University of Southampton

Faculty of Engineering and Physical Sciences

Electronics and Computer Science

Exploration of planar capaciflector for wearable respiration monitoring

by

Boyuan Zhao

ORCID ID 0009-0006-5988-3014

Thesis for the degree of Doctor of Philosophy

December 2024

University of Southampton

Abstract

Faculty of Engineering and Physical Sciences

Electronics and Computer Science

Doctor of Philosophy

Exploration of planar capaciflector for wearable respiration monitoring

by

Boyuan Zhao

Respiratory rate is an important physiological parameter, and its continuous monitoring plays a key role in health management. This study aims to evaluate the application of planar capacitive sensors with active shielding, capaciflectors, in respiratory monitoring. Previous studies have speculated that the change in sensor capacitance is mainly caused by skin deformation during breathing, but this theory has not been experimentally verified. In this study, an integrated wireless capaciflector respiratory sensor was developed based on the Texas Instruments FDC2214 capacitance-to-digital converter (CDC). Through experimental tests on 10 adult male volunteers, the results showed that the increase in sensor capacitance caused by skin stretching ranged from 0.01 to 0.1pF, which was in the same order of magnitude as the capacitance change caused by breathing, confirming that skin deformation is the main source of respiratory signals. In addition, the study explored the effect of operating frequency (200kHz to 7MHz) on sensor sensitivity and found that the sensor sensitivity at 200kHz was about 1.2 times higher than that at other frequencies, showing its potential as an optimised frequency, but due to the small effect, the current frequency selection can be more based on the needs of electronic devices. The study also explored the effect of electrode size on sensor sensitivity. The results showed that the design with an electrode length of 16 mm and a spacing of 4 mm showed a sensitivity improvement of about 2 times in some subjects, which may be a potential optimised design. However, due to individual differences, it is necessary to expand the sample size for further research. This study provides an important design reference for the design of capaciflector-based respiratory monitoring sensors.

Table of Contents

Table of Tables

Table of Figures

Research Thesis: Declaration of Authorship

Print name: Boyuan Zhao

Title of thesis: Exploration of planar capaciflector for wearable respiration monitoring

I declare that this thesis and the work presented in it is my own and has been generated by me as the result of my own original research.

I confirm that:

1. This work was done wholly or mainly while in candidature for a research degree at this University;
2. Where any part of this thesis has previously been submitted for a degree or any other qualification at this University or any other institution, this has been clearly stated;
3. Where I have consulted the published work of others, this is always clearly attributed;
4. Where I have quoted from the work of others, the source is always given. With the exception of such quotations, this thesis is entirely my own work;
5. I have acknowledged all main sources of help;
6. Where the thesis is based on work done by myself jointly with others, I have made clear exactly what was done by others and what I have contributed myself;
7. None of this work has been published before submission;

Submitted for review: Boyuan Zhao, Jack J. Tyson, Daniel C. Spencer, and Neil M. White. Comprehensive study of capaciflector-based respiration sensor performance: measurement principle, influence of operating frequency and electrode size. IEEE Sensors Journal, 2024

Signature: Date:

Acknowledgements

In the process of completing this doctoral thesis, I deeply appreciate the guidance and support of my two supervisors. Their expertise and thoughtful advice have been crucial in enabling me to understand and explore my academic field more deeply. Additionally, I am grateful to the fellow students who provided assistance during the research process. Their help in data collection and analysis was indispensable, and they offered significant perspectives during academic discussions. I would also like to extend special thanks to my parents, who have steadfastly supported and encouraged my academic pursuits. Their understanding and support have been a constant source of motivation on my journey towards academic goals. Finally, my gratitude goes to everyone who supported and assisted me on this research journey. Without their support, I could not have achieved what I have today. I am deeply grateful for their help and encouragement

Definition and Abbreviation

PTM Pneumotachometer

RIP Respiratory inductive plethysmography

MUT Material under test

BPM Breath per minute

CDC Capacitance-to-digital converter

ADC Analog-to-digital converter

BLE Bluetooth low energy

PDE Partial differential equations

ID Identifier

Chapter 1 Introduction

1.1 Background of respiration monitoring

Respiratory rate is a crucial vital sign and can serve as a predictor for serious illnesses. Clinical studies indicate that a respiratory rate exceeding 20 breaths per minute in non-exercise conditions suggests poor physical condition, while rates above 24 breaths per minute denote a high-risk state[1]. Respiratory rate is a valuable predictor because it reflects whether the concentrations of oxygen and carbon dioxide in the blood are within normal ranges[1]. Alveolar ventilation is regulated by the partial pressures of these gases in the arteries[1]. Low blood oxygen levels (hypoxaemia) and high blood carbon dioxide levels (hypercarbia) can lead to life-threatening symptoms such as arrhythmia, cerebral hypoxia, and cardiopulmonary arrest if not promptly treated[2]. The body compensates for these imbalances by increasing respiratory rate and tidal volume[1]. Therefore, monitoring respiratory rate allows for timely medical interventions to prevent the deterioration of these conditions. Additionally, opioids like methadone and morphine can reduce respiratory rate due to their side effects, making respiratory rate a critical indicator of adverse drug reactions[1].

Given its importance as a physiological parameter, there are currently three gold standards for respiratory rate measurement[3].

Figure 1 Two types of commercial pneumotachometer (PTM)[4][5].

The first method is based on the principle of airflow measurement and the related device is called pneumotachometer (PTM). The respiratory signal is obtained by measuring the flow velocity of the airflow on the nose and mouth area of the human body. Differential flowmeter and turbine flowmeter have been widely used for this type of respiration measurement. The principle of the differential airflow meter is to obtain the flow velocity by measuring the air pressure difference between the two ends of the pipe and then calculating the flow velocity

according to the linear relationship between the pressure difference and the flow velocity[6]. And the turbine flowmeter is based on the linear relationship between turbine spin speed and flow rate[6]. The similarity of these two methods is that they both require the subject to wear a facemask with pipe, because the measurement requires a pipe for airflow, as shown in Figure 1. Since these methods can directly obtain the flow rate of the inhaling and exhaling and the measured respiratory frequency are accurate and reliable, thus they are often used for clinical respiration monitoring or as a reference for evaluating the innovative respiratory measurement equipment. However, due to the bulky size of the entire device and the requirement to the facemask, they are likely not suitable for ordinary people to wear in daily life.

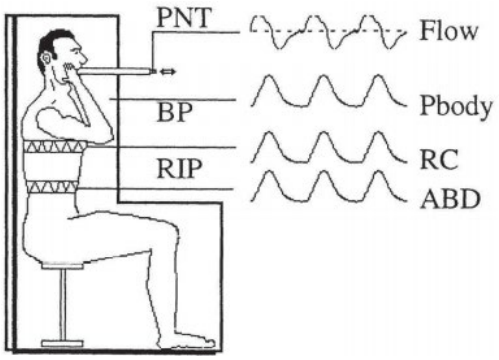

Figure 2 The schematic of respiratory inductive plethysmography (RIP) measuring the respiration signal from rib cage (RC) and abdomen (ABD)[7].

The second method is based on the measurement of chest or abdominal circumference. In the process of inhalation, the contraction of the diaphragm and the lifting of the ribs will increase the volume of the chest cavity[8], which cause air to be inhaled into the lungs under the action of the pressure difference between the body and the outside environment. At the same time, the longitudinal length of the abdominal cavity will be reduced due to the contraction of the diaphragm. This causes the increasing of the horizontal diameter of the abdominal cavity. During the exhalation phase, the relaxation of the diaphragm causes the drop of the pressure in the chest and abdominal cavity. This causes contraction of the chest and abdomen. Simply, the chest circumference and abdominal circumference increase during the inhalation period and decrease during the expiration period. Therefore, the respiratory signal can be obtained by measuring the chest circumference or abdominal circumference.

Respiratory inductive plethysmography (RIP) can measure changes in the circumference of the chest or abdomen during breathing process. The sensing front end of the device usually consists of an inductive coil integrated in an elastic cloth belt around the ribs (RC) or abdomen (ABD)[6], as shown in Figure 2. This coil work as an inductor that determine the frequency of the LC oscillating circuit. When the breathing activity causes the variation of the circumference of the

induction coil, the respiration signal will modulate the frequency of the oscillation circuit[6]. Finally, the breathing signal can be obtained through the demodulation of the output of oscillation circuit. At present, RIP has been proven to be a reliable respiration measurement system with an accuracy comparable to PTM[7]. However, since the movement of the torso also induces changes in the circumference of the coil, its measurement accuracy will be affected by motion artifacts (MA). In addition, in order to obtain a relatively reliable breathing signal, the cloth belt needs to be tightly wrapped around the chest or abdomen. This undoubtedly reduces the wearability and may even influence the normal process of breathing.

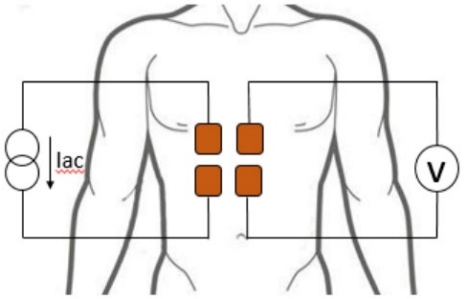

Figure 3 The schematic of four-electrode configuration of impedance pneumography[9].

The third method is based on measuring the thorax impedance. Since breathing will cause the movement of tissues inside the torso. When the current flows through the inside of the chest area, the path of the current will periodically change under the influence of breathing, which is manifested as the variation of thorax impedance from a macroscopic point of view. Therefore, the respiratory signal can be obtained by measuring the chest impedance. In practical measurement, the four-electrode configurated impedance measurement technology is usually used. For the four-electrode configuration, as shown in Figure 3, two electrodes are placed on opposite sides of the chest cavity and a low-amplitude current of about 50 kHz and 1 mA is injected into the chest cavity[6]. The other two electrodes are also connected to opposite sides of the chest cavity to measure the voltage change between them for impedance calculation. This method is called impedance pneumography and has also been proven to have comparable accuracy to the flowmeter. However, during the measurement process, the electrodes need to directly contact with the skin to obtain better measurement accuracy. Obviously, long-term monitoring will cause skin discomfort. In addition, the torso movement will change the contact condition between the electrode and the skin, thus the motion artifacts will influence the measurement accuracy of impedance pneumography[10].

Although these methods are accurate, their reliance on close contact with the body limits their comfort and suitability for long-term wearable applications. Therefore, there is a need to develop a technology that maintains high accuracy while improving wearability.

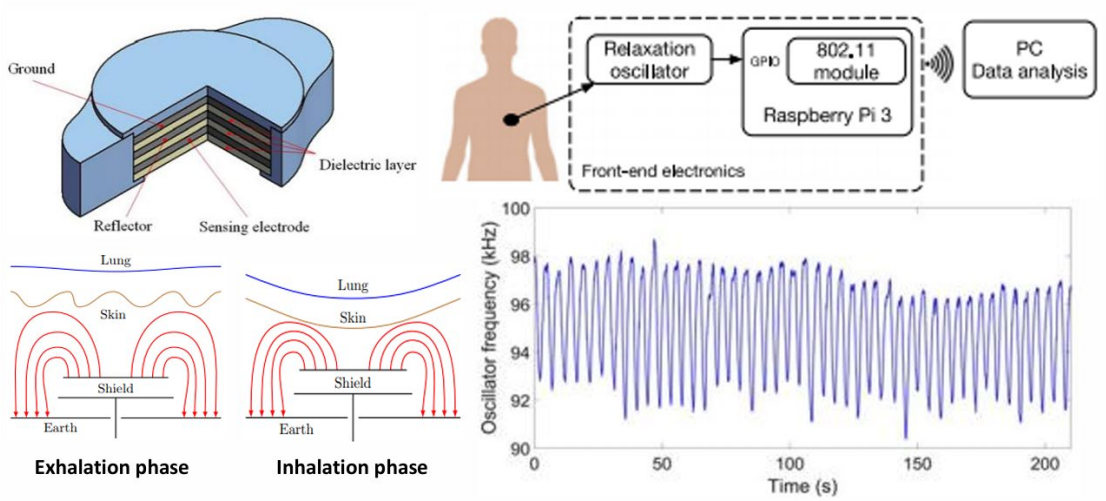

Figure 4 The prototype block diagram and the measured respiratory signal of the capaciflector based respiration sensor[11][12].

In recent years, White et al. have explored a respiration monitoring technology based on capacitive sensors, known as the capaciflector[12], as shown in Figure 4. This technology detects respiratory signals by measuring changes in capacitance during breathing. The capaciflector can be integrated into clothing, providing good wearability and does not require direct electrical contact, although skin contact can improve accuracy. In addition, this sensor technology has demonstrated its effectiveness for long-term monitoring of respiratory signals across various individuals. It has been proven capable of consistently and reliably collecting respiratory data from diverse subjects[13]. However, the exact working principle of this sensor is not fully understood and its measurements are affected by motion artifacts.

Given the potential advantages of capaciflectors in wearable respiratory monitoring, further research is essential to overcome the existing challenges. Understanding the underlying principles and optimising sensor design can significantly enhance performance and reliability. This study aims to explore these aspects in detail, contributing to the development of more effective wearable respiration monitoring technologies. Table 1 provides a comparison between the three gold standards for respiratory rate measurement and the capaciflector.

Table 1 Comparison of respiratory rate measurement technologies: three gold standards and capaciflector

Technology	**Measurement principle**	**Advantages**	**Disadvantages**
Pneumo-tachometer	Measures airflow velocity at the nose and mouth using differential or turbine flowmeters	Provides precise measurements of airflow, not affected by motion artifacts, useful in clinical settings	Requires the use of facemasks and tubing, which reduces comfort and wearability for long-term use.
Respiratory inductive plethysmography	Measures changes in chest and abdominal circumference	Offers detailed data on thoracic and abdominal movement, beneficial for comprehensive respiratory monitoring and detecting respiratory patterns	Susceptible to motion artifacts; requires tight-fitting belts around the chest and abdomen, which can be uncomfortable and impractical for extended wear.
Impedance pneumography	Measures thoracic impedance changes due to breathing	Suitable for continuous monitoring and detecting respiratory patterns	Sensitive to motion artifacts; requires direct skin contact with electrodes, which can cause discomfort and skin irritation over time; needs direct electrical contact with the skin.
Capaciflector	Likely measures capacitance changes due to breathing movements	Can be integrated into clothing, making it convenient for wearable applications; does not require direct electrical contact, though skin contact can improve accuracy	Susceptible to motion artifacts; exact measurement principle and influencing factors not fully understood.

1.2 Research questions and objectives

1.2.1 Research questions

To clarify the measurement principle of the capaciflector in respiratory monitoring and optimise its design, this study addresses the following specific research questions:

(1) Which physiological activity during breathing mainly affects the capaciflector's capacitance? Is it the motion of the lungs inside the thoracic cavity, or the motion of the skin, fat, and muscles outside the thoracic cavity?

(2) How does the operating frequency affect the capaciflector's sensitivity to respiration-induced capacitance changes? By conducting respiration measurements at different operating frequencies, observe the effects of these frequencies on sensor sensitivity.

(3) How does the size of the sensing electrode affect the capaciflector’s sensitivity to respiration-induced capacitance changes? Study the impact of different electrode sizes on sensor sensitivity and determine the optimal design.

1.2.2 Research objectives

The primary aim of this research is to answer the above research questions to elucidate the measurement principle of the capaciflector and optimise its design and operational parameters to enhance its performance in wearable respiration monitoring applications. The specific objectives are as follows:

(1) Verification of Measurement Principle: To experimentally verify that skin stretching is the main factor causing capacitance changes in the capaciflector during respiration monitoring.

(2) Assessment of Frequency Impact on Sensitivity: To investigate the effect of operating frequency on the sensitivity of the capaciflector.

(3) Assessment of Electrode Size Impact on Sensitivity: To evaluate the effect of different sensing electrode sizes on the sensitivity of the capaciflector and identify the optimal design.

(4) Validation of Results Across Different Subjects: To conduct repeated experiments on different subjects to verify the generality of the results.

1.3 Thesis contribution

Prior to this study, the research group had preliminarily verified the feasibility of capaciflector as a respiratory sensor[14], and also verified its stability and reliability in long-term monitoring between different subjects[13]. Compared with these previous studies, the innovation of this study lies in analysing the measurement principle of capaciflector as a respiratory sensor and analysing the influence of sensor operating frequency and electrode size on sensitivity.

Specific contributions to the field of wearable capacitive respiration measurement include:

(1) Innovative Electronic Design: A novel electronic design of an integrated wireless capacitive respiration device using the FDC2214 capacitive-to-digital converter is proposed and detailed in Chapter 4.

(2) Verification of Measurement Principle: The study verifies that the primary factor responsible for the capacitance change in a capaciflector-based respiration sensor is the stretching of the skin during breathing and detailed in Chapter 5.

(3) Frequency Sensitivity Analysis: Exploration of the impact of the capaciflector's operating frequency on its sensitivity to respiration-induced capacitance changes, demonstrating that frequency variations between 200kHz and 7MHz have limited impact on sensitivity and detailed in Chapter 6.

(4) Electrode Size Sensitivity Analysis: Investigation of the effect of different sensing electrode sizes on the capaciflector's sensitivity, identifying that an electrode length of 16mm with a spacing of 4mm offers higher sensitivity and detailed in Chapter 7.

These findings can provide important guidance for the design of capacitive reflectometer-based respiratory monitoring devices and help improve sensor performance in practical applications.

Chapter 2 Advancements in Wearable Projected Capacitive Respiration Sensors and Comparative Technologies

This chapter aims to provide a comprehensive background explanation of the study. First, the principle of projected capacitive sensing is discussed in depth to clearly build the theoretical basis of this study. Next, a detailed analysis of the capacitance measurement method is conducted to lay a solid foundation for establishing a subsequent experimental platform. In addition, this chapter will also comprehensively review the research progress of other wearable projected capacitive respiration sensors in respiratory monitoring applications in the existing literature. Finally, current alternative technologies will be reviewed and their advantages and limitations compared to projected capacitive sensors will be analysed. These comprehensive reviews and discussions provide solid theoretical support and practical guidance for the in-depth analysis of this study.

2.1 Principle of projected capacitive sensing

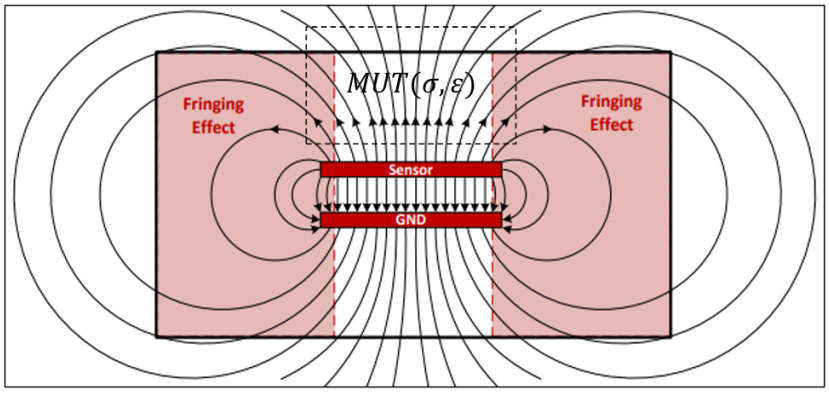

Figure 5 Schematic diagram of interrogation electric field of capacitive sensor with parallel plate structure[15]

The basic principle of capacitive sensing relies on the interaction between the material under test (MUT) and the interrogating electric field generated by the sensor electrodes[16]. The fringe electric field emitted by the capacitive electrode penetrates the MUT and induces an electrical displacement in it[16]. For an electrically neutral MUT, its internal displacement field is in the opposite direction to the interrogation field generated by the sensor, resulting in changes in the spatial potential distribution. This change changes the amount of charge stored

between the sensor electrodes, thereby changing the capacitance between the electrodes[16]. This is a common mechanism in which capacitive sensors work when measuring properties of objects in the environment, such as deformation or presence.

Under a quasi-static approximation of the electric field, the capacitance of a capacitive sensor can be described by Equation 1[16], [17]:

$$C = \frac{Q}{V} = -\frac{1}{V}\oint(\sigma(\mathbf{r}) + \varepsilon_0\varepsilon(\mathbf{r}))\nabla\Phi(\mathbf{r})\, d\Gamma \qquad \text{Equation 1}$$

where:

Q electric charges on a pair of electrodes (*C*).

V electric potential difference between a pair of electrodes (*V*).

$\mathbf{r}$ position vector (*m*).

$\sigma(\mathbf{r})$ spatial conductivity distribution (*S/m*).

ε_0 permittivity of vacuum (*Dimensionless*).

$\varepsilon(\mathbf{r})$ Distribution of spatial relative permittivity (*Dimensionless*).

$\Phi(\mathbf{r})$ Distribution of spatial electric potential distribution (*V*).

∇ gradient operator (*1/m*).

Γ electrode surface (m^2).

According to the guidance of Equation 1, it can be inferred that the capacitance of a capacitive sensor is affected by the conductivity, dielectric constant, potential, and the spatial distribution of the electrodes. Since the geometry of the sensor electrodes and the applied voltage are known conditions, capacitive sensors are able to measure the conductivity and dielectric properties of the material under test (MUT). Furthermore, by establishing the relationship between the electrical characteristics of the MUT and system variables (such as temperature, humidity, structural changes, etc.), accurate measurement of these system variables can be achieved[16]. In respiration measurement, the MUT can be regarded as a part of the human trunk. For such multilayer biological media, the electric displacement field within the medium is mainly caused by the Maxwell-Wagner (MW) effect or the interfacial polarization process[18]. The macroscopic electrical properties of materials can be characterized by using the dielectric constant ε and the electrical conductivity σ[19]. The ratio τ= ε/σ is the relaxation time of the material, which represents the diffusion time required for the charges in the material to reach a

steady state[19]. When current flows through the interface of two materials with different relaxation times, charges will accumulate on the interface[19]. This phenomenon is called the Maxwell Wagner effect, and the process of charge accumulation at the interface is called the interface polarization process.

According to Equation 1, the capacitance of a capacitive sensor depends on the spatial electric field distribution within its sensing range. When the multilayer medium is located inside the interrogation electric field of the sensor, the electric field distribution in the medium depends not only on the electric field formed by the applied voltage V, but also on the displacement field formed by the accumulated charges at the interface[19]. Therefore, it is critically important to characterise the accumulated charges at the interface of the medium.

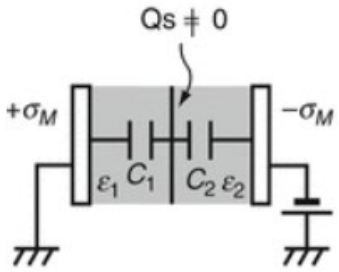

Figure 6 Schematic of double-layer dielectric between two meatal plates with voltage applied[19]

For simplicity, Figure 6 shows a parallel plate capacitor composed of double-layer dielectrics with different relaxation times. Equation 2 describes the charge accumulation process at the interface of the double-layer dielectric:[19]:

$$\sigma_s(t) = \sigma_s(1 - \exp(-t/\tau_{MW})) \qquad \text{Equation 2}$$

$$\tau_{MW} = \frac{C_1 + C_2}{G_1 + G_2}$$

$$C_1 = \varepsilon_1 S/L_1 \qquad C_2 = \varepsilon_2 S/L_2 \qquad G_1 = \sigma_1 S/L_1 \qquad G_2 = \sigma_2 S/L_2$$

where:

σ_s interface charge density (C/m^2).

t time variable (s).

τ_{MW} Maxwell's dielectric relaxation time of double-layer dielectric (s).

C_1, C_2 capacitance of the dielectric films (F).

G_1, G_2 admittance of the dielectric films (S).

S area of electrode (m^2).

$\varepsilon_1, \varepsilon_2$ dielectric constant of the dielectric films (*Dimensionless*).

σ_1, σ_2 conductivity of the dielectric films (S/m).

L_1, L_2 thickness of the dielectric films (m).

According to Equation 2, due to the existence of Maxwell's dielectric relaxation time. The charge density at the interface of two dielectric materials depends not only on their electrical properties, but also on their thickness[19]. Thus, the variation in the thickness of a certain dielectric layer or the displacement of the dielectric boundary in the double-layer dielectric will cause the change of the interface charge density. In addition, since the capacitance between the two metal plates in Figure 6 is related to the distribution of the spatial electric field that partly depends on the interface charge density. Therefore, the displacement of the dielectric boundary in a capacitor has double-layer dielectric can change the capacitance of the capacitor. More generally, for a multilayer dielectric medium that is penetrated by the interrogation electric field of a capacitive sensor, the movement of the dielectric boundary within the medium will cause the change of sensor capacitance.

2.2 Capacitance measurement

2.2.1 Reflector – active shielding

Capacitive coupling sensing technology detects objects in space by utilizing the fringe electric fields generated by capacitive sensors. The sensing range of this technology is directly affected by the design structure and size of the sensor electrodes. For example, in a parallel plate capacitor, its fringe electric field is usually relatively weak due to the strong coupling between the sensing electrode and the ground electrode, limiting its ability to detect distant objects. However, by applying active shielding technology, a reflective electrode with the same potential as the sensing electrode can be added between the sensing electrode and the ground electrode[20]. This design effectively weakens the coupling between the sensing electrode and the ground electrode, thereby expanding the fringe electric field generated by the sensing electrode. The result is a significant increase in the sensor's detection range, allowing detection of objects at greater distances. Figure 7 shows how active shielding technology changes the sensing range of a sensor, allowing it to cover a wider area.

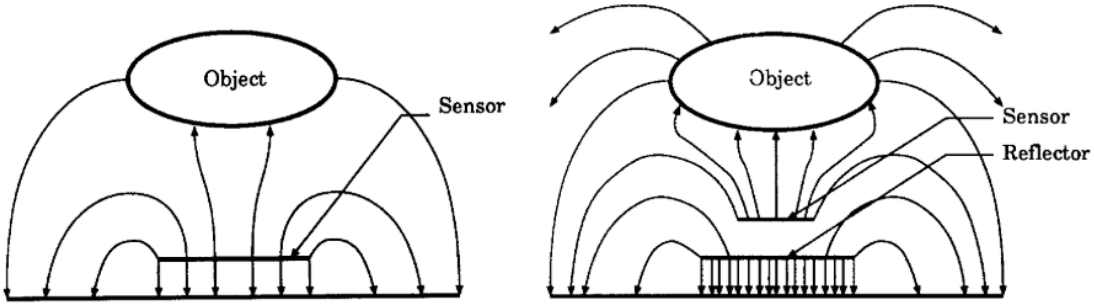

Figure 7 The schematic of the fringing filed of capacitor and capaciflector[20]

2.2.2 Impedance analysis

Impedance analysis is a measurement technique used to determine the impedance and phase difference of circuit components such as capacitors. Impedance is a combined expression of resistance and reactance, while phase difference reflects the time offset between current and voltage waveforms. By measuring these parameters, the capacitance value at a specific operating frequency can be calculated. Typically, the sensor needs to be connected to the impedance analyser through a test fixture. When performing frequency-dependent testing, it is necessary to know the frequency range supported by the test fixture. Since this experiment requires driving the sensor at different operating frequencies, an impedance analyser is an ideal measurement tool.

The main difference between capaciflectors and traditional capacitors is the addition of active shielding. The function of this shielding layer is to weaken the capacitance between the sensing electrode and ground, and at the same time make the sensor have unidirectional sensing characteristics. However, impedance analysers do not natively support active shielding. Simply introducing a voltage follower into the analyser's excitation signal may directly affect the measurement results because the input impedance of the voltage follower affects the measurement. Nonetheless, the presence or absence of active shielding does not change the basic working principle of the sensor. Therefore, impedance analysis can be performed without a reflective layer. Considering the high accuracy and stability of the impedance analyser, it can be used in the early verification stage of the experiment to ensure that the capacitive sensor achieves the expected performance at different frequencies.

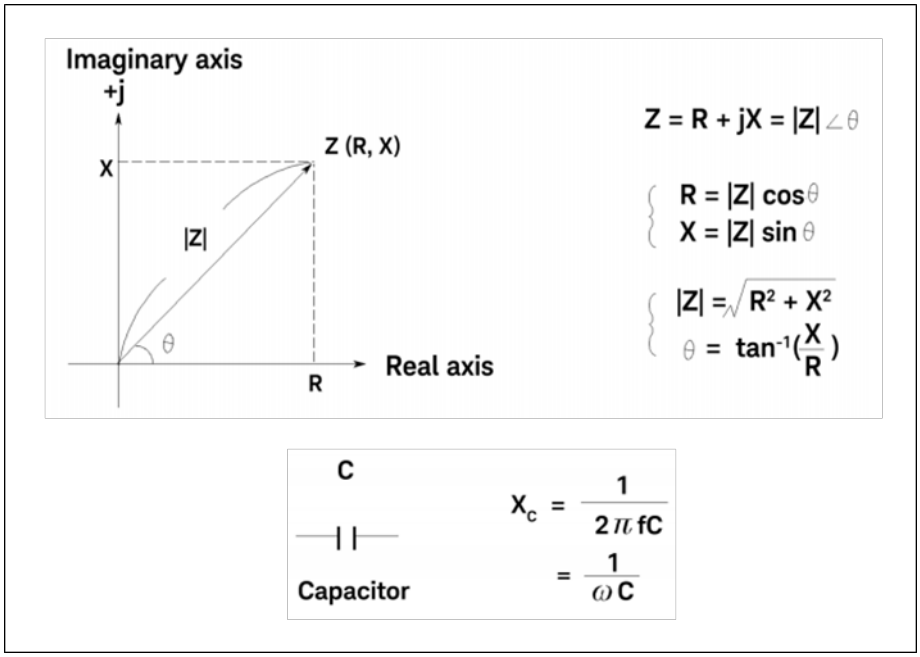

Figure 8 Impedance Z consists of resistance R (real part) and reactance X (imaginary part) and capacitance a form of reactance[21].

2.2.3 Resonance-based capacitance measurement

Capacitance measurement can be achieved through resonant circuits directly related to capacitance, including two main types: RC (resistance-capacitance) circuits and LC (inductance-capacitance) resonant circuits. RC circuits, especially relaxation oscillator circuits, mainly produce a delay effect through a combination of resistance and capacitance, and are often used to generate timing signals and adjust the response time of the circuit[22]. The characteristic of this circuit is that the time of voltage change during capacitor charging and discharging can be precisely controlled by the RC time constant[22]. An LC resonant circuit combines an inductor and a capacitor to form a system capable of oscillating at its natural frequency. In such a circuit, any change in capacitance will affect the resonant frequency of the system[23]. In both circuits, any change in capacitance affects the resonant frequency of the system. In practice, for example, in proximity sensing applications, when a target (such as a human hand) approaches the capacitive sensing electrode, the capacitance of the sensor changes. This change is reflected as a change in frequency, which can be recorded and analysed by a frequency counter.

The capacitance measurement method based on resonant frequency changes is highly sensitive, can accurately capture small capacitance changes, and has good anti-interference ability. However, the design of the resonant circuit needs to consider many factors, such as the

characteristics of the circuit components, ambient temperature, physical properties of the electrodes, etc., all of which may affect the resonant frequency. Therefore, when designing and optimising the resonant circuit, these factors need to be taken into consideration to ensure measurement accuracy and stability.

2.3 Capacitive sensing-based respiration measurement

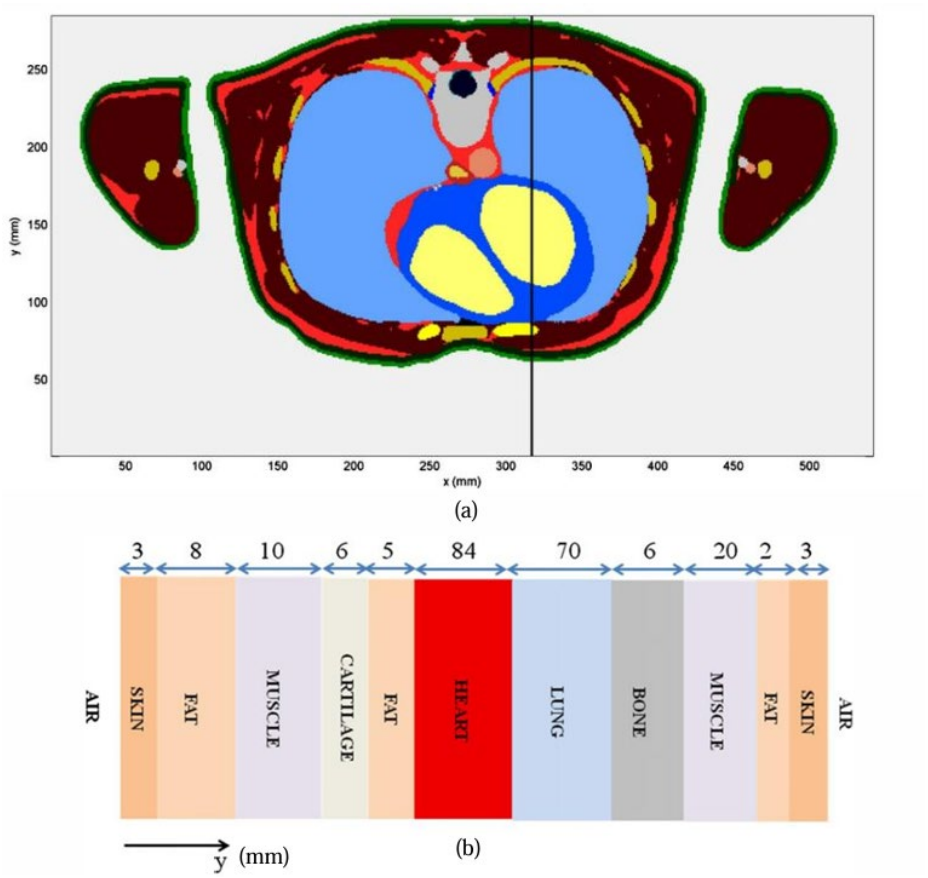

Figure 9 (a) Axial cross-sectional anatomy of the chest area of an adult male. The lines provide sequence and thickness information for the multilayer tissue model[24]. (b) The planar multi-layer tissue model[24].

The human body is composed of multiple layers of biological tissue, as shown in Figure 9. The electrical properties and the relaxation time of various tissues are quite different, as shown in Table 2. Respiration is a complex physiological process that can cause simultaneous movement of multiple layers of tissue, such as the expansion of the lungs and the stretching of skin and fat. In other words, breathing causes displacement of the dielectric boundary in the torso region of the body. Therefore, when the interrogation electric field of the capacitive sensor penetrates the tissues inside the torso, due to the interface polarisation effect, the displacement of the

dielectric boundary inside the torso caused by respiration will change the capacitance of the sensor. This is the general principle of capacitive respiration sensing.

Table 2 The basic electric properties and relaxation time of biological tissues at 3MHz

Electrical properties	**Skin**	**Fat**	**Muscle**	**Bone**	**Heart**	**Lung (inflated)**	**Lung (deflated)**
ε	642.68	20.92	522.35	148.34	759.79	363.54	462.21
σ (S/m)	0.29	0.03	0.57	0.10	0.41	0.18	0.39
τ (s)	2216.14	697.33	916.40	1483.40	1853.15	2019.67	1185.15

Based on this sensing principle, in 2011 Wartzek et al. proposed a capacitive sensor that can monitor breathing from the back of the human body.

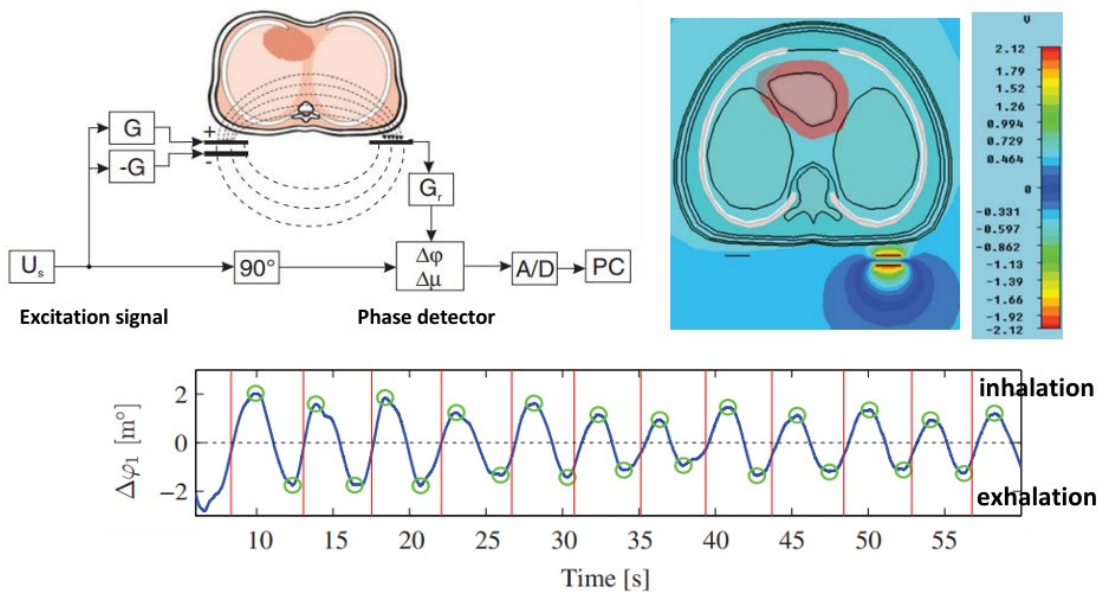

Figure 10 Schematic of Wartzek et al. proposed respiration measurement system and the measured respiratory signal[18].

The sensor uses a co-planar parallel plate capacitor structure, the excitation electrode and the receiving electrode are placed on both sides of the body. The generated 20MHz electric field can cross the entire chest area. Since the human body is a complex dielectric with a multilayer structure, when the electric field passes through this type of dielectric, the phase difference between the signals on the two electrodes is not completely equal to 90 degrees. In addition, the phase difference will vary with the permittivity, conductivity and dimension of the dielectric[25]. According to Impedance pneumography, the impedance of the human body will change with breathing[6]. Therefore, the respiratory signal can be obtained by measuring the

phase difference between the signals on the two electrodes. The implementation phase measurement is conducted by a commercial phase detector, as shown in Figure 10. Because the performance of this sensing method is related to the electric field strength in the area being measured[18]. In order to obtain a higher electric field strength under the same applied voltage, the author cancelled the passive shielding and added an extra with the signal that completely opposite to the signal applied on excitation electrode so that the electric field strength on the sensing side can be improved[18]. Although this configuration makes the sensor sensitive to the approaching object at non-sensing side, for indoor monitoring scenes, the sensor can be integrated into the mattress or seat back to carry out respiration monitoring.

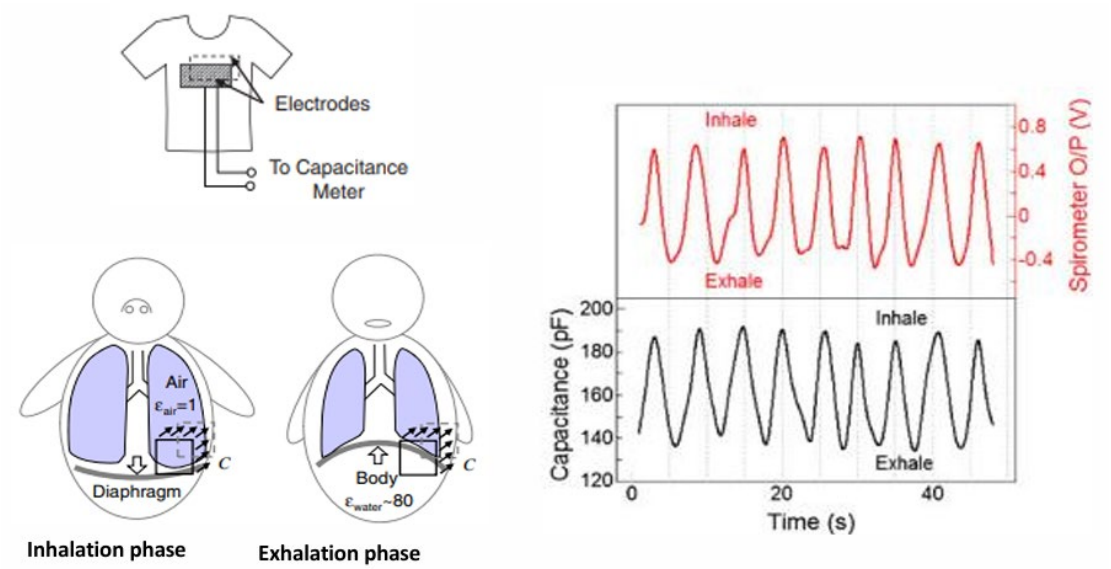

Figure 11 Schematic of Kundu et al. proposed wearable capacitive respiration sensor and the measured respiratory signal[26].

Although the impedance of the human body changes with respiration, the details of the principle are still unknown. In 2013, Kundu et al. proposed a wearable capacitive respiration sensor that can be integrated in a T-shirt. The proposed sensor utilizes a parallel plate capacitor structure, and two electrodes are located on the chest and the corresponding back area. The torso is sandwiched between two electrodes as a dielectric. The author believes that air (relative permittivity 1) being inhaled into the lungs will change the dielectric property of the chest area. In addition, inhalation makes the chest circumference increase, so the distance between the two plates will increase. According to the formular of the parallel plate capacitor, the capacitance is inversely proportional to the distance between the plates and proportional to the relative permittivity. If the working principle proposed by the author is correct, the capacitance of the sensor should be reduced during the inhalation process. However, according to the measured breathing signal given in the article, there is an upward trend during inhalation. This means that there might be a problem with the proposed working principle. In addition, the intensity of the

electric field generated by the sensor attenuates severely with distance in the human body[27]. Therefore, changes in the electrical properties of the inner layer of the tissues are difficult to change the capacitance of the sensor.

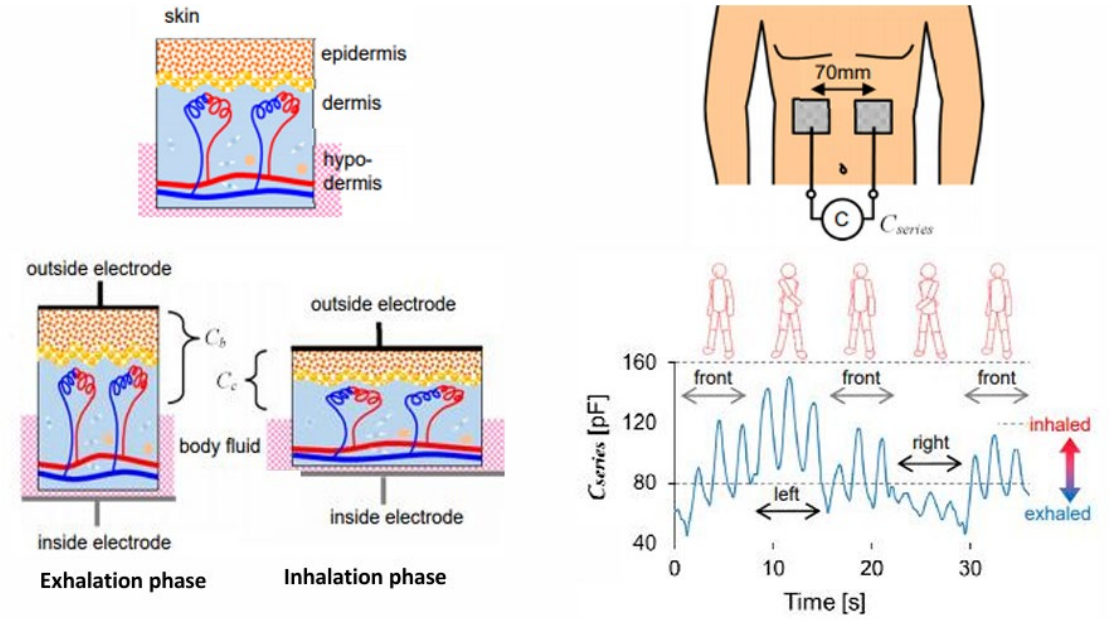

Figure 12 Schematic of Terazawa et al. proposed wearable capacitive respiration sensor and the measured respiratory signal[28].

Therefore, to solve the problem of unclear working principle, in 2016, Terazawa et al. proposed another possible working principle. The author believe that the change of the sensor's capacitance is caused by the compression and relaxation of the skin. Specifically, since the human skin has a multilayer structure, the epidermis at the outer layer has almost no conductivity due to lack of moisture, and the electrolyte solution with high conductivity is held in the subcutaneous tissue, such as sweat glands[29]. Under the influence of the electric field generated by the sensor, a virtual electrode will be formed in the subcutaneous tissue by the ions in electrolyte solution[29]. The inside electrode and the electrode of the sensor form a parallel plate capacitor and the dermis and epidermis are work as dielectric. Inhalation causes an increase in the chest circumference, which stretches the outer tissues of the chest cavity and reduces their thickness. For parallel plate capacitors, the capacitance is inversely proportional to the thickness between the plates. Therefore, the capacitance will rise during the inhalation process.

Based on this working principle, in 2018, the author changed the configuration of sensor to a coplanar parallel plate capacitor structure, and moved the deployment position of the sensor from the chest to the abdomen. The reason is that the increase in abdominal circumference during inhalation is greater than the change in chest circumference[28]. Although Terazawa et

al. proposed the working principle of the sensor is matched with the measured respiratory signal, the author utilised flexible textile electrodes in the process of experimental verification. The strain of the flexible electrode will also cause a change in the capacitance of the sensor. Therefore, it cannot be fully proved that the change in sensor capacitance is caused by the change in skin thickness. In addition, the connecting wire between the electrode and the capacitance measuring unit also causes changes in capacitance when vibrating, mainly due to parasitic parameters in the stranded wires. Although in subsequent studies, the team reduced the impact of wire movement on capacitance measurements by using coaxial wires instead of stranded wires[30], this method still failed to completely eliminate the impact of vibration on capacitance changes.

In summary, the research on capacitive respiration sensors has been carried out for many years. Although this type of sensor has been proven to be able to obtain clear breathing signals which caused by changes in the electrical properties of the tissues inside the torso during breathing, it is still unknown which part of the tissue dominate the production of the signal. Therefore, it is necessary to conduct further research on this issue.

2.4 Comparative wearable respiration measurement technologies

For the research topic of wearable respiratory rate monitoring, the capacitive-based respiration sensor is not the only method that use to detect breathing. In the past decade, several research groups have conducted research on breathing measurement based on capacitive sensing and the specific content about it is discussed in the summary in 2.1.1. In addition, some respiration monitoring methods based on other sensing principles will also be discussed in Section 2.1.

2.4.1 Strain sensing-based techniques

In addition to capacitive sensors, the chest belt with integrated strain gauges can also be used to measure breathing signal. Piezoresistive sensors can convert strain into resistance variation, which is a typical strain gauge. For wearable applications, the woven conductive yarns can work as a piezoresistive sensor. And the yarns can be used to measure the respiratory signal when it be integrated into the chest belt[6]. Specifically, the expansion of the thorax during inhalation stretches the chest belt around the thorax, which cause the conductive yarn to be stretched. The stretching affects the number of conductive contacts inside the yarn. The reduction of contact points will lead to an increase in resistance[6]. During the exhalation process, the ribs contract and the yarn returns to its original state, which increases the number

of conductive contacts, resulting in a decrease in electrical resistance. The resistance change can be measured by the Wheatstone bridge circuit.

Generally, the chest belt equipped with a single strain sensing unit are seriously susceptible to motion artifacts. To reduce the interference caused by motion. In 2020, Massaroni et al. A respiratory monitoring garment with 6 independent piezoresistive sensing elements is proposed. The sensing element is deployed on the front of the garment, as shown in Figure 13. In order to reduce motion artifacts, 4 of the 6 measured respiratory signals with higher signal-to-noise ratio are select first[31]. Then the selected 4 respiratory signals are averaged and normalized. Finally, they can be used to calculate the respiratory rate[31]. In the author's experiment, 10 male volunteers took part in walking and running experiment on a treadmill (walking: 1.6 km/h, running: 8 km/h)[31]. Compared with the measurement results of a single piezoresistive sensing element, the fusion of the six independently sensing elements shows better consistency with reference pneumotachometer. And the average error of the respiratory frequency measured in the running state is ±3 BPM[31].

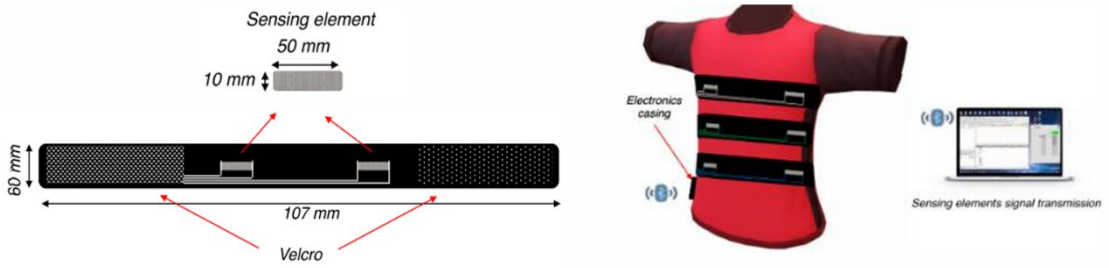

Figure 13 The respiration monitoring garment with 6 piezoresistive sensing elements and measured respiration signal[31].

Although the chest belt can provide reliable breathing signals according to its working principle, in order to ensure the accuracy of the measurement results, the chest belt needs to be tightly wrapped around the chest. This will limit the expansion of the chest cavity in a certain extent. For patients with respiratory diseases such as chronic obstructive pulmonary disease (COPD), the chest belt may even change the patient's normal breathing. To this end, some researchers are dedicated to the study of miniature strain sensors, which can be attached to the surface of the skin to measure local chest wall and abdominal wall movements during breathing.

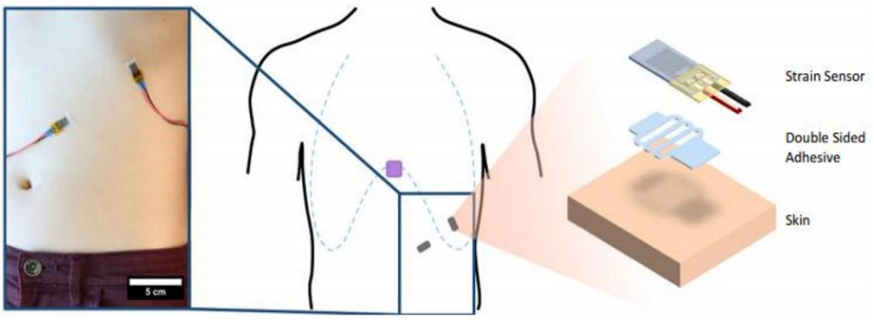

Figure 14 Two miniature strain sensors attached on the skin surface of ribs and abdomen for respiration measurement[32].

In 2019, Chu et al. proposed a miniature flexible piezoresistive wireless strain sensor, which can be attached to the skin of the ribs and abdomen to monitor the respiratory rate, as shown in Figure 14. The sensor front end is a piezoresistive metal film encapsulated in silicone elastomer substrate[33]. When tension is applied to the silicone elastomer, the metal film will rupture slightly and cause an increase in electrical resistance[33]. The micron-scale wrinkle of the metal film will not be simply developed to cracks, so that the sensor can be reused[33]. At present, the sensor has been verified to be reusable 2000 times under the strain of 156%-226% [32]. 7 volunteers with no respiratory diseases participated in the experiment. The spirometer is used as a reference system. In the static state, through correlation evaluation, the average correlation coefficient between the respiratory signal measured by the strain sensor and the reference signal is 0.962[32]. Under running conditions at a speed of 12.9km/h, the average correlation coefficient between the strain sensor and the reference system is 0.75[32]. It can be seen from this that motion artifacts can also contaminate the respiratory signal measured by the strain sensor deployed on the skin surface.

In addition to the above two types of piezoresistive materials, capacitors with interdigital structures can also be used as strain sensors. When the interdigital electrode is stretched or bent under applied force, the gap between the interdigital fingers decreases, which cause the increase in capacitance. Thus, there is a linear relationship between the capacitance and the applied force.

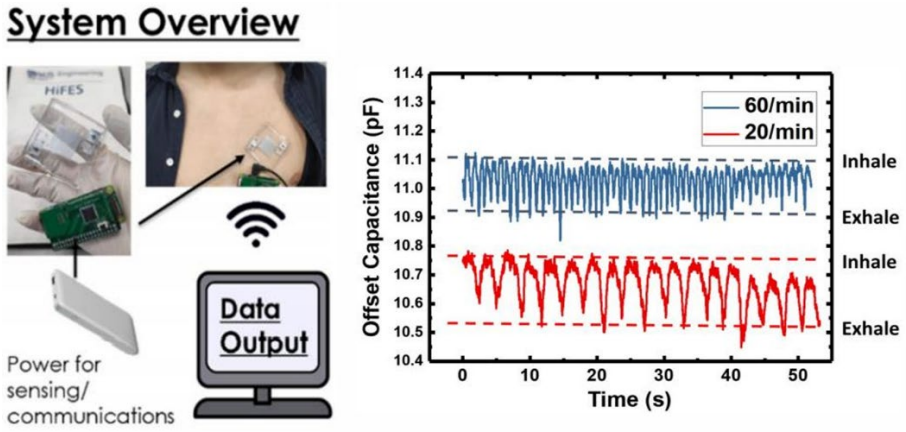

Figure 15 PDMS and liquid alloy based-interdigital capacitive sensor and its measured respiration signal[34].

In 2019, Li et al. proposed a flexible interdigital capacitive respiration sensor based on polydimethylsiloxane (PDMS) and liquid-phase GaInSn alloy (Galinstan) material. The interdigital electrodes are formed by liquid-phase alloy embedded in interdigital microfluidic tubes in PDMS[34]. This flexible sensor can be directly attached to the skin surface of the chest and measure the stress caused by the expansion of the chest during inhalation process[34].

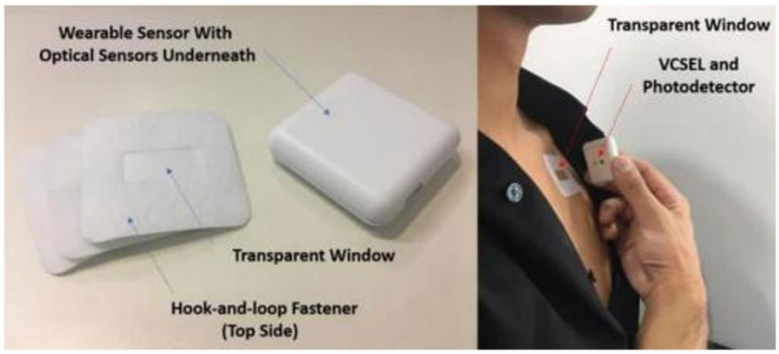

Figure 16 Measuring skin deformation using optical sensors to obtain respiratory signals[35].

In a 2020 study, Singh et al. explored a breath measurement scheme that combined wearable technology with adaptive optics methods. This solution uses the principle of direct contact optical diffuse reflection to measure the deformation of the skin during the respiratory cycle[35]. The research team developed an adaptive algorithm to initially calculate the breathing frequency and select the most suitable frequency band accordingly[35]. On this basis, they also developed a bracelet device that uses optimised algorithm parameters to improve the detection accuracy of respiratory frequency[35]. This method was validated in an experiment involving 82 patients with respiratory illnesses, compared with traditional manual counting methods. Experimental results show good agreement between the new method and reference

manual counting. Performance evaluation revealed that its 95% confidence interval deviation ranged from -3.34 to 3.67 breaths per minute, with the mean and standard deviation being 0.05 breaths/minute and 2.56 breaths/minute respectively[35]. This shows that the method performs well in terms of accuracy and stability, providing an effective alternative for respiratory rate measurement.

In summary, due to the clear working principle, the development of strain-based respiratory sensor has been relatively mature. The existing problems include motion artifacts and the trade-off between measurement accuracy and wearability. In terms of improving wearability, in the past, the chest belt sensor needed to surround the chest may affect the normal breathing of wearer. Recently, the skin-adhesive miniaturized sensor can obtain breathing signals by measuring the local strain variation of the chest, ribs or abdomen area during breathing. This undoubtedly greatly improves wearability of the sensor. However, compared with the chest belt, the method of measuring local body strain is more sensitive to torso movement, thus further research is still needed to improve reliability of it.

2.4.2 Airflow velocity sensing-based techniques

As mentioned in the introduction, airflow velocity measurement is the gold standard for respiratory monitoring. This method is usually not portable enough because it requires obtaining the respiratory signal by measuring the pressure difference between the two ends as the air flows through the tube. However, some research groups have simplified this measurement mode based on MEMS (microelectromechanical systems) airflow sensors, reducing the size of the required pipes to improve its portability.

In 2018, Taffoni et al. developed a device for monitoring human respiratory frequency during exercise, as shown in Figure 17 (a). The monitoring device is cleverly integrated into the earphones, and its sensing unit is located where the microphone stick of the original earphones is, about 10 centimetres away from the mouth[36]. The device consists of a commercial air flow meter (SpiroQuant P, EnviteC by Honeywell) and an accompanying digital differential pressure sensor (SDP610, Sensirion)[36]. Since the sensor is at a certain distance from the mouth, it mainly measures the exhaled airflow, as shown on the right side of (a) below. However, since the device is only used to measure respiratory rate, this deployment method does not affect the accuracy of the measurement. The device has been experimentally verified by mechanical ventilation in two breathing modes of 12 times/min and 32 times/min. The results show that the respiratory frequency measured by the monitoring device is consistent with the setting of the

mechanical ventilator[36]. Testing on healthy adult men also showed that the measurement error was approximately ±1 BPM, whether at rest or running[36]. Therefore, the respiratory frequency monitoring device has high accuracy, and since it does not require a mask to collect airflow, its wearing experience is more comfortable than traditional instruments and is suitable for long-term monitoring. However, the device mainly measures airflow exhaled through the mouth and is not ideal for monitoring breathing conditions through the nose. Studies have pointed out that during exercise of moderate intensity and below, airflow mainly enters and exits the respiratory tract through the nose[37].

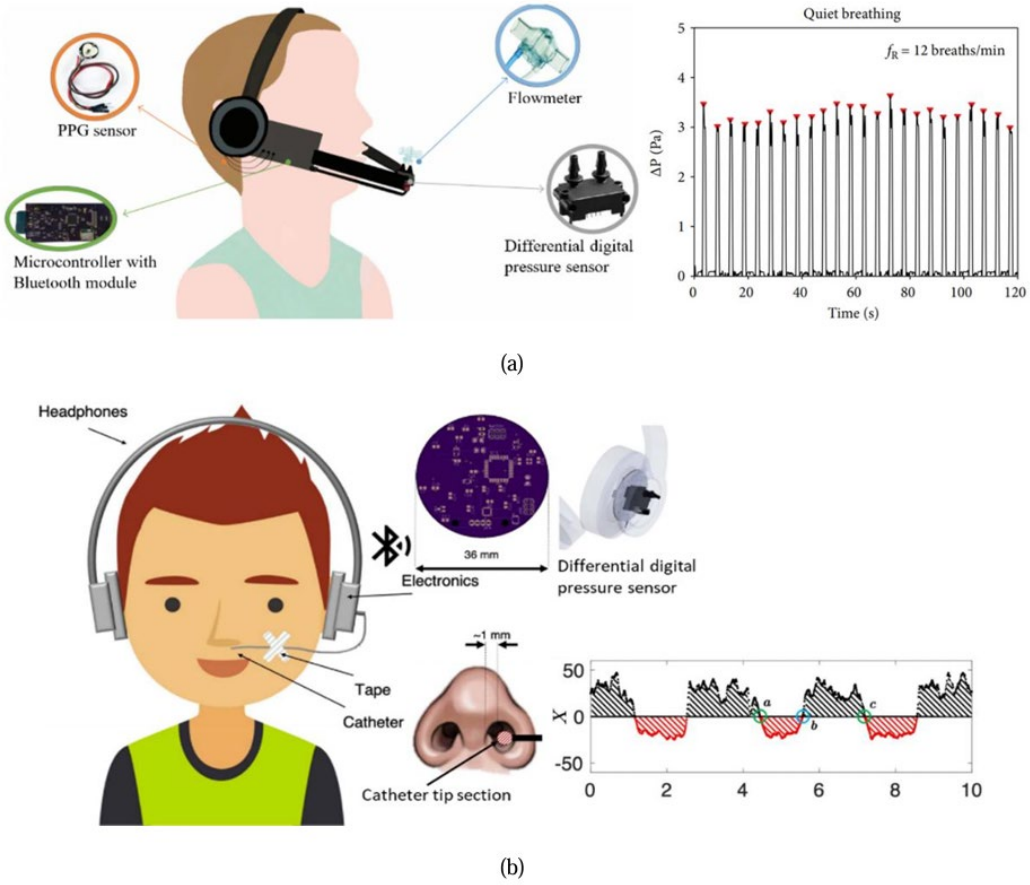

Figure 17 Respiration measurement technologies based on air flow velocity monitoring: (a) Sketch of the differential air flow monitoring device built into the headset and its sensor output signal[36]; (b) Sketch of the respiration monitoring device and the sensor output signal of the headset integrated differential flow meter[38].

In order to improve this problem, Massaroni et al. optimised the above-mentioned device in 2019 with the aim of monitoring airflow through the nose more effectively. Their improvements included removing the microphone stick and commercial flow meter and integrating the differential pressure sensor directly into the headset. In addition, they designed a flexible catheter with a diameter of 0.5cm, which was connected to one end of the sensor, and the other

end was fixed to the edge of the nostril with medical tape[38]. In the experiment, a total of 10 volunteers were recruited, and the newly designed sensor was tested for 10 to 15 minutes of cycling and compared with a commercial respirometer (used as a reference system). The research team evaluated the differences between the new monitoring system and a reference system using Bland-Altman analysis[39], which quantifies the agreement or difference between two measurement methods by calculating the deviation between them. The analysis results showed that when the recorded breathing data was calculated at 30-second intervals, the average deviation of the 10 volunteers was -0.03±1.60 BPM[38]. When the data was calculated at single breath intervals, the deviation was -0.06±6.27 BPM[38]. This research result shows that although the newly designed device can effectively capture the respiratory signal, there is a certain synchronization error between the start and end points of its signal and the reference system when analysing a single breath. This error may be due to limitations in the sensor's location, which prevents the sensor from responding quickly to exhaled airflow. However, this synchronization issue has relatively little impact on overall respiratory rate measurements. Therefore, although there are certain limitations in accurate monitoring of single breaths, the device still shows good performance in long-term or continuous respiratory frequency monitoring.

2.4.3 Airflow temperature sensing-based techniques

For air flow detection, in addition to using differential flow meters and turbine flow meters, hot film/hot wire flow sensors can also be utilized. This type of flow sensor can be designed to be flat to reduce the volume of the device. Hot-wire/film flow sensors use hot-wire/film resistors as their sensing front ends. The resistor is firstly heated to a constant temperature by the current flowing through it[40]. In this state, since the Joule heat generated by the resistor is in equilibrium with the heat transferred to the environment[41], if the heat transfer process between the resistor and the environment is not affected, the resistance of the hot wire/film resistor will stay in constant. When the airflow velocity at the surface of the resistor increases, the resistor will be cooled and cause its resistance value to change non-linearly[42]. Therefore, there is a non-linear relationship between the resistance value of the hot wire resistor and the air flowrate at its surface[6].

In 2015, Jiang et al. proposed a flexible wireless hot-film anemometer. The sensor uses a platinum film with a temperature coefficient of resistance (TCR) $38 \times 10^{-4}\ °C^{-1}$, which works at 23°C, as a thermal film resistor[41]. A Wheatstone bridge is used to measure the change in resistance of the hot film. A Bluetooth module is used to record the output of the Wheatstone

bridge. The entire system is powered by a 5mm thick button battery. All components are integrated into a flexible substrate with a length of 100mm and a width of 25mm to make the complete system flexible[41].

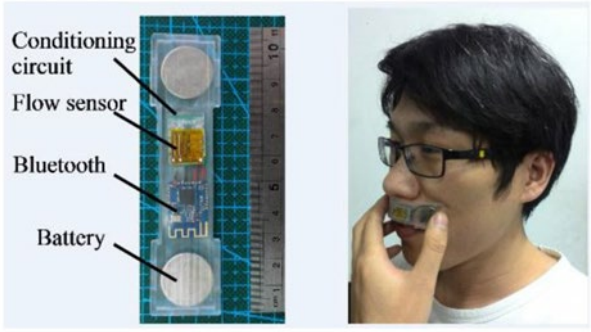

Figure 18 The platinum-based flexible hot film flow sensor proposed by Jiang et al. and its state of being deployed on the upper part of the lips[41].

At present, the author has tested the performance of the sensor using the 14L/min airflow generated by air pump. According to the experimental results presented by the author, the air flow measured by the proposed sensor is almost the same as the air flow set by the air pump within 2 minutes. Since the flowrate for nasal breathing is also about 14L/min. Therefore, it can be considered that the sensor has the ability to accurately measure respiration. In 2020, in order to further improve the sensitivity of the sensor, Jiang et al. replaced platinum with aluminium with a higher TCR ($43 \times 10^{-4}\ °C^{-1}$) and lower working temperature, which reduce the power consumption of the system[43].

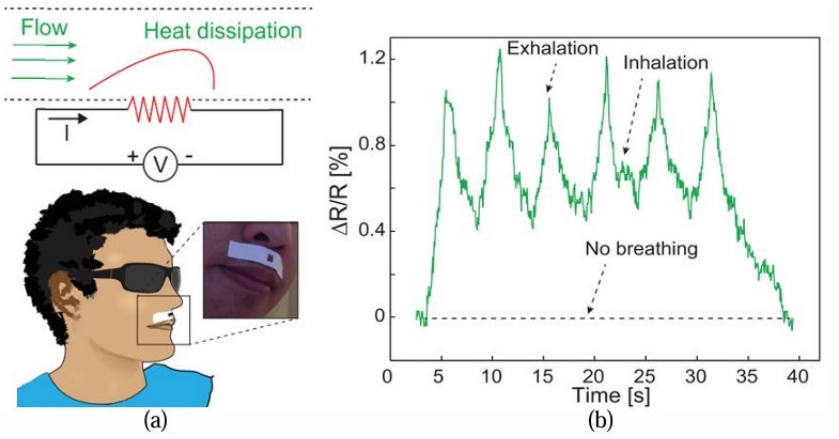

Figure 19 (a) The graphite-based flexible hot film flow sensor proposed by Dinh et al. and its state of being deployed on the upper part of the lips. (b) The respiratory signal measured by GOP-based hot-film anemometer[44].

In addition to hot film resistors based on metal materials, graphite with TCR $-5.6 \times 10^{-4}\ °C^{-1}$ can also be used as a hot film resistor to measure airflow. In 2017, Dinh et al. graphite-based

hot film anemometer, as shown in Figure 16. The sensing front end of the system is a rectangular graphite pattern drawn on paper. Compared with the research of Jiang et al., the deposition of graphite does not require the use of thin film deposition technology and a clean room-level production environment, which means the fabrication cost for the sensor is low[44]. In addition, graphite is a degradable material and therefore has the potential as a disposable sensor[44]. However, its lower TCR makes the sensitivity of graphite-based hot film sensors unstable during long-term measurement[44]. Therefore, the further research is still required for improve the stability of the material.

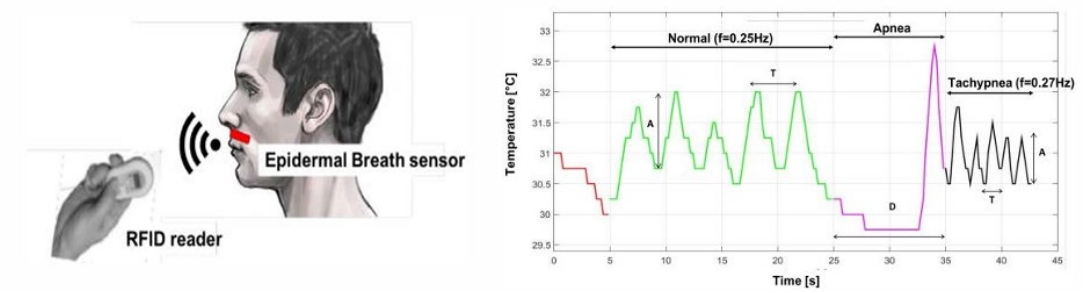

Figure 20 Battery-less RFID epidermal temperature sensor mounted on the upper or lower lips for breath monitoring[45].

In addition to thermistors, some researchers also use commercial temperature sensors for respiratory monitoring. For example, in 2018 Occhiuzzi et al. developed a respiration sensor based on a commercial RFID chip (EM4325 IC). This design takes advantage of the chip's battery-less operating mode and the integrated on-chip temperature sensor (measurement range -40°C to +64°C with ±0.25°C resolution). The sensor is placed on the upper or lower lip to monitor temperature changes in areas near the nose and mouth caused by respiratory airflow. In tests carried out on 20 volunteers, the average temperature changed by about 1.5°C, from 32°C when exhaling to 30.5°C when inhaling. The study also demonstrated the RFID system's ability to identify apnea events. However, the accuracy of this device has not been verified as it was not compared to a reference system.

2.4.4 Airflow humidity sensing-based techniques

Since the exhaled air contains water vapor, the environmental humidity in the mouth and nose area will suddenly rise during exhaling phase. Therefore, the humidity sensor can be used to measure the humidity near the human nose to obtain the respiratory signal. For miniaturized humidity sensors, the common structure is an interdigital capacitor structure. By placing some hygroscopic materials between the interdigital electrodes, when the environmental humidity

rises, the material absorbs the water vapor in the environment to change its dielectric constant and conductivity, resulting in a change in capacitance.

In 2016, Güder et al. used cellulose paper as a moisture-absorbing material. For reducing the cost, the author printed graphite electrodes directly on the surface of the paper. In order to reliably measure the humidity change, the sensor is integrated into the mask. As shown in Figure 17, the capacitance of the sensor is mainly determined by the conductivity of the cellulose paper. When the paper absorbs the exhaled moisture, the fibres of the material are wrapped in water to increase the conductivity[46]. When the dry air flow through the surface of the paper, the water on the fibres will leaves immediately, resulting in a decrease in electrical conductivity[46]. Due to the materials used for fabrication is very common, this sensor has a very low cost (paper chip is 0.005 US dollars, mask is 1.5 US dollars)[46]. One obvious disadvantage is that this sensor is not durable. Due to the limited mechanical strength of the paper itself, this device is more suitable for use as a disposable sensor. For the same interdigital electrode structure, other researchers have used leather with higher mechanical strength as the moisture-absorbing material of the sensor[47].

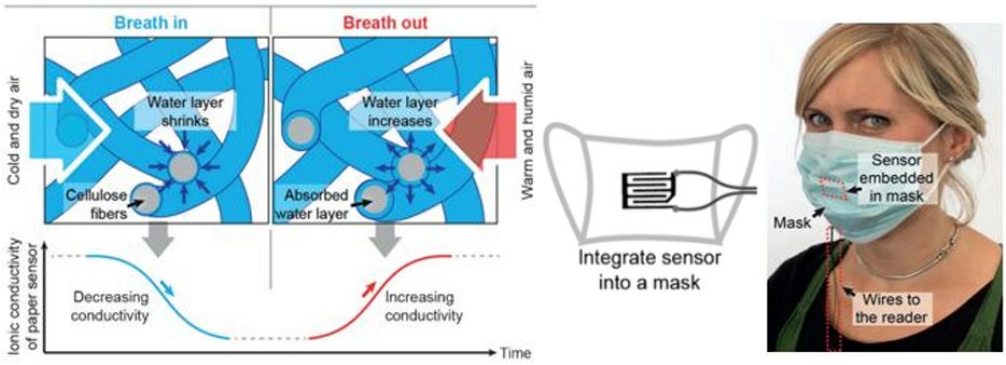

Figure 21 Paper-based humidity sensor for exhaled air measurement[46].

In 2019, Xie et al. proposed a humidity sensor based on silver nanowires and leather materials. The grain leather is used as the moisture absorption material and the substrate of the sensor, and the interdigital electrodes formed by nano silver wires are directly fabricated on the surface of leather as shown in Figure 18[47]. And the working principle is the similar with the sensor based on paper and graphite.

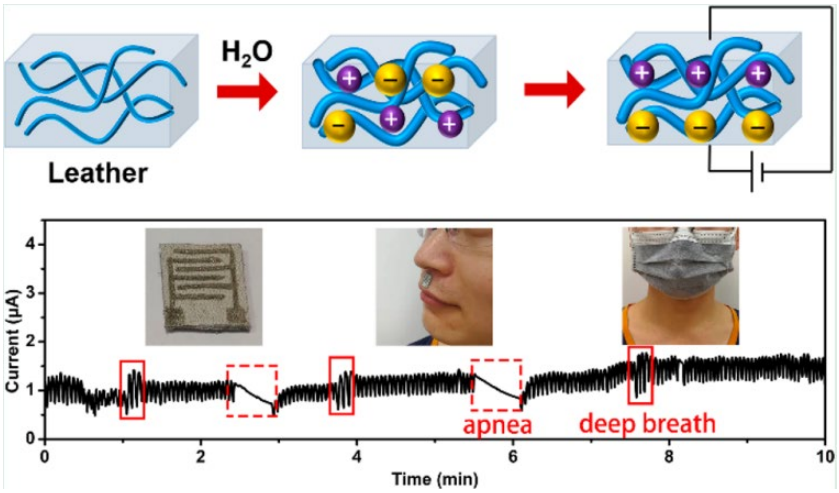

Figure 22 Mechanism of leather-based humidity sensor and a facemask with embedded leather-based sensor[47].

In 2017, Caccami et al. proposed a graphene oxide-based humidity respiration sensor design. This design utilizes the hydrophilic properties of graphene oxide (GO) as a humidity sensing material. Graphene oxide is obtained by oxidizing graphene with strong acids. The oxygen groups exposed on its surface give it significant hydrophilicity[48]. In the study, commercial graphene oxide was deposited on the surface of parallel gold electrodes on Si/SiO2 substrates by drop casting and dried at room temperature. Using the sensing port of the AMS SL900A microchip, humidity changes (60 ohms/relative humidity) between two gold electrodes can be measured continuously[49]. Humidity change data near the sensor is wirelessly transmitted to an external RFID reader through a radio frequency identification tag (RFID) antenna to achieve measurement of humidity changes[50]. Due to the low-power nature of RFID, the sensor can operate in battery-less mode when periodically interrogated by an external reader, thereby reducing the overall weight of the sensor and increasing its durability.

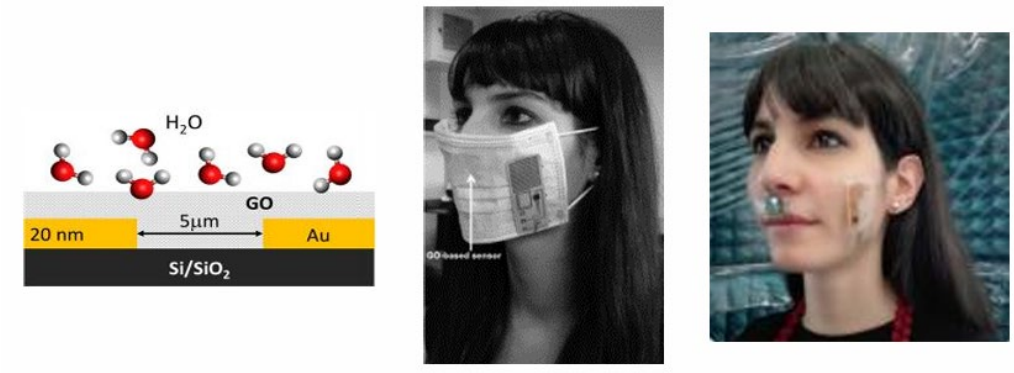

Figure 23 Schematic diagram, prototype d actual deployment of graphene oxide humidity sensor[49][50].

In 2018, Caccami et al. improved the design by fixing the sensor on the FR4 substrate and attaching it directly to the upper part of the lips so that the test subject's breathing was not restricted by the mask. Although the respiration sensor has been tested on ten volunteers under static conditions and proven capable of acquiring valid respiration signals, its systematic errors and reliability have not been fully evaluated due to the lack of a reference system.

2.4.5 Airflow sound sensing-based techniques

In addition to directly detecting the airflow generated by breathing, the envelope of the sound signal generated by the airflow in the trachea has been proved to be in good agreement with the breathing signal recorded by the capnometer[51]. Since the nature of the acoustic signal is mechanical vibration, it is susceptible to interference from environmental noise. In order to extract the respiratory signal from the complex acoustic signal, the signal first needs to be filtered. Specifically, the airflow sound signal with a frequency of 200 Hz to 800 Hz will be filtered and recorded. Then, the breathing signal can be extracted from the recorded breathing sound signal by Hilbert transform.

Figure 24 ACURABLE AcuPebble wireless acoustic based respiration sensor mounted on the neck of a subject[52].

In 2004, Sierra et al. tried to extract the breathing signal from the breathing sound signal for the first time. The author used a piezoelectric film deployed on the throat of the subject to measure the breathing sound[51]. By extracting the envelop of the sound signal, the extracted breathing signal has shown good consistency with the measurement result of pneumotachometer. In addition, performance of the acoustic-based breathing measurement method is not affected by motion artifacts. At present, this kind of sensor has been used for clinical respiratory monitoring, as shown in Figure 19 (a), the main application is with some patients who cannot use or cannot tolerate face-mask respiratory monitoring. A miniaturized device based on acoustic respiration measurement has been proposed by Corbishley et al. in 2008[53]. The main challenge of this

research is the trade-off between the measurement accuracy, device power consumption and device size. Since the acoustic sensor front end is a passive component, it has the advantage of low power consumption compared to other sensors that need to be driven by electricity[53]. In the author's research, a miniature wireless microphone is used as the sensor front end. The respiratory signal can be obtained through filtering and envelope detection. Recently, commercial products based on this device have been clinically verified to be used for sleep breathing monitoring[54].

2.5 Discussion

The working principle of projected capacitive sensors is based on detecting the electrical properties of materials within the range of an electric field. Capacitance is typically measured with an impedance analyser, but active shielding often requires resonance-based measurement methods. Early studies, such as this 2011 work, mainly used large-size electrodes to monitor changes in the electrical properties of the lungs during breathing. However, in recent years, as sensor sizes have decreased, research has begun to hypothesize that respiratory signals may originate from deformation of the skin during breathing. In fact, the skin in the trunk area does deform when breathing, and this phenomenon has been verified by optical sensors, but rigorous experimental verification for projected capacitive sensors has not yet been performed. In addition, in the process of obtaining respiratory signals by measuring skin deformation with miniaturized projected capacitive sensors, the impact of the driving frequency and size of the electrodes on improving the sensitivity of respiratory measurement has not been fully studied. These studies are necessary in order to better understand this theory and design miniaturized projected capacitive respiration sensors with higher sensitivity.

In addition, the study also covers the review and analysis of other respiration measurement techniques. According to the literature review on wearable respiration sensors, it is obvious that the current trend is to miniaturize the sensor and improve its wearability. For example, the hot-film flow meter that measures the airflow of the nose and the humidity sensor integrated inside face mask that measures the humidity of the airflow of the nose. The size, fabrication cost and wearability of these two types of innovative respiration sensors are obviously better than pneumotachometer, which is known as the gold standard. For the strain sensing, compared with the traditional respiratory inductive plethysmography method, the patch sensor that measures the local strain of the ribs and abdomen does not need to surround the chest, so it will not affect the subject's normal breathing. In addition, for an acoustic breathing sensor based on breathing sound detection, although it is susceptible to interference from environmental noise, the way

that measure the breathing from neck position is not available in other breathing detection methods. For some special scenes, such as scenes where the torso and face are not suitable for wearing sensors, neck breathing detection can provide an additional breathing monitoring option.

Table 3 Respiration measurement methods summary

Respiration measurement methods	**Deployment position**	**Working principle**	**Limitations**
Projected capacitive sensing	Chest, abdomen	Thorax impedance	Motion artifact
Strain sensing	Chest, abdomen, ribs	Measuring chest circumference change	Required body contact; Motion artifact
Airflow rate sensing	Nose	Measuring the airflow	Required body contact
Temperature sensing	Nose	Measuring the airflow	Required body contact;
Humidity sensing	Nose	Measuring the airflow humidity	Required facemask
Acoustic sensing	Neck	Measuring the sound of breathing	Required relative quiet environment

Compared with other technologies, projected capacitive sensors have the advantage of being able to be placed in torso areas (such as the chest), which makes them less disruptive to daily life during long-term monitoring. However, this sensor also has several limitations, such as its inherent sensitivity to ambient temperature and humidity, which is mainly due to parasitic parameters in its design. In addition, the current ambiguity about its measurement principle and common motion artifacts are also challenges that need to be solved in its application. If these problems can be overcome, the capacitive sensor's inherent low cost, low power consumption, simple design, and rapid response to environmental changes, coupled with its mature development history, will give it significant advantages in the field of respiratory monitoring.

Chapter 3 Screen-Printed Capaciflector: Development and Testing

The current main research question is which tissue interface movement in the chest area dominates the generation of the respiration signal of the capacitive sensor. According to a literature review, two possible tissue interfaces are the lungs inside the thoracic cavity and the skin outside the thoracic cavity respectively. During normal breathing process, these two kinds of tissue boundaries move at the same time. In order to be able to study their effects on the sensor capacitance separately, two controlled experiments were designed. The detailed experimental setups and corresponding simulation setup are described in the section 3.2 and 3.3 below.

In addition, considering that the sensor ultimately will work as a wearable sensor, the sensor itself needs some flexibility to provide a certain degree of wearability. For this reason, thick film production technology has been used to fabricate the capacitive sensor used in this research, and the specific fabrication process is described in section 3.1. Since flexible capacitive sensor is sensitive to deformation of itself such as bending, thus related experiment has been designed to evaluate the effect of bending on the capacitance of the sensor.

3.1 Screen printed fabrication process

The sensors used in this chapter are fabricated screen-printing technology. This is a type of thick film deposition process that requires the use of a thick film screen and screen printer to implement material deposition. The screen is a finely woven mesh made of stainless steel, polyester or nylon[55]. It is typically fixed on the metal frame under tension and has a printable area with desired pattern[55]. Generally, the screen will be fixed at a position 0.5mm away from the surface of the substrate by a screen printer[55]. Materials such as conductive or dielectric ink are evenly poured on the printable area of the screen surface. Then, the ink passes through the screen under the pressure of the squeegee while the screen is in contact with the substrate so that the ink is deposited on the surface of the substrate in the shape of desired pattern.

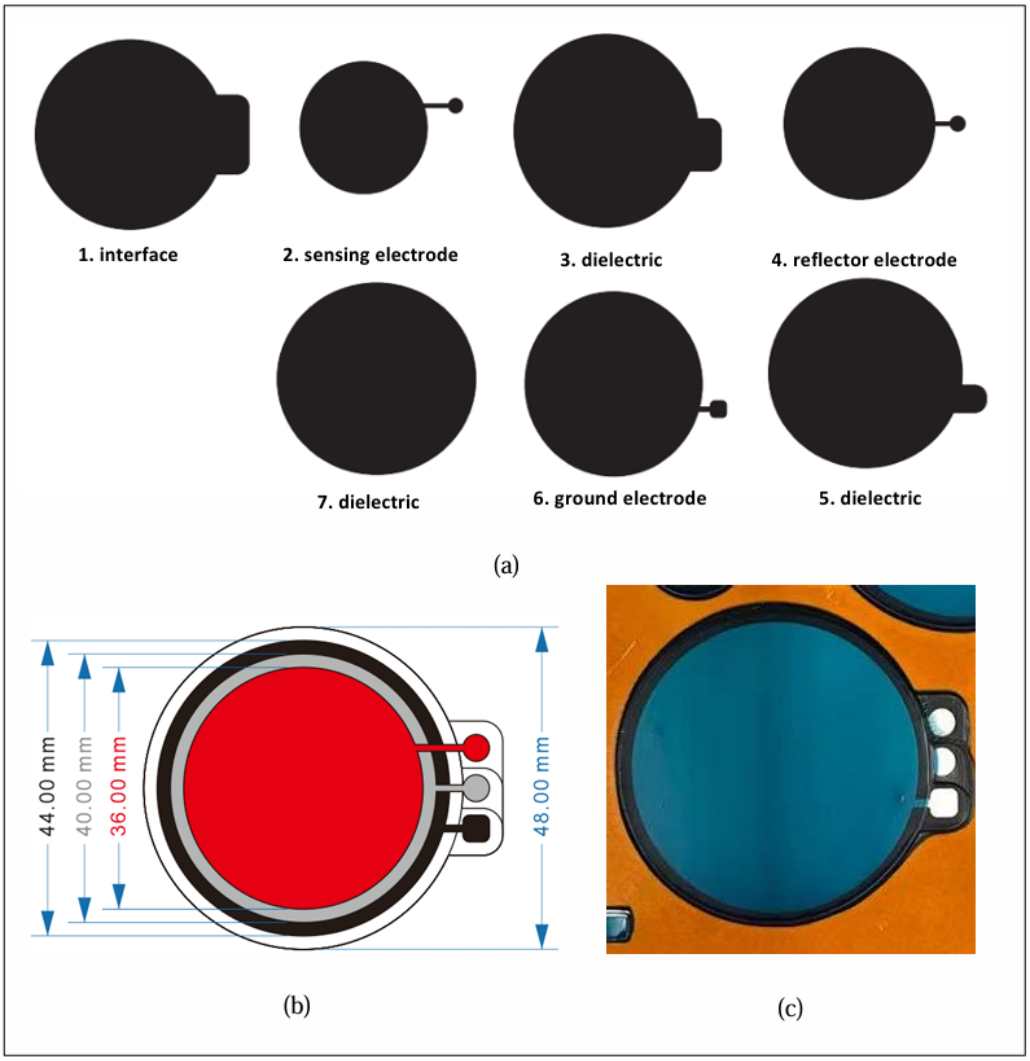

Figure 25 Customized structure of the screen printed capaciflector: (a) shape of the pattern for each layer of the screen; (b) bottom view after 7-layer stacking; (c) printed capaciflector on Kapton substrate.

The fabrication process flow of the sensor used in this research is described in Table 4. Figure 25 shows the patterns of each layer of the screen printing and the printed samples.

Table 4 Fabrication process of screen printed capaciflector

Print order	**Layer**	**Typical diameter (mm)**	**Material**	**Typical number of depositions**	**Curing process after every 2 depositions**
1	Interface	48	UV Curing Flexible Coverlay	4	365nm UV exposure for 30 sec
2	Sensing electrode	36	Silver	2	80°C heating for 30 min
3	Insulation layer	48	UV Curing Flexible Coverlay	4	365nm UV exposure for 30 sec
4	Reflector electrode	40	Silver	2	80°C heating for 30 min
5	Insulation layer	48	UV Curing Flexible Coverlay	4	365nm UV exposure for 30 sec
6	Ground electrode	44	Silver	2	80°C heating for 30 min
7	Insulation layer	48	UV Curing Flexible Coverlay	2	365nm UV exposure for 30 sec

3.2 Capacitance measurement based on impedance analysis

Since the experiment needs to drive the sensor at different working frequency, an impedance analyser (6500B, Wayne Kerr) is used to measure the capacitance of the sensor. Considering that the difference between a capaciflector and a typical capacitor is only an added active shielding, and the main function of the active shielding is to weaken the capacitance between the sensing electrode and the ground. Therefore, the presence or absence of the reflector layer does not change the working principle of the sensor. In addition, since the impedance analyser

cannot provide active shielding, thus all tests in this chapter use parallel plate capacitors composed of sensing electrodes and reflector electrodes where the reflector work as ground.

Impedance analyser can measure the impedance and phase difference between the two electrodes of the sensor, and then calculate the capacitance based on these two measured results and the working frequency. In general, the sensor needs to be connected to the impedance analyser through a test fixture, and in frequency dependent tests, it is necessary to know the support frequency range of the test fixture. The working frequency of the test fixture (Kelvin Clips 1EVA40100, Wayne Kerr) used in this experiment is between 20Hz and 3MHz. Therefore, the highest operating frequency that the sensor can reach in the experiment is 3MHz.

3.2.1 Respiration experiment setup

The respiration experiment mainly studies how the capacitance changes during breathing, and the relationship between the magnitude of the change and the frequency.

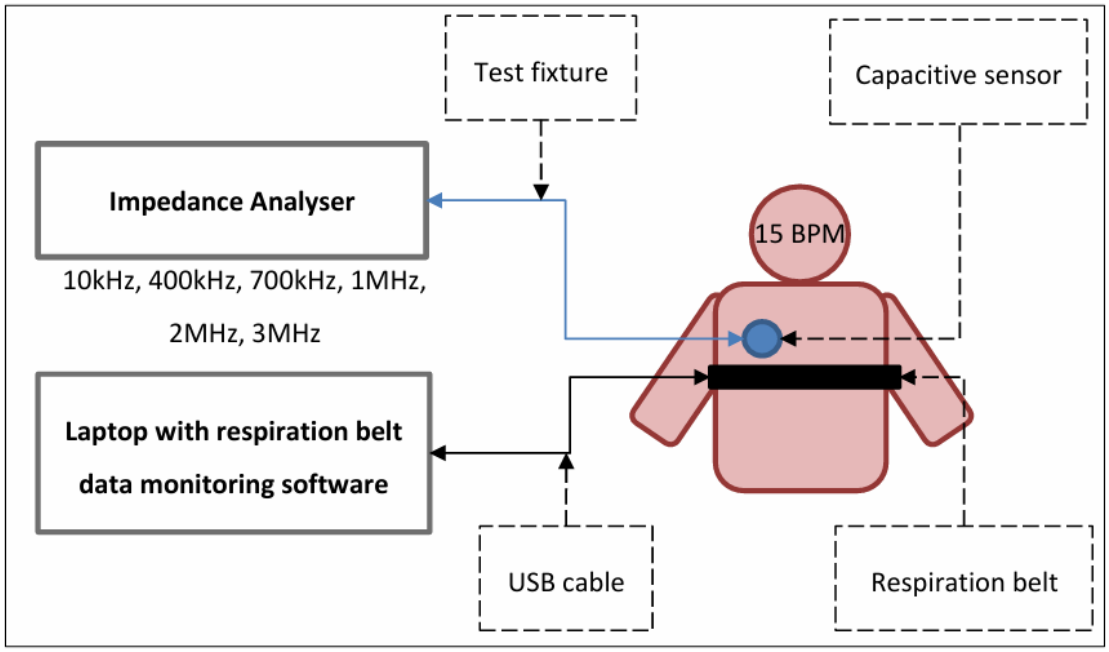

Figure 26 Schematic of respiration experiment setup.

In order to avoid the proximity sensing characteristics of the capacitive sensor, the sensor is attached on the skin surface of the right chest by masking tape to ensure that the distance between the sensor and the skin surface remains constant during the measurement. In addition, because the sensor has a certain level of flexibility, in order to avoid the influence of sensor strain on the capacitance, an insulating plastic disc with the size that similar to the sensor is

tightly attached to the non-sensing side of the sensor to prevent the deformation of sensor during the experiment.

A respiration belt (Go Direct® Respiration Belt, Vernier) is wrapped around the rib cage as a reference system. It can measure the force exerted on the belt caused by the rise of the chest circumference. During the experiment, the breathing of subject was guided by 30 beats per minute. Specifically, the subject inhale when one beat is heard, and when the subject hears the next beat, the exhalation is conducted. By repeating this process, the subject's breathing rate can be stabilized at 15 breaths per minute (BPM). After the test starts, the impedance analyser continuously records the capacitance of the sensor for 1 minute. The experiment has been repeated at 10kHz, 400kHz, 700kHz, 1MHz, 2MHz and 3MHz.

3.2.2 Stretching skin experiment setup

The stretching skin experiment mainly studies how the capacitance changes when skin is stretched, and the relationship between the magnitude of the change and the frequency. The increase in the chest circumference caused by inhalation will stretch the tissues of the outer layer of the chest cavity, which might be the cause of the capacitance change.

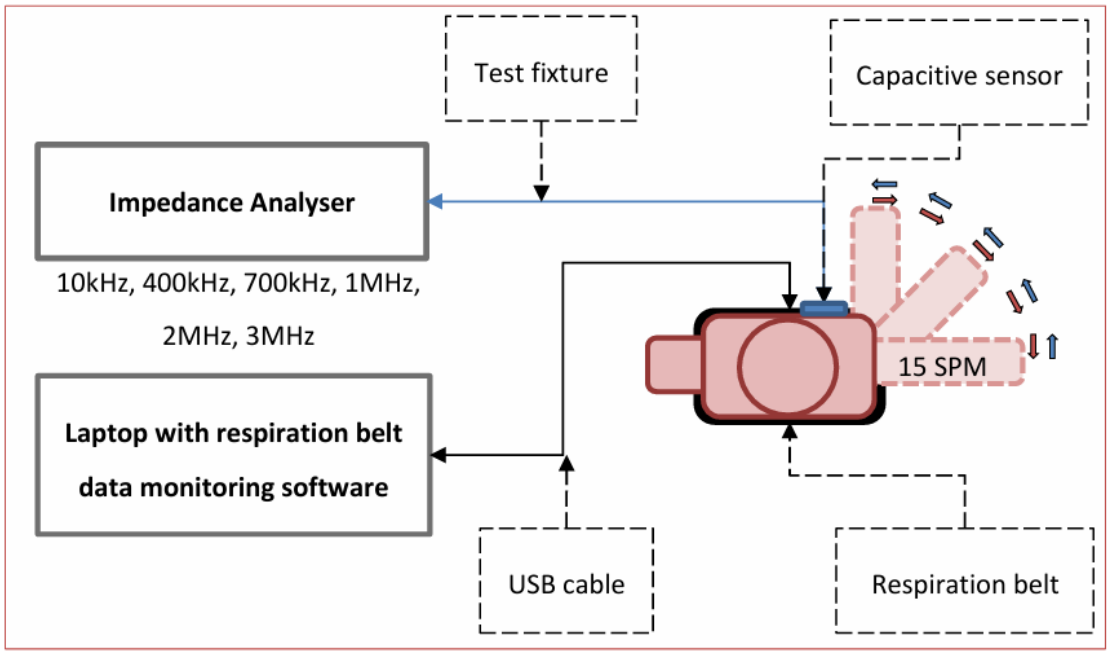

Figure 27 Schematic of stretching skin experiment setup; the right part is the top view of the subject.

In order to study the effect of skin stretching on the capacitance of the sensor independently, the subject was asked to hold his breath to ensure that the chest cavity would not expand or contract throughout the single test. The subject then conducts the right arm horizontal movement under the guidance of 30 BPM metronome, as shown in Figure 27. The chest skin is in a relaxed state when the arm at front, and the skin is stretched when the arm at side. Similar to the respiration experiment, the frequency of the skin being stretched can be stabilized at 15 stretches per minute (SPM). In addition, in order to avoid long-term breath holding, the single test only lasts 15 seconds. More samples require multiple tests to be repeated. Except for the test protocol, the remaining experimental settings are consistent with the breathing experiment. The experiment has also been repeated at 10kHz, 400kHz, 700kHz, 1MHz, 2MHz and 3MHz.

3.3 Finite element analysis for tissue under E-field

The physical phenomena in the real world are normally described by partial differential equations (PDE)[56]. For describing the behaviours of object with complex geometric structure, it is very difficult to solve the analytical solution of the equation[56]. Usually, complex structures are discretized to obtain the equations which approximate to the actual situation. And this kind of equations can be solved using numerical methods[56]. The final result will be similar to the analytical solution of the original partial differential equation that directly describe the actual phenomena[56]. The finite element method (FEM) is used to find approximate solutions of these partial differential equations.

In the finite element method, firstly the continuous geometric model is divided into discrete elements by a mesh. For 2D models, the typical mesh element is triangle. For each node on the mesh, the laws of physics can be applied on the node. Then, the needed physical parameters on the nodes are solved according to the boundary conditions.

Since our research mainly focuses on the interaction between the alternating electric field generated by the capacitive sensor and the human body. Ampere-Maxwell's Law is used to describe the system composed of capacitive sensors and the human body. Since the magnetic effect can basically be ignored, the model can be simplified by electro-quasistatic approximation. The simplified law can be written as:

$$\nabla \cdot (\mathbf{J} + \frac{\partial \mathbf{D}}{\partial t}) = 0 \qquad \text{Equation 3}$$

where:

$\mathbf{J} = \sigma\mathbf{E}$ conductive current density.

$\mathbf{D} = \varepsilon_0\boldsymbol{\varepsilon_r}\mathbf{E}$ displacement current density.

$\mathbf{E} = -\nabla V$ electric field is negative gradient of electric potential.

By reorganizing these equations, Ampere-Maxwell's Law under quasi-static approximation can also be written as:

$$-\nabla \cdot (\sigma\nabla V + \frac{\partial(\varepsilon_0\varepsilon_r\nabla V)}{\partial t}) = 0 \qquad \text{Equation 4}$$

where:

ε_0 permittivity of vacuum (*Dimensionless*).

ε_r relative permittivity of space (*Dimensionless*).

σ conductivity of space (*S/m*).

V electrical potential (*V*).

Equation 4 can be applied on the nodes and used to calculate the spital potential distribution in space based on the electrical conductivity and dielectric distribution in space under given boundary conditions of potential.

3.3.1 Layered body model setup

In order to study the electric field distribution of the capaciflector in different tissue layers, a layered human body model was established using COMSOL Multiphysics software. The model includes skin, fat, muscle and lung tissue, and the dielectric properties of each layer are based on existing bioelectric properties data.

In this study, Electric Current simulation in AC/DC module of COMSOL was used to analyse how the capacitance of the sensor changes during the respiration process. The model geometry is composed of 3 parts including the environment (air, relative permittivity 1), the human body and the sensor. To reduce the time-consumption of the simulation, the geometry of the model is based on 2D axisymmetric structure.

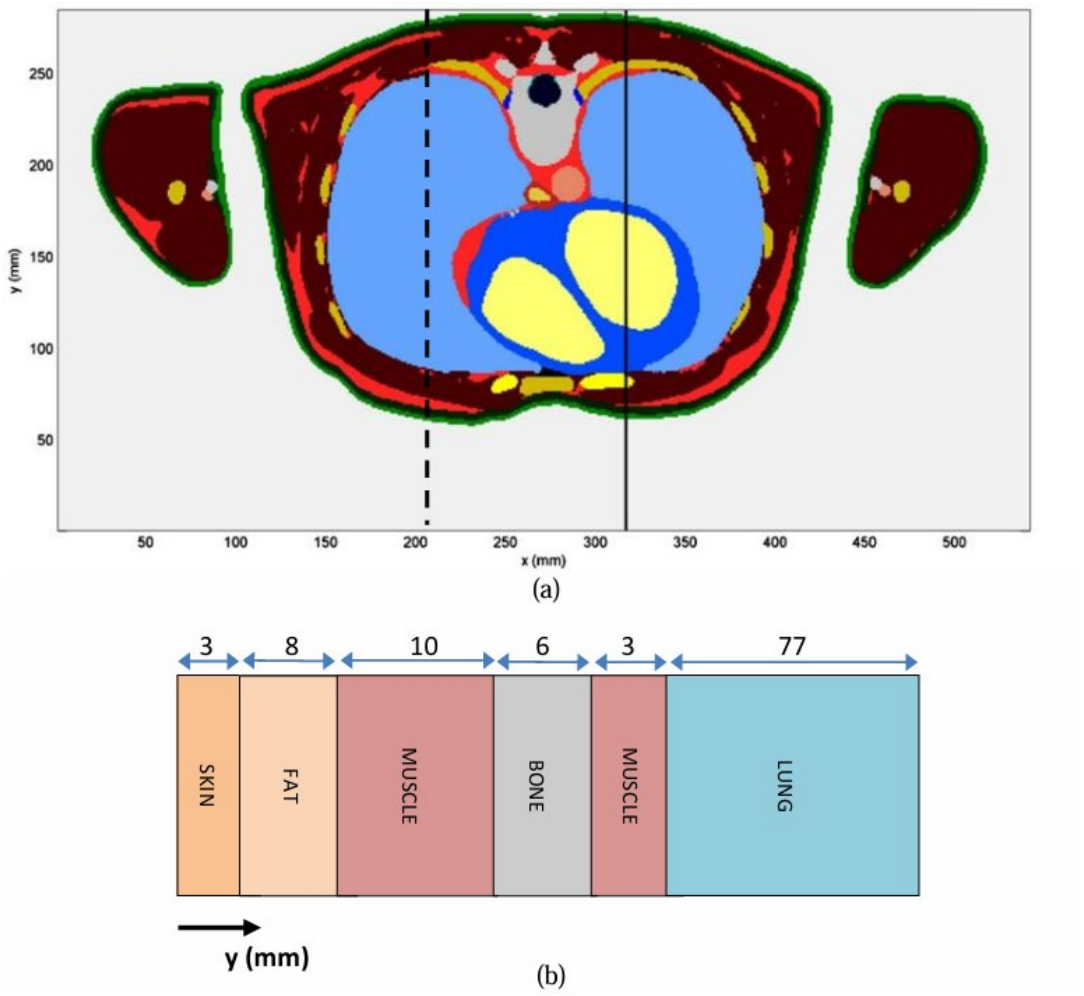

Figure 28 (a) Axial cross-sectional anatomy of the chest area of an adult male. The dash lines provide sequence and thickness information for the multilayer tissue model used in the simulation[24]. (b) The planar multi-layer tissue model.

The multilayer tissue model is used to describe the human body. Since the sensor is relatively small and located on the front side of the chest, only half of the body model is used, as shown in Figure 28. The radius of the environment and the tissue model are set as 80 mm to avoid the fringe field effect in the capacitance simulation[57].

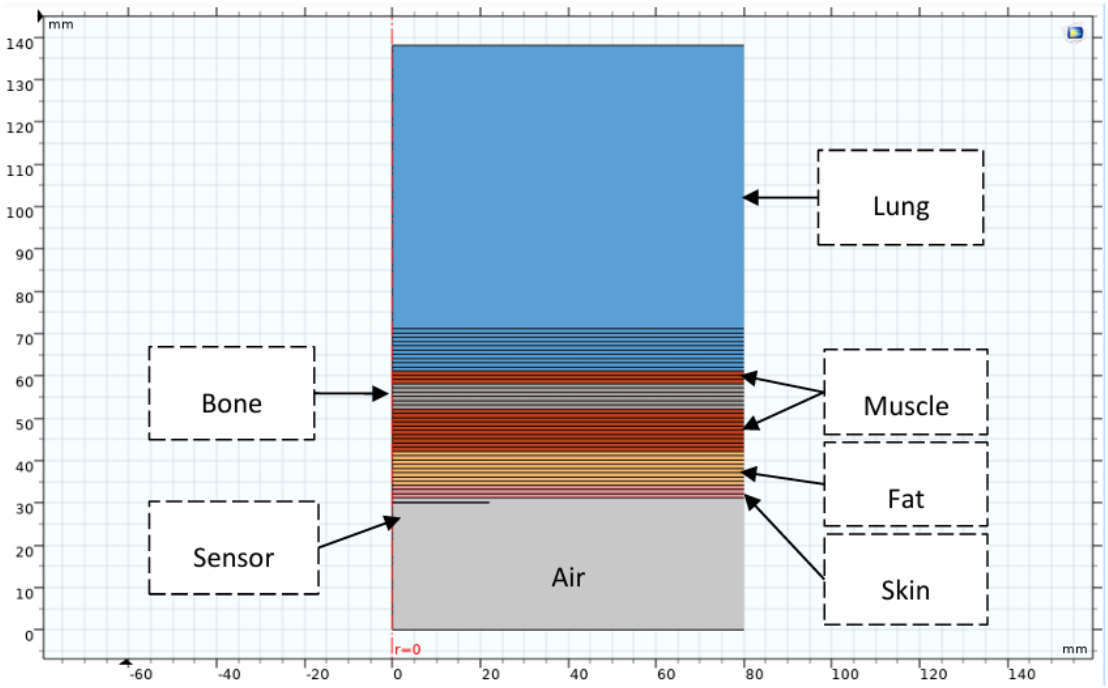

Figure 29 2D Axisymmetric COMSOL Model of multi-layer human tissues.

Since the simulation of breathing is implemented by the changes in the thickness of the skin or fat layer, in order to avoid errors caused by changes in the mesh. Each layer of tissue is layered at 1 mm intervals to avoid mesh changes caused by changes in geometry.

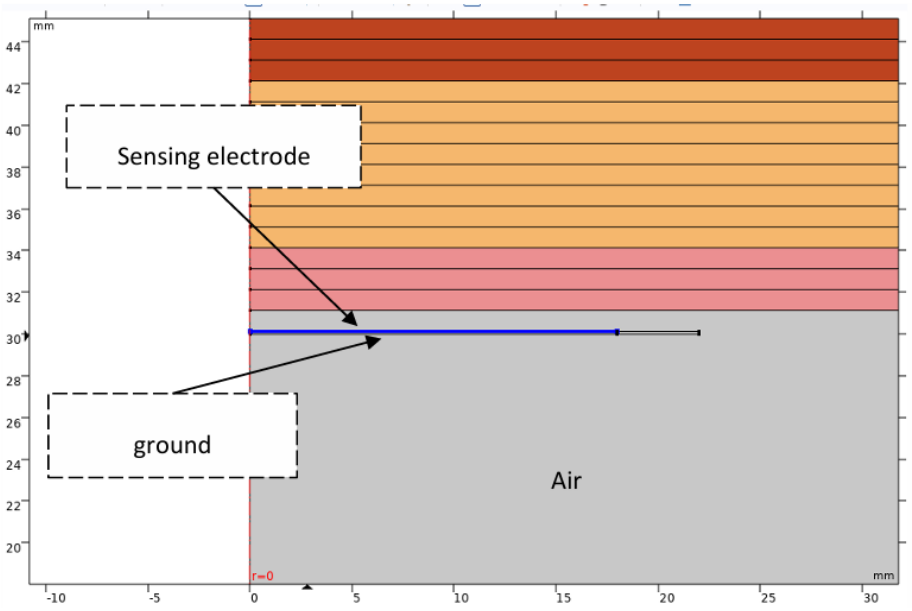

Figure 30 The sensor is located 1 mm below the tissue model.

The sensor is placed 1mm below the tissue model. Since the thickness of the sensor electrode is only about 20 microns, in order to avoid generating an extreme fine mesh, only the geometry of the dielectric (FR-4, relative permittivity 4.5) with thickness 0.13 mm is built. The boundary

conditions of the terminal (1V) and the ground are respectively applied on upper with radius 18 mm and bottom side with radius 20 mm of the dielectric, which work as the electrodes, as shown Figure 30.

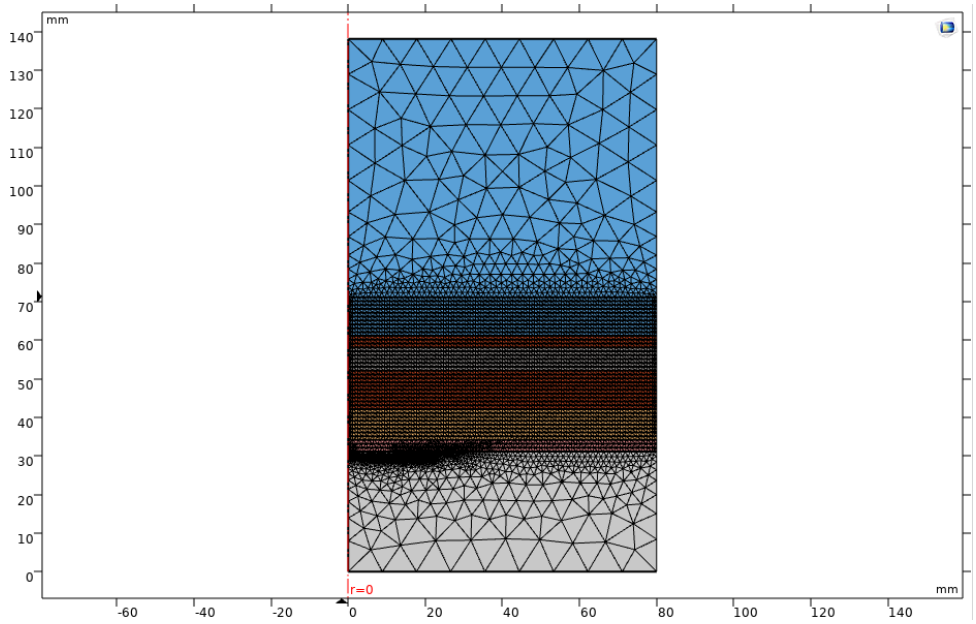

+86Figure 31 Meshing of the simulation geometry

Figure 31 shows that the meshing the model geometry, and the relative permittivity and conductivity of the tissue model material are obtained from[58].

By calculating the admittance between the terminal and the ground, the capacitance can be extracted according to the equation below:

$$Y(\omega) = G + j\omega C;\ C = \frac{Imag(Y(\omega))}{\omega};\quad \text{Equation 5}$$

where:

Y admittance

ω angular frequency of excitation

G conductance

C capacitance.

Since the Young's modulus of the dermis (about 200kPa) is about 4 times that of subcutaneous fat (about 50kPa)[59], this means that the strain of the fat layer is about 4 times of the skin layer under the same stress. Therefore, the inhalation is simulated by the decreasing the thickness of the fat layer. The change in capacitance during inhalation can be obtained by subtracting the

capacitance of the sensor in the exhalation state from the capacitance of the sensor in the inhalation state. Then, the repeated the simulations at 10kHz, 400kHz, 700kHz, 1MHz, 2MHz, 3MHz, 10MHz and 20MHz are conduct to observe the frequency response of the sensor.

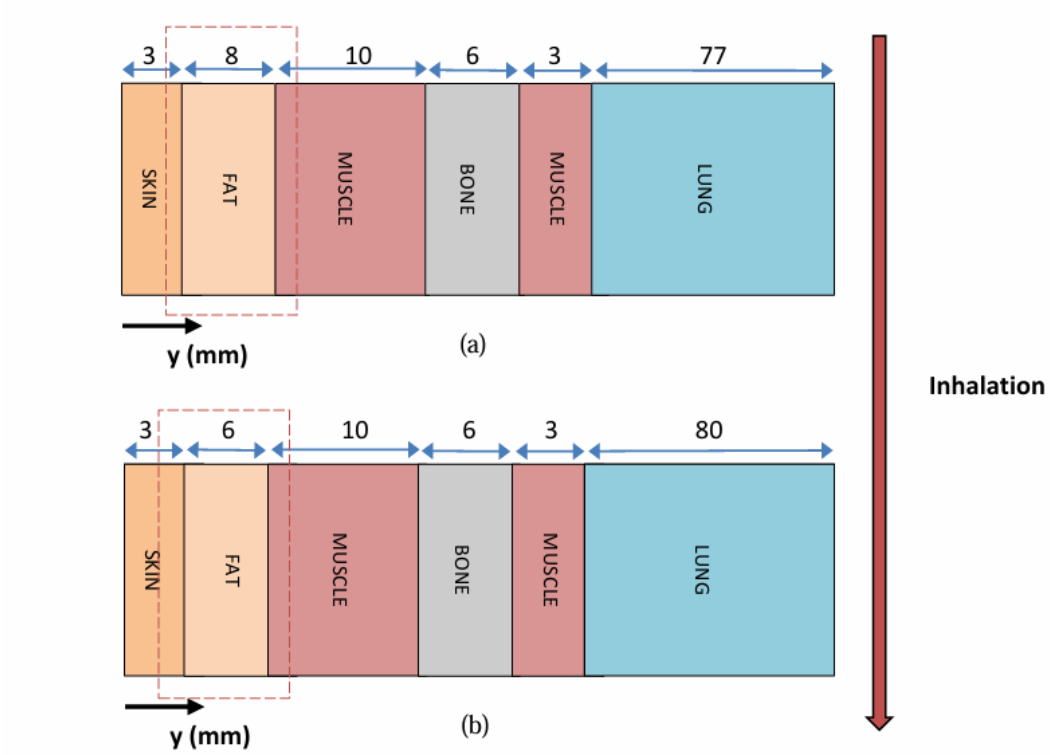

Figure 32 Inhalation process is simulated by reducing the thickness of the fat layer: (a)exhalation (b) inhalation.

Notably, this model includes several significant simplifications. One major simplification is that it does not account for changes in the dielectric constant and conductivity of biological tissues when they deform. The only exception is the lung tissue, where the model considers the decrease in dielectric constant caused by air entering the lungs during inhalation, supported by some experimental data[60]. The dielectric constant and conductivity of biological tissues depend on their composition and structure. Deformation typically alters their electrical properties. Ignoring these changes can lead to inaccuracies in the simulation results. However, since these changes are difficult to quantify, their impact on the simulation can only be assessed through experimental observations and further simulations.

3.4 Result

This section focuses on presenting the results of experimental and simulation studies. The experimental section delves into the complex relationship between the sensor's sensitivity to respiratory activity and its operating frequency. This included an exhaustive analysis of the

sensor's capacitance changes in response to respiration at different frequencies to reveal the effect of frequency on sensor performance. At the same time, how the sensor's sensitivity to skin stretch changes with changes in operating frequency was also studied, which was evaluated through precise measurements of capacitance changes. The simulation results section supplements the experimental observations, provides an in-depth understanding of the factors affecting sensor performance, and helps explain the phenomena observed in the experimental data.

3.4.1 Respiration experiment

Figure 33 shows the first 30 seconds of typical measurement data obtained at a test frequency of 10kHz during a breathing experiment, set to 15 breaths per minute. The frequency of the respiratory signal is approximately 0.25Hz. By using a low-pass filter with a cutoff frequency of 0.72Hz, part of the signal noise is filtered out. The red circle in the figure marks the end point of inhalation determined from the local maximum of the signal, and the blue circle marks the start point of inhalation determined from the local minimum. The capacitance during inhalation increases by approximately 1pF.

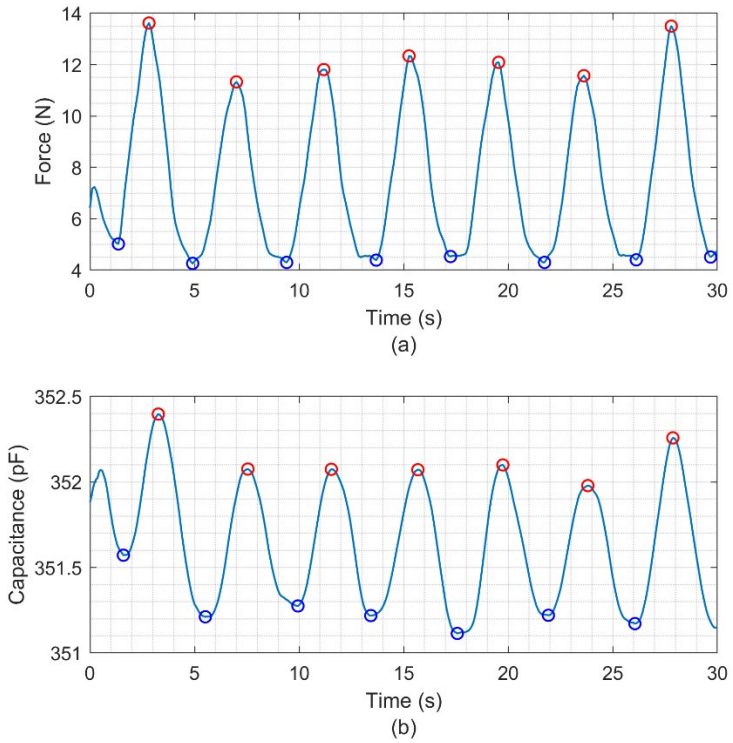

Figure 33 30-second measurement results: (a) Reference breathing signal measured by the respiration belt; (b) Respiration signal recorded by impedance analyser at 10kHz with breathing rate 15 BPM.

The capacitive sensor used in the experiments is configured as a parallel plate capacitor, so it has an intrinsic capacitance of approximately 352pF. In the experiment, the capacitance change is mainly determined by the fringe electric field, so the influence of this inherent capacitance can be ignored. The stretch data in Figure 33 (a) shows the relative intensity of breathing. Respiration-induced force changes and capacitance changes can be quantified by calculating the difference between local maxima and minima, which demonstrates the sensitivity of both sensors to respiratory activity. Statistical analysis is performed on the sensitivity data at all test frequencies and displayed in the form of box plots to more intuitively observe the sensitivity changes of the sensor at different frequencies.

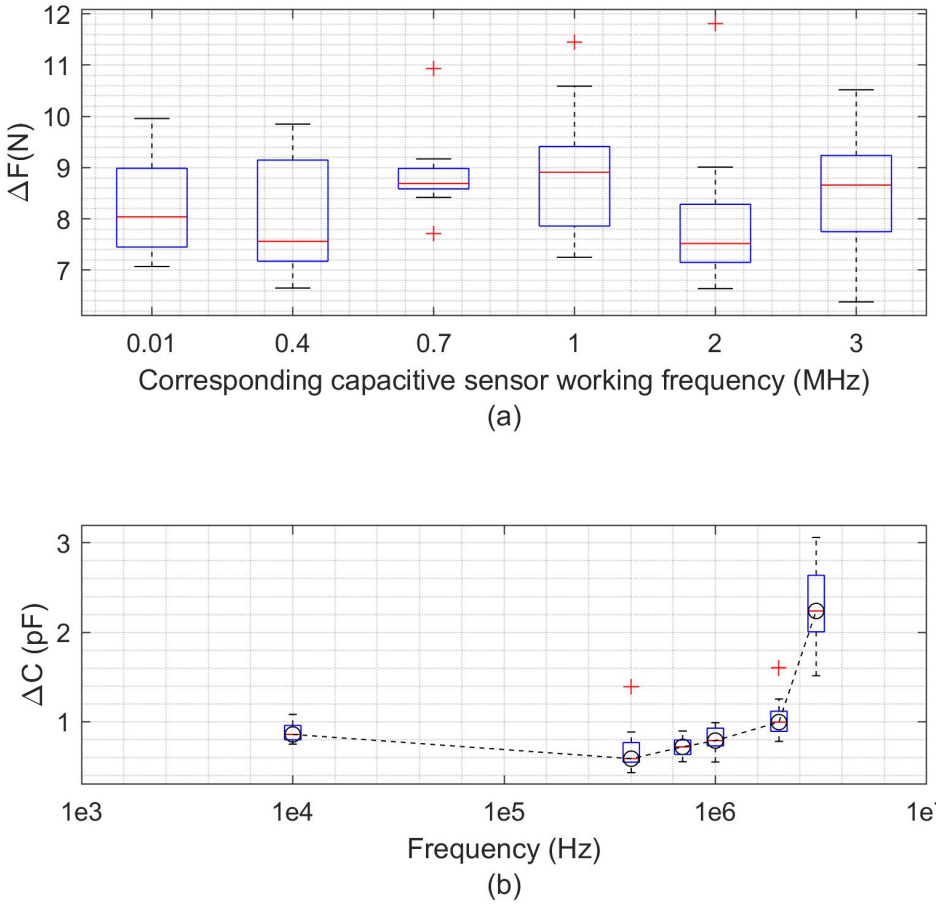

Figure 34 (a) Corresponded force difference data measured by the respiration belt; (b) Frequency response for the difference of capacitance between inspiratory state and expiratory state.

It can be seen from the data that the sensitivity of the capacitive sensor to respiration has slight change in the frequency range below 3MHz. The capacitance change caused by breathing is reduced by approximately 25% in the frequency range from 10kHz to 400kHz. Then in the interval from 400kHz to 2MHz, the capacitance change gradually increases, increasing by approximately 67%. In the frequency range of 2MHz to 3MHz, the sensor's sensitivity is

approximately doubled. These results reflect that there is a certain correlation between the sensor's sensitivity to capacitance changes caused by breathing and the operating frequency.

Although breathing intensity varied slightly when tested at different frequencies, these changes were around ±1% in terms of median differences. A current limitation is that the linear relationship between stretch and capacitive sensors in respiration measurements has not yet been established, so the results of the stretch sensor cannot yet be used to compensate for the results of the capacitive sensor. However, given that these differences are not particularly large, this issue can be ignored for the time being.

3.4.2 Stretching skin experiment

Figure 35 below shows typical measurement data obtained during a skin stretch experiment at a 10kHz setting. In the experiment, the frequency was set to 15 times of skin stretching per minute, and the corresponding stretching signal frequency was approximately 0.25Hz. In order to remove part of the signal noise, a low-pass filter with a cutoff frequency of 0.72Hz was applied. The red circle in the figure marks the end point of the stretching action determined by the local maximum of the signal, while the blue circle marks the local minimum, which is the starting point of the stretching action. In independent skin stretching experiments, a capacitance change of approximately 0.7 pF was observed.

It should be noted that although the tension sensor is mainly used to measure breathing rather than local deformation of the skin, the movement of the arm causing the chest skin to stretch also involves the movement of the rib area. Therefore, the respiration belt sensor wrapped around the rib area can also detect the relevant signal changes.

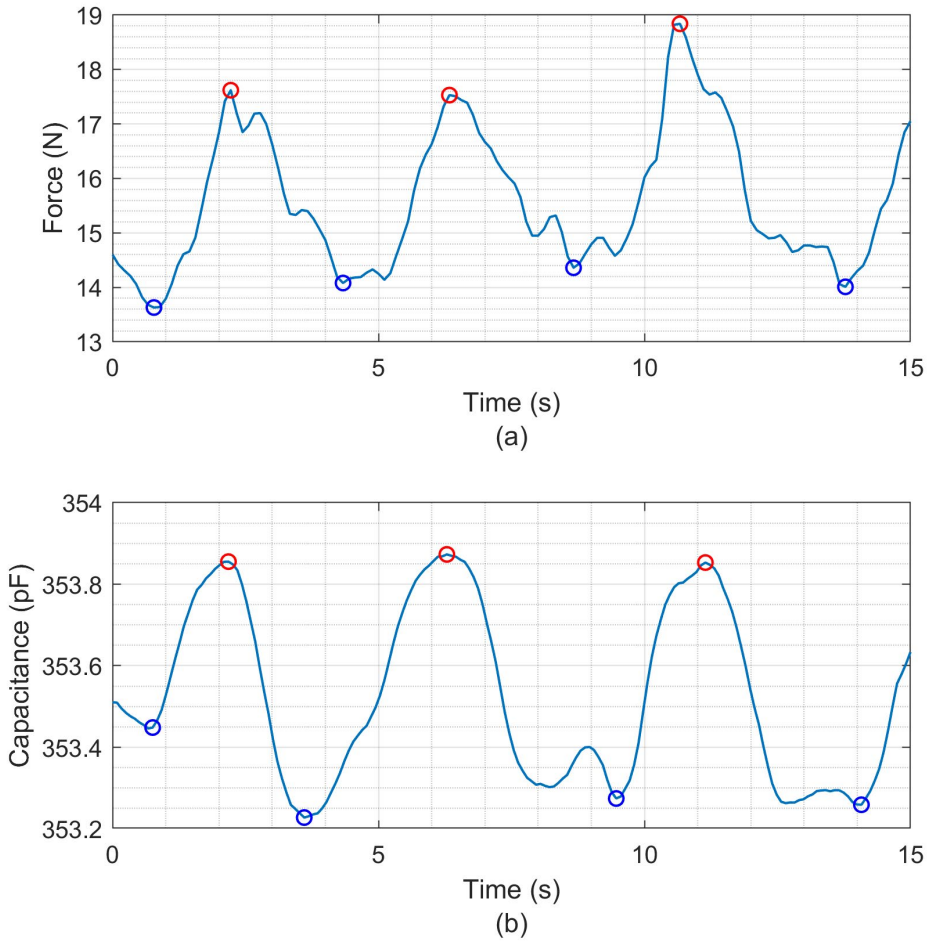

Figure 35 15-second measurement: (a) Corresponded reference stretching skin signal measured by the respiration belt; (b) Stretching skin signal recorded by impedance analyser at 10kHz with frequency of 15 stretch per minute.

Similar to the analysis method for breathing experiments, capacitance changes caused by skin stretching can be quantified by calculating the difference between local maxima and minima of the signal. This data analysis process reflects the sensitivity of both sensors to skin stretch. In order to evaluate the performance of the sensor more comprehensively, the sensitivity data at all test frequencies were statistically analysed and the results were presented in the form of box plots. Such statistical analysis helps reveal the changing trends and differences in the sensor's response to skin stretch under different testing frequencies.

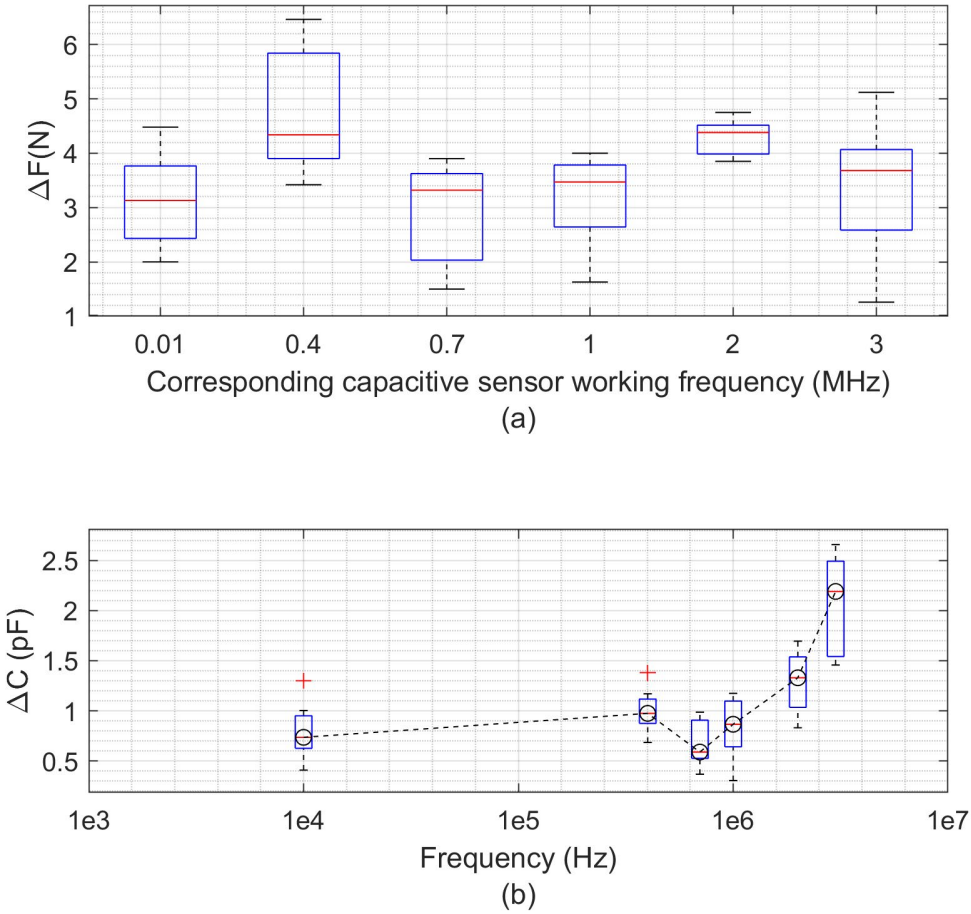

Figure 36 (a) Corresponded force difference data measured by the respiration belt; (b) Frequency response for the difference of capacitance between skin stretched state and skin relaxed state.

It can be seen from the data that the sensitivity of the capacitive sensor to breathing shows a certain degree of change in the frequency range below 3MHz. Between 10kHz and 400kHz, the capacitance changes show an increase of about 5% with breathing. Then, in the frequency range from 400kHz to 700kHz, the sensitivity gradually decreased by about 35%. In the frequency range from 700kHz to 3MHz, the sensitivity increases significantly, by about 4 times. The increase in capacitance change at 400kHz may be related to the increase in stretch amplitude, suggesting that there may be differences in the sensor response to skin stretch at different frequencies.

3.4.3 Simulation

The COMSOL simulation results, as shown in the Figure 37, display the spatial electric potential distribution across different layers at a frequency of 3 MHz.

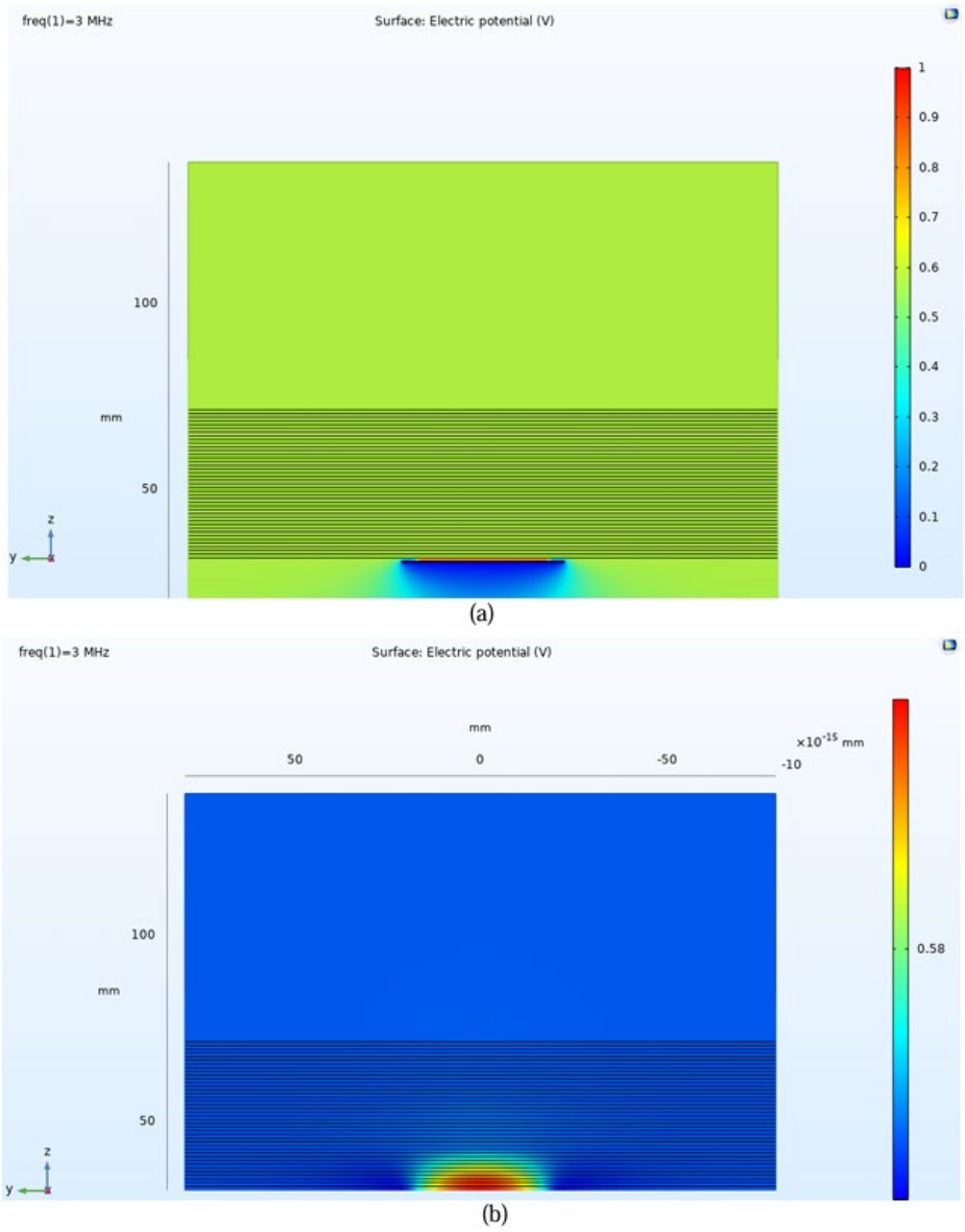

Figure 37 The computed spatial potential distribution: (a) the entire model; (b) inside the human tissue model.

The colours in the Figure 37 represent the magnitude of the electric potential. It can be observed that the electric potential is primarily concentrated within 8 mm from the bottom of the tissue model, which mainly includes the skin and fat layers. The potential significantly diminishes in deeper layers such as muscle and lung tissue.

This result indicates that changes in the dielectric constant of the skin layer have a greater impact on the capaciflector. Although the simplified model could not replicate the exact magnitude of the capacitance changes observed in the experiments, the spatial potential distribution map reveals the distribution characteristics of the electric field in the skin layer and

deeper tissues. Specifically, the electric potential is higher in the skin layer compared to the deeper tissues, suggesting that variations in the dielectric constant of the skin layer are more likely to cause changes in the sensor's capacitance.

Table 5 shows the capacitance at different test frequencies of a model similar to the capacitive sensor structure used in the experiment calculated through simulation. Actual sensor capacitance values may deviate from theoretical expectations due to small differences in electrode spacing during manufacturing.

Table 5 COMSOL simulation result

Frequency (MHz)	**Exhalation state capacitance (pF)**	**Inhalation state capacitance (pF)**
0.01	318.91910267671	318.919110144894
0.4	318.918081857029	318.918148619301
0.7	318.917447942052	318.917535008137
1	318.916732298699	318.916838062974
2	318.913749105156	318.91390627073
3	318.909837157015	318.910036563539
10	318.868292357922	318.868792271514
20	318.816179874335	318.817102069224

By calculating the difference between the capacitance value in the inhalation state and the capacitance value in the exhalation state, the capacitance change caused by breathing activity in the simulation can be determined. These capacitance changes as a function of test frequency are shown in Figure 38. The graph depicts the trend of capacitance changes at different frequencies, providing an intuitive understanding of the performance changes of capacitive sensors when capturing respiratory activity. These data reflect the sensitivity of the sensor to capacitance changes caused by breathing and are helpful for analysing and comparing the response characteristics of the sensor at different frequencies.

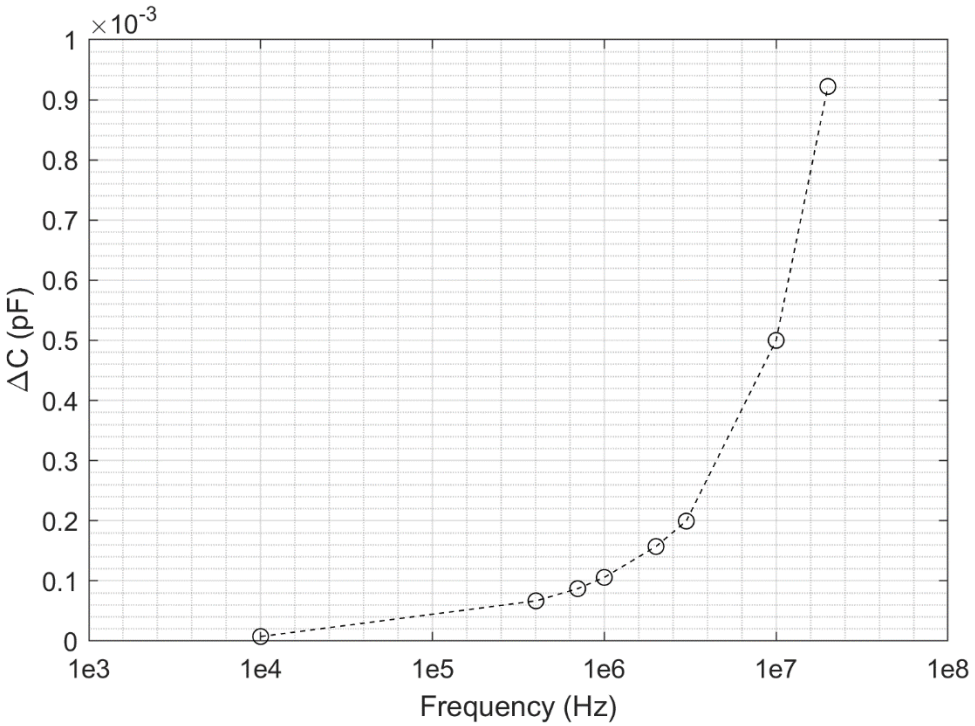

Figure 38 Simulation of frequency response for the difference of capacitance between inspiratory state and expiratory state.

Overall, the simulation results show that as the sensor excitation frequency increases, its sensitivity to capacitance changes caused by breathing shows an increasing trend. This is somewhat different from the results of actual experiments. In addition, the magnitude of the capacitance change is also different. In the simulation results, within the test frequency range from 10kHz to 3MHz, the magnitude of the capacitance change is approximately 0.1fF. In actual experiments, the corresponding capacitance change is about 1pF. This difference may be due to oversimplification of the simulation model.

3.5 Discussion

3.5.1 Experiment

The study found that both inhalation and independent skin stretching will cause the capacitance of the sensor to increase, and the change range is roughly around 1pF. Generally speaking, frequencies at the MHz level can achieve higher sensor sensitivity to breathing and skin stretching than frequencies at the kHz level. This phenomenon may be consistent with the common idea that increasing the frequency of an electric field can increase its penetration depth

into human tissue, thereby making changes caused by the dielectric properties of the tissue in the body more easily detected.

However, there is still a certain potential error in the entire measurement system. First, the 3MHz frequency is close to the upper frequency limit of the test cable, which may cause some unexpected effects, such as resonance, which in turn leads to an increase in additional capacitance values. In addition, the length of the test cable is about 1 meter. The rise and fall of the chest during breathing and skin stretching will inevitably cause the test cable to move slightly, which may also have a certain impact on the capacitance value. Standard capacitance measurements often require avoiding test cable or fixture movement that could interfere with the measurement. To achieve more accurate and reliable measurements, future work requires the design of a more compact system that minimizes the distance between the sensing electrodes and the capacitance measurement equipment to eliminate the influence of parasitic parameters in the test cable on the experimental results.

3.5.2 Simulation

The main purpose of the COMSOL simulation is to analyse the distribution of the capaciflector's electric field in the human body and whether the change in sensor capacitance is caused by the change in thickness of different layers of tissue. In theory, the simplified layered model helps to observe the electric field distribution, but ignores the effect of biological material deformation on electrical properties, which may be one of the reasons for the difference between the simulation results and experimental data.

In simulation studies, the capacitance detected by the sensor increased as the subcutaneous fat layer became thinner. This phenomenon is mainly due to changes in material composition within the detection range of the sensor. The fat layer, which has a lower relative permittivity, is reduced by approximately 25%, while the muscle layer (which has a higher relative permittivity) becomes closer relative to the sensor, causing an increase in capacitance. Since the effective dielectric constant of a composite material is related to the ratio of its component materials, the combination of a decrease in material with a lower dielectric constant and an increase in material with a higher dielectric constant within the detection range of the sensor results in an increase in capacitance. The monotonic increase in capacitance change with frequency reflects the decrease in the effective dielectric constant with frequency, which weakens the dielectric obstruction of the sensor's detection of the electric field.

Compared with the actual experimental results, the magnitude of the capacitance change in the simulation results is significantly different, indicating that the current simulation model cannot

fully simulate the changes in dielectric constant and conductivity of human tissue under dynamic conditions. This may be related to oversimplification of the model. The relative dielectric constant of various human tissues is closely related to their composition and structure. At present, it seems that to accurately simulate the impact of human tissue deformation on its dielectric constant, a more detailed model is needed to simulate the structural changes of tissue under stress.

Despite the limitations of the model, the simulation results still provide a reference for the subsequent experimental design. For the results of the electric field distribution under static simulation, it can be observed that the electric field generated by the sensor is higher in the shallow tissue, which means that under the same electrical property changes, the changes in the shallow material are easier to detect than the deep tissue. The sensor design in the subsequent experiments can be based on the capacitive sensor structure of non-destructive material detection. Then design the experiment and analyse whether the sensor can obtain the respiratory signal only by detecting the deformation of the shallow tissue.

For the optimisation of the COMSOL model in the future, it may be necessary to use a hybrid physical field simulation of mechanics and electricity to simulate the effect of changes in tissue structure under dynamic conditions on its electrical properties. This will include more complex tissue structure simulations and consider the anisotropy of material deformation and its electrical properties. Through these improvements, it is expected to more accurately predict the relationship between the deformation of biomaterials and their electrical properties, and provide a theoretical basis for the verification of the measurement principle of capacitive respiratory sensors attached to the chest skin.

3.5.3 Screen-printed capaciflector

In terms of the physical properties of the capacitive sensor, the design of the capacitive sensor manufactured by screen printing technology needs to ensure that there is no short circuit between different layers of electrodes. Therefore, multiple depositions of dielectric materials are performed between the electrode layers to achieve a certain interlayer thickness. The sensor exhibits the characteristics of a rigid device to a certain extent, although it retains a certain degree of bending flexibility. In addition, due to limitations in material properties, the sensor is prone to breakage during installation, which affects its durability. Such limitations in physical properties may introduce additional variables in repeated experiments, affecting the stability and reproducibility of the experiments. In order to reduce the impact of sensor material on experimental results, future research plans to conduct experiments using capacitive sensors manufactured with standard printed circuit boards (PCBs). This approach is expected to

improve sensor durability and reliability while reducing experimental bias due to sensor material properties.

Additionally, measurement data across multiple subjects were also missing from the current study, which limits the ability to generalize experimentally observed trends to different individuals. To ensure that the observed trends are generalizable across individuals, more subjects need to be measured and analysed. Such data will not only increase the credibility of the research results, but also help more accurately evaluate the effectiveness of capacitive sensors in different populations.

Chapter 4 Integrated design and evaluation of capacitiflector-based respiration sensor

This chapter focuses on the experimental platform used in subsequent chapters of the study. The platform consists of two main parts: a wireless capacitive sensor and a wireless stretch sensor for reference measurements. This platform is designed to provide the necessary measurement functions and data recording capabilities for experiments to ensure the accuracy and completeness of research data.

The capacitive sensor under study was designed to address specific issues identified in previous studies. The excitation frequency of the capacitive electrode of the sensor can be adjusted so that it can meet the requirements of experiments at different excitation frequencies. The sensor also includes active shielding to reduce the effects of external interference. In addition, the sensor realizes the need for miniaturization and battery power to enhance experimental portability and flexibility. At the same time, the device has wireless data transmission functions.

A key part of the experimental platform uses Texas Instruments' FDC2214 capacitor-to-digital converter, which is based on an LC resonant circuit and can operate on a 3.3V power supply. It supports an excitation frequency adjustment range of 10kHz to 10MHz and is available in active shielding configurations. Wireless data transmission uses Texas Instruments' CC2650STK development board. The development board can transmit the data measured by FDC2214 to the computer through the Bluetooth low energy (BLE) protocol to complete data recording.

The reason for choosing this type of capacitance measurement chip is that it can significantly reduce the distance between the capaciflector and the capacitance measurement unit, effectively reducing the influence of parasitic parameters in the test connection cable. Battery operation and wireless data transmission are designed to increase flexibility in the testing process. This ensures that subject movement within the experiment is not restricted by power and data transmission cables.

In subsequent experiments, the developed wireless capacitive sensor will be deployed in the middle of the subject's right chest. This arrangement is used to capture chest-related capacitance change signals. At the same time, a wireless stretch sensor will be located on the lower side of the right chest, aiming to provide a reference signal for chest deformation caused by breathing or other movements. This mounting configuration ensures that both sensors can effectively capture physiological and motion signals related to the chest area.

The content of this chapter first provides a general overview of the experimental platform, and then introduces each subsystem of the platform in detail, including capacitive sensors, stretch sensors, and wireless data acquisition units. Next, the deployment process and preliminary test results of the experimental platform are described. These parts are directly related to the practical application and performance evaluation of platform design.

Based on the above content, the purpose of building this experimental platform is to improve the reliability of research data and the application scope of the experiment. In particular, the design of capacitive sensors is not only a key part of this research, but also provides a practical case for the prototype design of future wearable capacitive respiration sensors. This design facilitates future development of more compact systems suitable for practical applications.

4.1 System overview

This system is an experimental platform specially built to study the working principle of capacitive respiration sensors and their different design performances. The platform is divided into two main parts: a wireless capacitive sensor and a wireless stretch sensor for reference measurements.

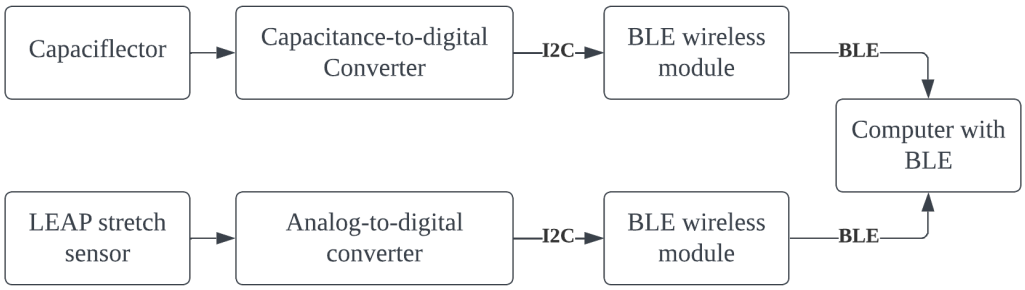

Figure 39 Experimental platform for testing capaciflector-based respiration sensor

Key components of the wireless capacitance measurement system include the capaciflector, FDC2214 capacitance-to-digital converter (CDC), and the CC2650STK wireless data transmission unit. The CC2650STK uses I2C interface to collect capacitance data from the FDC2214 and transmits it to the computer via the Bluetooth Low Energy protocol. In the reference measurement system, a commercial stretch sensor produced by LEAP Technology[61] is used to convert the deformation into a voltage signal. The signal was then recorded by a Texas Instruments ADS1115 analog-to-digital converter (ADC). Another CC2650STK obtains these voltage data from the ADS1115 through the I2C interface and transmits the data to the

computer through the Bluetooth low energy protocol. The MATLAB Bluetooth Low Energy toolkit running on the computer is responsible for receiving data from the two wireless sensors. The operation of the entire system, including the startup and timing of measurements, is mainly controlled by MATLAB.

The details of each component of the system are discussed in depth in subsequent sections.

4.2 Subsystem functional details

4.2.1 Capaciflector design

As mentioned in the previous chapter, a capaciflector is a fringe field capacitive sensor equipped with active shielding. The sensor is designed to detect the conductivity and dielectric properties of materials near its fringe field. In the sensor system of this study, capaciflectors exploit this principle to detect changes in the electrical properties of skin tissue in the chest area. Alterations in the capaciflector's capacitance arise from these changes, which are subsequently recorded by an interfaced capacitance-to-digital converter.

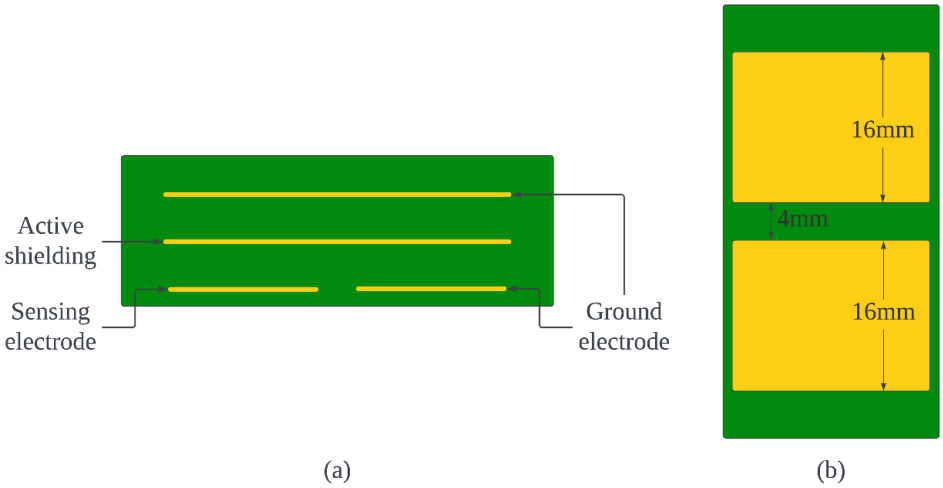

Figure 40 Schematic diagram of the structure of a coplanar parallel plate capacitive sensor with active shielding: (a) side view; (b) bottom view.

Compared with the traditional capaciflector structure based on a single-electrode capacitive sensor, this study adopts a coplanar parallel plate capacitive sensor design. This is the basic structure of capacitive sensors in non-destructive material detection applications. This configuration controls the electric field range by adjusting the electrode spacing and length. The electrode shape is changed from circular to rectangular. The main reason is that rectangular

electrodes can provide relatively consistent electrode edge spacing. This can relatively ensure the uniformity of the electric field distribution, which is convenient for predicting the detection depth of the sensor. In contrast, two circular electrodes placed in parallel may complicate the electric field distribution and increase the difficulty of analysis due to inconsistent edge distances. Although electric field distortion may occur at the right angles of the rectangular electrode, this distortion is limited to the edge area, and the electric field in most of the detection area is still relatively reliable. Circular electrodes have the advantage of avoiding the problem of electric field inhomogeneity caused by tip discharge. In future work, electrodes with different geometric shapes will be further designed to compare their performance. However, the current study starts with the basic structure so that the experiment is not affected by too many factors.

The sensor used in this study adopts a 1.6mm thick four-layer PCB board design. The bottom layer of PCB constitutes a coplanar parallel plate capacitive sensor, which is mainly used to detect the electrical properties of skin tissue. The sensor contains two electrodes with dimensions of 16mm long and 22.5mm wide. The distance between the two electrodes is 4mm. One of the electrodes is connected to the excitation signal for detection of the capacitance-to-digital converter, while the other electrode is connected to the ground plane. At a position 0.6mm above the bottom layer, there is an active shielding electrode with dimensions of 38mm long and 24.5mm wide, and its edge is extended by 1mm relative to the sensing electrode and ground electrode at bottom layer. The active shielding electrode is connected to the unity gain buffer output with the excitation signal as input. This isolates electromagnetic interference from the non-sensing side and enables unidirectional measurements. There is a ground plane 0.6mm above the shielding layer. Its dimensions are the same as the active shield electrode. An interface layer is set up 0.2mm above the ground plane layer, using SAMTEC 1.54mm pitch pin header to facilitate connection to the capacitance-to-digital converter.

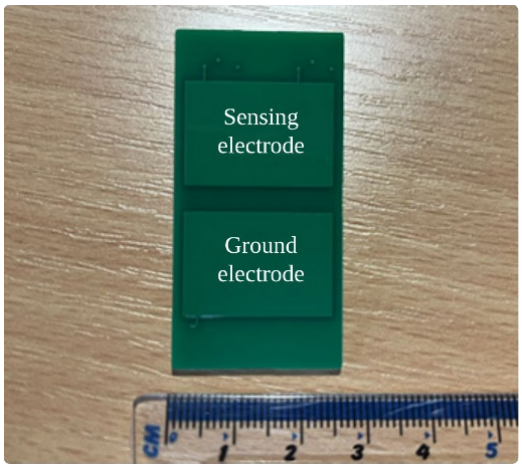

Figure 41 Sensing electrode side of capaciflector manufactured by JLCPCB

Capaciflector's sizing is based on earlier research that used coplanar parallel plate capacitive sensors to detect water intrusion inside composite panels[62]. In the study, when a water exists inside the material being measured and causes a capacitance change of at least 3%, the distance between the liquid and the material surface is defined as the penetration depth (d) of the capacitive sensor. This penetration depth can be calculated from the linear combination of electrode length (l) and spacing (g), the formula is d = 0.675g + 0.65l[62]. According to this formula, the sensor used in this study can theoretically reach a penetration depth of 13.1mm in composite panel water intrusion detection applications.

Although the dielectric constant of human tissue is significantly higher than that of composite plate materials, which will reduce the actual detection range, this dimensional parameter was still used as a benchmark for preliminary testing. After preliminary testing, further adjustments to the size of the sensor will be made based on the results.

4.2.2 Capacitance-to-digital converter

The FDC2214 capacitor-to-digital converter used in this study is based on the LC resonant circuit method. The LC resonant circuit generates an oscillation signal of a specific frequency through its configured inductor and capacitor.

$$f_{SENSOR} = \frac{1}{2\pi\sqrt{LC}}$$

When the sensing electrode of the capaciflector is connected to one end of the LC tank circuit, any change in its capacitance will affect the oscillation frequency. Frequency changes can then be monitored using measurement components such as frequency counters. Since the inductance and capacitance in the LC tank are known, the capacitance of the capaciflector can be accurately calculated based on changes in frequency.

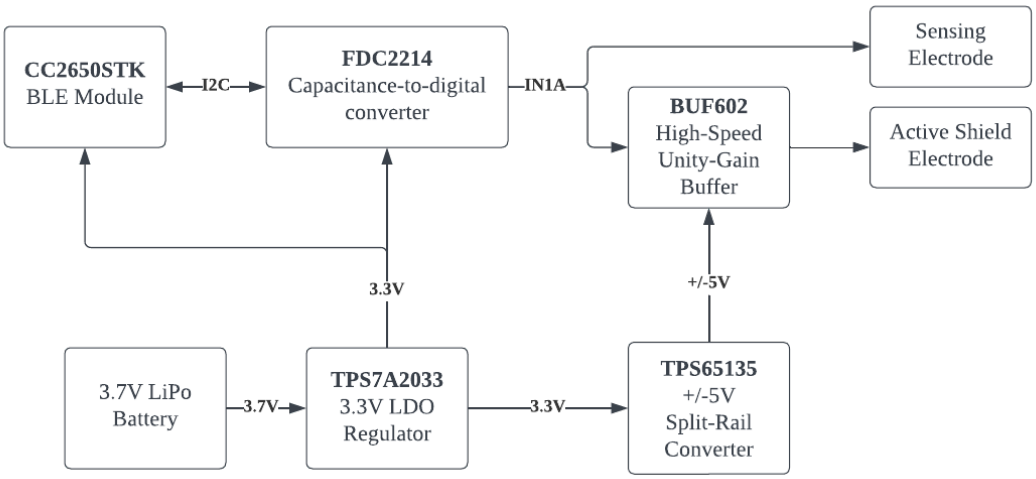

Figure 42 Schematic of the active shield configured capacitance-to-digital converter

In terms of active shielding, a BUF602 wideband unity gain high-speed buffer is used. Its input end is connected to the sensing electrode, and the output end is connected to the active shielding electrode to effectively isolate interference and ensure accurate one-sided sensing.

The power supply part of the system consists of a lithium polymer battery and a 3.3V low-noise LDO regulator. Since the BUF602 buffer requires bipolar power supply, a split-rail voltage converter is introduced to convert the 3.3V output of the LDO to +/-5V to meet the power supply needs of the BUF602.

Finally, the initialization and data transmission process of FDC2214 is controlled by the CC2650 BLE microcontroller on the CC2650STK development board through the I2C interface.

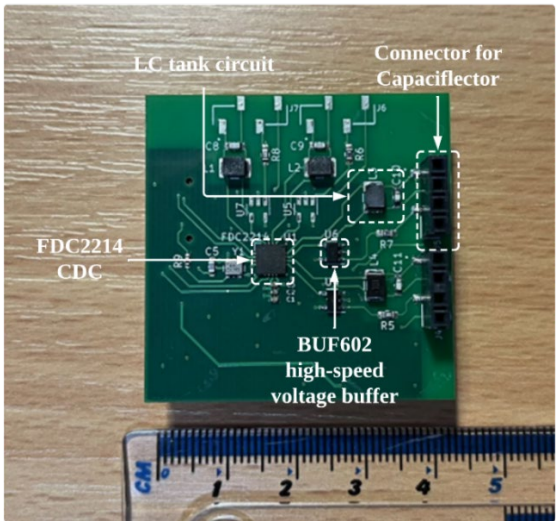

Figure 43 Capacitance-to-digital converter module PCB (manufactured by JLCPCB).

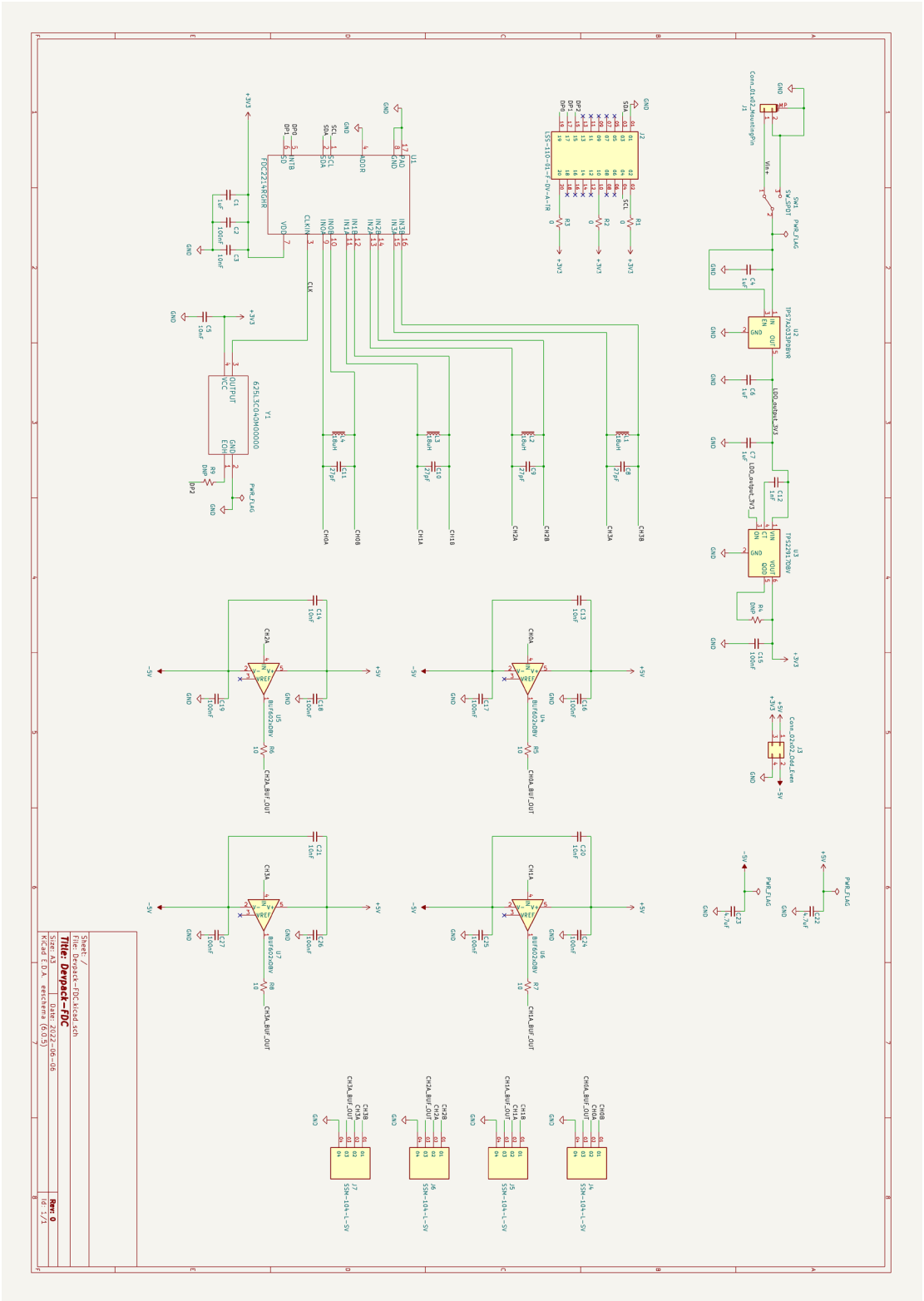

Figure 44 Schematic of capacitance-to-digital converter module.

4.2.2.1 Technical specifications of FDC2214

The attached table lists the main technical indicators of FDC2214. The device provides four measurement channels from CH0 to CH3, and only CH1 was used in this study.

In the preliminary experimental configuration of this study, the excitation signal of the FDC2214 was set to 1MHz, in the form of a half-sine wave, oscillating between 0 and a specific voltage value. According to the device specifications, this oscillation amplitude needs to be maintained in the range of 1.2V to 1.8V. To achieve this goal, by adjusting the I_drive code parameter of the FDC2214, the amplitude can be adjusted to approximately 1.5V.

Table 6 FDC2214 technical specifications[63]

Category	**Description**
Number of channels for measurement	4
Maximum input capacitance	250nF
Sensor excitation frequency	10kHz to 10MHz
Noise floor at 100sps	0.3fF
Supply voltage	2.7 to 3.6V
Runtime power consumption	2.1mA
Interface	I2C

Since skin has a higher dielectric constant than air, the capacitance of the capaciflector will increase by several picofarad compared to when it is not mounted on the skin surface. Since the increase in capacitance will reduce the amplitude of the excitation signal, the capacitance in the LC tank needs to be carefully selected. In order to avoid that the excitation signal amplitude exceeds 1.8V in the uninstalled state, which may cause damage to the chip, the capacitor and inductor are accurately set in the LC tank circuit design, as shown in the Table 7. Although higher capacitance values (such as 220pF) may reduce the resolution of capacitance measurements due to limitations of the chip's internal frequency counter, testing has shown that the selected settings are capable of achieving a capacitance measurement resolution of at least 10fF. The selection of the inductor needs to ensure that its self-resonant frequency is higher than the resonant frequency of the designed LC tank circuit.

Table 7 Designed LC tank circuit parameters

Category	**Description**
Capacitor	220pF, NP0/C0G, +/-1%
Inductor	100μH, RF inductor, +/-10%
Theoretical resonant frequency	1.07MHz
Designed oscillation amplitude	1.5V

In addition, in order to accurately obtain the amplitude and frequency of the excitation signal, an oscilloscope was used for measurement in the experiment. Adjusting the I_drive code to ensure that the amplitude is maintained at approximately 1.5V. Since the actual capacitance and inductance values may deviate from the theoretical values, we used an impedance analyser (wayne kerr6500B) to make precise measurements at their operating frequency to reduce errors in frequency calculation of capacitance. Table 8 shows the results of these measurements, which were also used to calculate the capacitance measurement results.

Table 8 Measured LC tank circuit parameters

Category	**Description**
Measured capacitance	224.81pF
Measured inductance	104.51μH
Measured resonant frequency	1.03MHz
I_drive code	0x50
Measured oscillation amplitude	1.66V

4.2.2.2 Active shielding

As mentioned before, active shielding is mainly used in sensor systems to implement unidirectional sensing functions. Although a ground plane (passive shielding) on the back of the sensing electrode can achieve a similar effect, such a configuration will result in a certain inherent capacitance between the sensing electrode and the ground plane. The size of this inherent capacitance depends on the design, typically ranging from tens to hundreds of picofarads, which can adversely affect the sensor operating frequency setting of the LC circuit configuration. Adding an active shielding layer between the ground plane and the sensing

electrode can effectively reduce the coupling between the two and reduce the inherent capacitance of the sensor, thereby making it easier to adjust the operating frequency of the sensor.

Theoretically, the signal on the active shield should be the same as the excitation signal on the sensing electrode. However, due to performance limitations such as bandwidth and slew rate of the unity gain op amp, there is usually a phase difference between the two signals[64]. This phase difference can result in a small potential difference between the sensing electrode and the active shield, which can create a certain amount of capacitance. In order to reduce this phase difference as much as possible, this study selected the BUF602 high-speed unity-gain buffer. The key parameters of BUF602 are shown in the Table 9. Considering that the FDC2214 only operates in the 10kHz to 10MHz frequency range, the BUF602 can meet the needs of active shielding function as long as it uses +/-5V power supply.

Table 9 BUF602 technical specifications[65]

Category	**Description**
Bandwidth at 1Vpp	920MHz
Slew rate	8000V/μs
Typical power supply	±5V
Quiescent current	5.8mA
Input impedance	1MΩ || 2pF

It should be pointed out that BUF602 is not the only choice, other op amps that meet the requirements can also be used to implement active shielding. In actual applications, the appropriate op amp can be selected and replaced according to the specific situation.

4.2.2.3 Power supply configuration

The main operating voltage of this system is 3.3V, which is powered by a combination of a small lithium polymer battery and a low-dropout regulator (LDO). Considering that the BUF602 op amp requires a +/-5V power supply, the system uses a split-rail voltage converter to meet this requirement. In terms of voltage regulator selection, this system uses the TPS7A2033 produced by Texas Instruments, which was selected for its low noise performance. The split-rail voltage converter uses the TPS65133 produced by Texas Instruments. The battery is a 3.7V 150mAh lithium polymer battery produced by Adafruit[66]. In the overall design,

special attention was paid to selecting electronic components with low noise levels to improve the performance and reliability of the system. It should be noted that other alternative components that meet the specification requirements can also be selected based on specific system requirements.

4.2.2.4 Register configuration

Proper operation of the FDC2214 relies on the correct configuration of its internal registers. After each power-on, the values specified in the following table must be written into the corresponding registers through the I2C interface to complete initialization. This configuration procedure activates measurement channel 1 and sets it to continuous measurement mode.

Table 10 Typical initial register configuration for FDC2214

Address	**Value**	**Register Name**	**Comments**
0x15	0x2001	CLOCK_DIVIDER_CH1	10MHz Deglitch filter setting
0x1A	0x5E01	CONFIG	Enable device
0x1F	0x5000	DRIVE_CURRENT_CH1	LC tank circuit driving current
0x19	0x0001	ERROR_CONFIG	Error state checking
0x1B	0x020D	MUX_CONFIG	Enable channel 1
0x09	0x2089	RCOUNT_CH1	Setting for sampling rate
0x11	0x0400	SETTLECOUNT_CH1	Setting for sampling rate

Table 11 Measurement data register

Address	**Default Value**	**Register Name**	**Comments**
0x02	0x0000	DATA _CH1	MSB of channel 1 measurement result
0x03	0x0000	DATA_LSB_CH1	LSB of channel 1 measurement result

Channel 1 measurement results can be read from specific registers as described in Table 11. The result of each measurement consists of two 16-bit numbers combined in order MSB (most

significant bit) and LSB (least significant bit). The resulting 32-bit data can be converted into capacitance data using specific calculation methods.

4.2.2.5 Deriving capacitance value from measurement data

In order to derive the capacitance of the sensor from the measured data, the following two formulas are used.

$$C_{SENSOR} = \frac{1}{L*(2\pi*f_{SENSORx})} - C \text{ [63]}$$

First, use the resonant frequency of the LC resonant circuit to infer the capacitance value of the sensor. In this formula, C represents the fixed capacitance in the LC tank circuit, and L is the fixed inductance in the circuit.

$$f_{SENSORx} = \frac{CH1\_FIN\_SEL*f_{REF1}*DATA1}{2^{28}} \text{ [63]}$$

The resonant frequency can be calculated by another formula, where DATA1 is the 32-bit measurement data of channel 1. CH1_FIN_SEL is the system configuration parameter of channel 1, and its value needs to be set to 2 according to the data table.

4.2.3 LEAP stretch sensor

The main cause of changes in sensor capacitance is the deformation of the skin during breathing. Based on this, an elastic stretch sensor is selected as a reference sensor to measure the local deformation of the thorax. The commercial LEAP elastic stretch sensor uses a rubber-based design that converts physical stretch changes into a voltage signal output. The sensor features high linearity and sensitivity. Its specific dimensions and actual object are shown in Figure 45.

In practical applications, in order to ensure that deformation can be accurately transmitted to the sensor, the attachment area of the sensor needs to be fixed on the surface of the object being measured. For this purpose, two clamps 3D printed from PLA (polylactic acid) were designed to stably clamp the connection areas at both ends of the sensor. The underside of these clamps is designed to be flat, allowing them to be easily attached to the surface of the skin using double-sided tape.

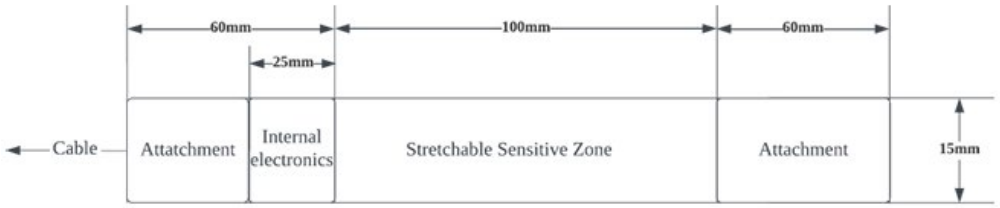

(a)

(b)

Figure 45 LEAP stretch sensor: (a) specified design dimensions; (b) actual appearance

Additionally, the sensor's supply voltage requirements are compatible with battery-powered systems. Table 12 details the specific technical parameters of the sensor. The output voltage signal is converted into a digital signal by an analog-to-digital converter, then recorded by the CC2650STK development board and transmitted to the computer.

Table 12 LEAP stretch sensor technical specifications[61]

Category	**Description**
Sensitivity	0.05V/mm stretch
Output voltage range	0.5 – 4.5V
Power supply	5V
Sample rate	1000 SPS
Power consumption	<0.2W

4.2.4 Analog-to-digital converter

In this system, the key role of the analog-to-digital converter (ADC) is to convert the voltage signal output by the LEAP stretch sensor into a digital signal to facilitate more efficient data storage and transmission. For this purpose, the ADS1115 analog-to-digital converter was selected to meet the accuracy and performance requirements of the system. The ADS1115 provides a measurement range of ±6.144V and a voltage resolution of 187.5μV, allowing it to accurately detect voltage changes caused by tiny deformations at the level of 0.1 mm. This performance specification is critical for detecting subtle stretch sensor signals in this system.

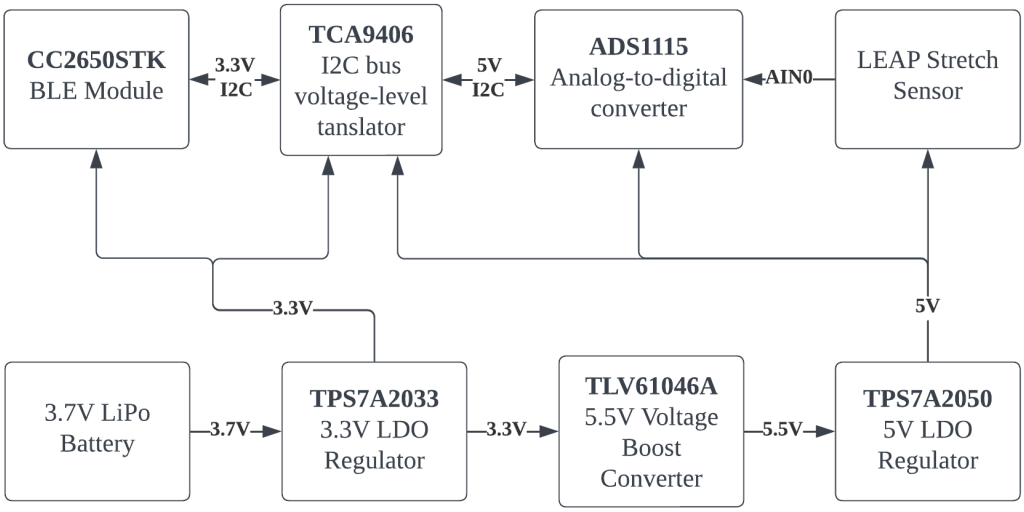

Figure 46 Schematic of the wireless LEAP stretch sensor system.

Regarding the system power supply, this system mainly has two power supply voltage levels: 5V and 3.3V. The 5V voltage is used to support the ADS1115 analog-to-digital converter to accommodate the 0.5 to 4.5V output voltage range of the LEAP stretch sensor. The 3.3V voltage is to meet the power requirements of the data transmission module CC2650STK. To power these two voltage levels, the system uses a combination of a lithium polymer battery and an LDO regulator to first generate 3.3V. Then a boost converter and another LDO regulator are used to generate 5V.

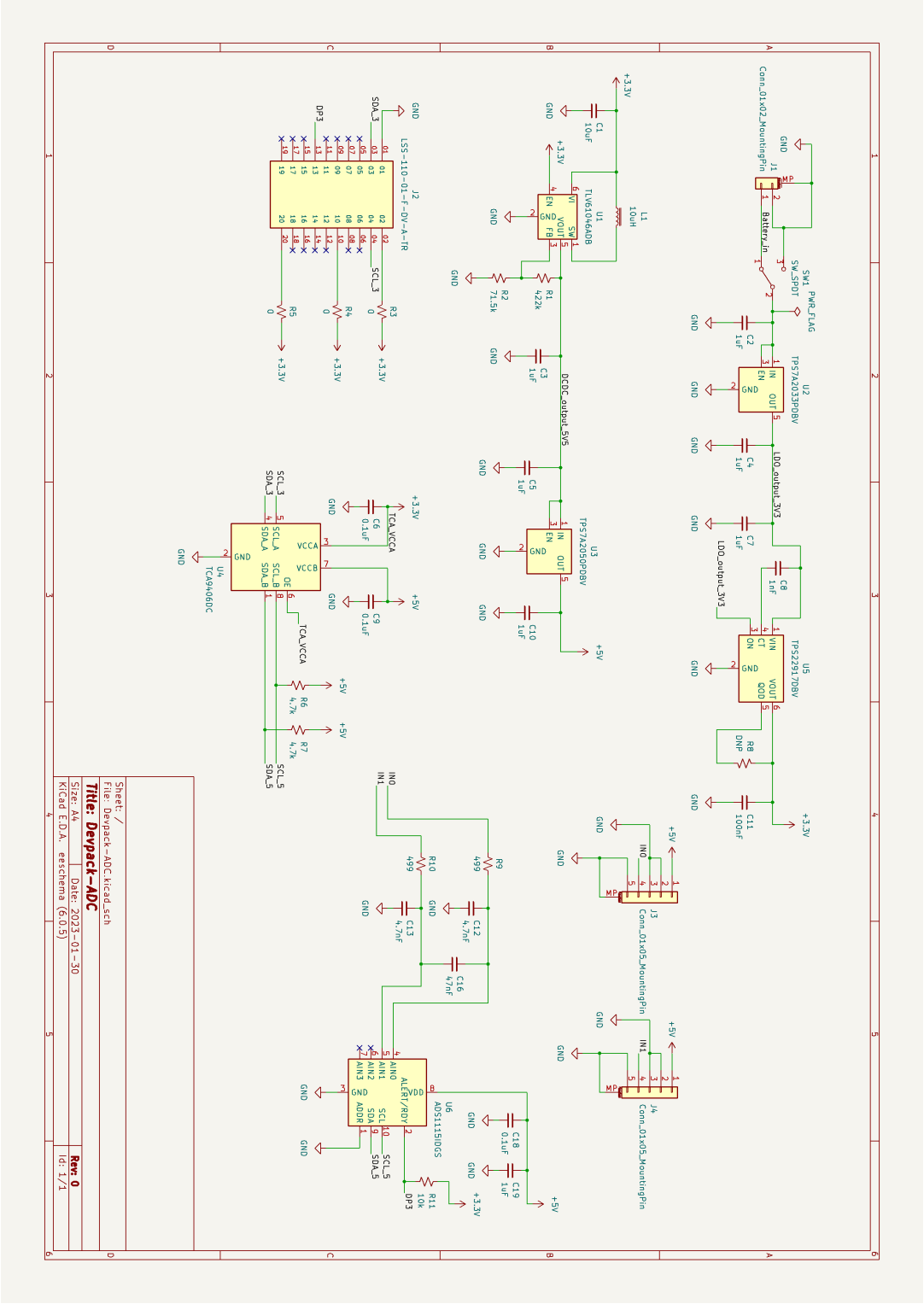

Figure 47 Schematic of analog-to-digital converter module.

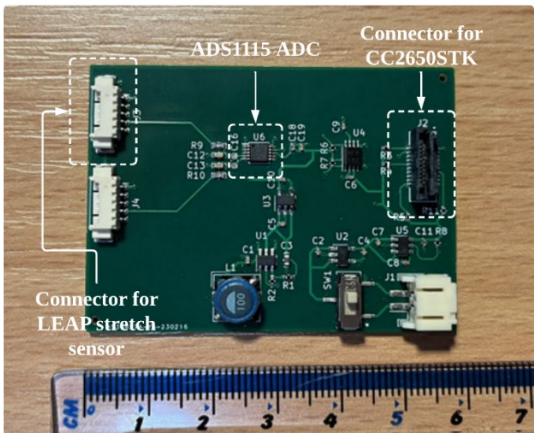

(b)

Figure 48 Analog-to-digital converter module PCB (manufactured by JLCPCB).

In addition, in view of the voltage difference between CC2650 and ADS1115 during I2C communication, the system specially integrates an I2C voltage translator. This measure is designed to ensure effective communication between the two modules and ensure the stable operation of the entire system.

4.2.4.1 Technical specifications of ADS1115

The attached table lists the main technical parameters of ADS1115. The device provides four inputs from AIN0 to AIN3, and only AIN0 is used in this study.

Table 13 Technical specification of ADS1115

Category	**Description**
Resolution	16-bit
Number of channels for measurement	4
Maximum sample rate	860 SPS
Maximum full-scale range (FSR)	+/-6.144V
Supply voltage	2 - 5.5V
Interface	I2C

In the experimental configuration, the sampling rate of the ADC was set to 860 SPS. Its measurement mode is set to continuous conversion mode.

4.2.4.2 Power supply configuration

The system has two main power supply voltage levels: 3.3V and 5V. 3.3V is first generated by a 3.7V 350mAh Li-polymer battery combined with a TPS7A2033 LDO regulator. The TLV61046A boost converter and another TPS7A2050 LDO regulator are then used to generate 5V. In the overall design, special attention was paid to selecting electronic components with low noise levels to improve the performance and reliability of the system. It should be noted that other alternative components that meet the specification requirements can also be selected based on specific system requirements.

4.2.4.3 Register configuration

Proper operation of the ADS1115 relies on the correct configuration of its internal registers. After each power-on, the values specified in the following table must be written into the corresponding registers through the I2C interface to complete initialization. This configuration procedure activates measurement channel 0 and sets it to continuous measurement mode.

Table 14 Typical initial register configuration for ADS1115

Address	**Value**	**Register Name**	**Comments**
0x01	0x40E3	Config register	Enable 100ms sampling gap continuous measurement

Channel 0 measurement results can be read from specific registers as described in Table 15.

Table 15 Measurement data register

Address	**Default Value**	**Register Name**	**Comments**
0x00	0x0000	Conversion register	The last conversion result

4.2.4.4 Extracting length value from measurement data

In order to derive the length of the sensor from the measured data, the following formula is used.

$$Length = DATA_{AIN0} * \frac{0.1875mV}{50\,mV/mm}$$

First, the voltage value output by the stretch sensor can be calculated by multiplying the measurement data by the measurement resolution (0.1875mV) set by the ADS1115. This voltage value is then converted to length data by dividing it by the sensor's sensitivity (50mV/mm). It is important to note that the calculated initial length itself has no practical meaning. However, the measured data changes are consistent with changes in the actual length of the sensor.

4.2.5 BLE wireless module

The main function of the BLE wireless module in this system is to control the sensor for data collection and wirelessly transmit the collected data to the computer through the Bluetooth Low Energy protocol. In the experimental setting of this study, wireless transmission significantly reduces the interference caused by the data connection line and improves the freedom of movement of the tested subject, which is of great significance to the accuracy and reliability of the experimental results.

4.2.5.1 CC2650STK development board

In order to simplify the design and development of wireless modules, this study selected the CC2650STK development board produced by Texas Instruments. This development board is a miniaturized evaluation platform based on the CC2650 wireless microcontroller. It integrates four commercial sensors on the board, each communicating through the I2C interface, the details of which are shown in Figure 49.

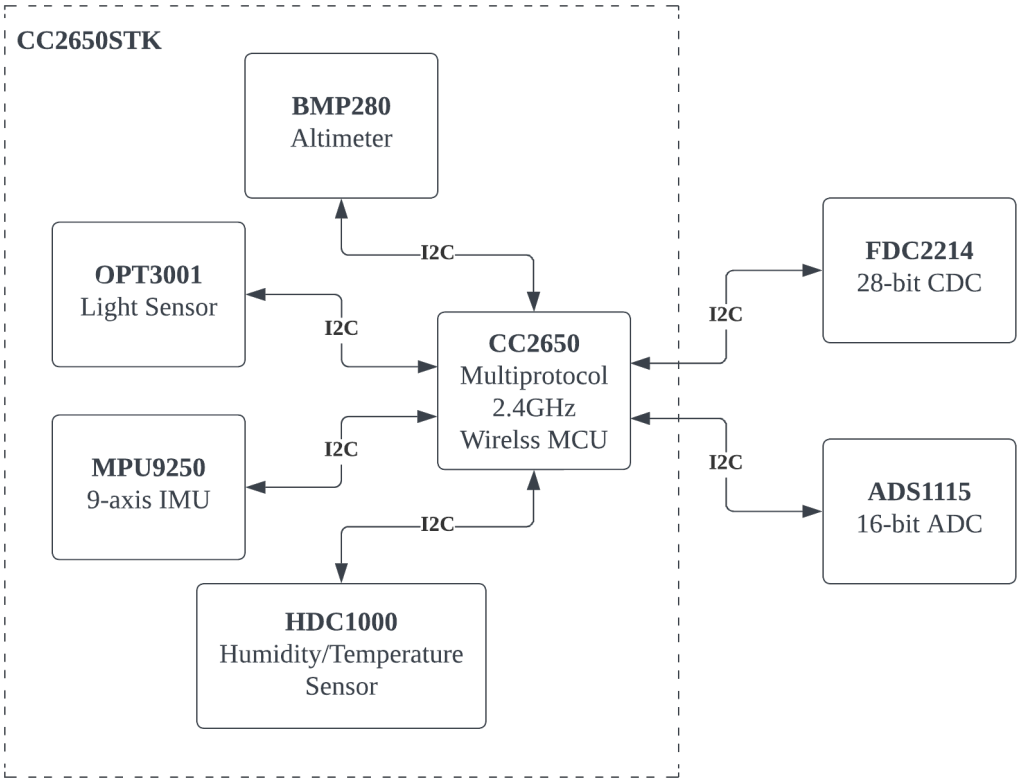

Figure 49 CC2650STK system overview

In this study, the FDC2214 CDC and ADS1115 ADC are connected to the CC2650 through the on-board expansion hardware interface on the CC2650STK development board.

4.2.5.2 Development of CC2650 firmware based on TI's example

The development example provided by Texas Instruments for the CC2650STK development board shows how the four on-board I2C peripheral sensor data can be transmitted wirelessly through BLE. The project software runs on TI RTOS and adopts a layered software architecture common in IoT applications, including the middleware layer, service layer and application layer.

The middleware layer is responsible for the read and write operations of I2C peripherals. It encapsulates the startup, initialization and data reading operations of the sensor. The service layer abstracts these operations, converts them into operations on specific sensors, and encapsulates the read data in the BLE protocol stack of CC2650 for BLE transmission. The application layer is responsible for the business logic of the software and calls the functions of the service layer to implement specific functions such as data collection and system scheduling.

The software of example project adopts a modular design, building independent middleware, service and application layer code for each I2C peripheral. Each peripheral sensor is equipped with independent services and characteristics for BLE data collection. In practical applications, computer can interact with each peripheral sensor through unique identifier (UUID) of its services and characteristics.

In this study, in order to reduce the development workload, data transmission was not implemented by adding new middleware, service and application layer codes dedicated to FDC2214 and ADS1115. On the contrary, the original sensor-specific middleware layer code was adjusted, and the I2C read and write operations were changed to adapt to the operations of FDC2214 and ADS1115. This approach avoids the need to write additional service layer and application layer code, thereby effectively reducing the overall development burden.

```
#define SENSOR_SELECT()    SensorI2C_select(SENSOR_I2C_0,Board_HDC1000_ADDR)

/*********************************************************************
* @fn        SensorHdc1000_init
* @brief      Initialize the humidity sensor driver
* @return     true if I2C operation successful
*********************************************************************/
bool SensorHdc1000_init(void) {
   uint16_t val;

   // Check the current I2C address is for HDC1000
   if (!SENSOR_SELECT()) {
      return false;
   }

   // Enable reading data in one operation
   val = SWAP(HDC1000_VAL_CONFIG);
   success = SensorI2C_writeReg(HDC1000_REG_CONFIG, (uint8_t*)&val, 2);

   SENSOR_DESELECT();
   return success;
}
```

During the actual implementation of this project, the original middleware code for the HDC1000 temperature and humidity sensor was changed to adapt to the operation of FDC2214.

The core components of middleware usually include function definitions for initialization, startup, and data reading. This article takes the definition change of the initialization function as an example to show the specific replacement of the code. It should be pointed out that the display of some macro definitions is omitted here. The original code is for the HDC1000 sensor. It first verifies whether the address of the device currently connected through I2C is the address of HDC1000. Then, use the I2C write register function to send the predefined 16-bit data to the specified address to complete the initialization setting.

```
#define SENSOR_SELECT()    SensorI2C_select(SENSOR_I2C_0,Devpack_FDC2214_ADDR)

/*****************************************************************************
* @fn         FDC2214_init
* @brief      Initialize the capacitance to digital converter driver
* @return     true if I2C operation successful
*****************************************************************************/
bool SensorHdc1000_init(void) {
   uint16_t val;

   // Check the current I2C address is for FDC2214
   if (!SENSOR_SELECT()) {
      return false;
   }

   // Initialize all necessary registers
   val = FDC2214_VAL_RCOUNT_CH1;
   val = SWAP(val);
   SensorI2C_writeReg(FDC2214_REG_RCOUNT_CH1, (uint8_t *)&val, REGISTER_LENGTH);

   val = FDC2214_VAL_SETTLECOUNT_CH1;
   val = SWAP(val);
   SensorI2C_writeReg(FDC2214_REG_SETTLECOUNT_CH1, (uint8_t *)&val, REGISTER_LENGTH);

   val = FDC2214_VAL_CLOCK_DIVIDER_CH1;
   val = SWAP(val);
   SensorI2C_writeReg(FDC2214_REG_CLOCK_DIVIDER_CH1, (uint8_t *)&val,
REGISTER_LENGTH);

   val = FDC2214_VAL_ERROR_CONFIG;
   val = SWAP(val);
   SensorI2C_writeReg(FDC2214_REG_ERROR_CONFIG, (uint8_t *)&val, REGISTER_LENGTH);

   val = FDC2214_VAL_MUX_CONFIG;
   val = SWAP(val);
   SensorI2C_writeReg(FDC2214_REG_MUX_CONFIG, (uint8_t *)&val, REGISTER_LENGTH);

   val = FDC2214_VAL_DRIVE_CURRENT_CH1;
   val = SWAP(val);
   success = SensorI2C_writeReg(FDC2214_REG_DRIVE_CURRENT_CH1, (uint8_t *)&val,
REGISTER_LENGTH);

   SENSOR_DESELECT();
   return success;
}
```

During the modification process, the main work is to modify the I2C address to the address of FDC2214 and replace the initialization write register part with the corresponding configuration required by FDC2214. This simple modification method effectively adapts to new sensors without requiring a large-scale rewrite of the entire middleware architecture.

At the same time, the middleware code that originally served the OPT3001 light sensor was also modified to adapt to the ADS1115. Through these adjustments, the example project can be

modified with a lower development effort to realize the function of transmitting FDC2214 and ADS1115 data to the computer via BLE.

On the computer side, in order to obtain the data collected by FDC2214, it is necessary to use the UUID corresponding to the service and characteristics originally assigned to the HDC1000 humidity/temperature sensor. Similarly, to obtain the data of ADS1115, you need to use the UUID of the original OPT3001 light sensor service and characteristics.

4.2.6 Data collection using MATLAB

On the computer side, the BLE toolkit of MATLAB[67] is used to perform the recording and real-time display functions of measurement data. The toolkit supports connection with BLE peripherals and provides the function of reading and writing peripherals based on UUID.

In this experiment, the execution of part of the MATLAB code includes the following steps:

1. Connect the wireless capacitive sensor (FDC2214) and the wireless stretch sensor (ADS1115);

2. Start these two sensors and set the sampling interval to 0.1 seconds;

3. From the two sensors respectively Read the data;

4. Plot and display the data from the two sensors;

5. Repeat step 3 for a total of 300 iterations.

It should be pointed out that although the set sampling interval of each sensor is 0.1 seconds, theoretically the total sampling interval of the two sensors should be 0.2 seconds. However, in practical applications, due to computer performance limitations, the actual total sampling interval between two sensors is usually about 0.25 seconds. Although this is not entirely ideal, this sampling rate is still sufficient to test respiratory signals with a period of approximately 2 to 4 seconds.

4.3 Sensor mounting and testing

4.3.1 3D-printed case

In order to ensure that the sensor can be stably attached to the skin surface, the housing is specially designed for the capaciflector and fabricated through 3D printing. The material used is PLA. The capaciflector housing and its components are fixed with Blu Tack[68], a reusable adhesive tack, to ensure stability during the measurement process.

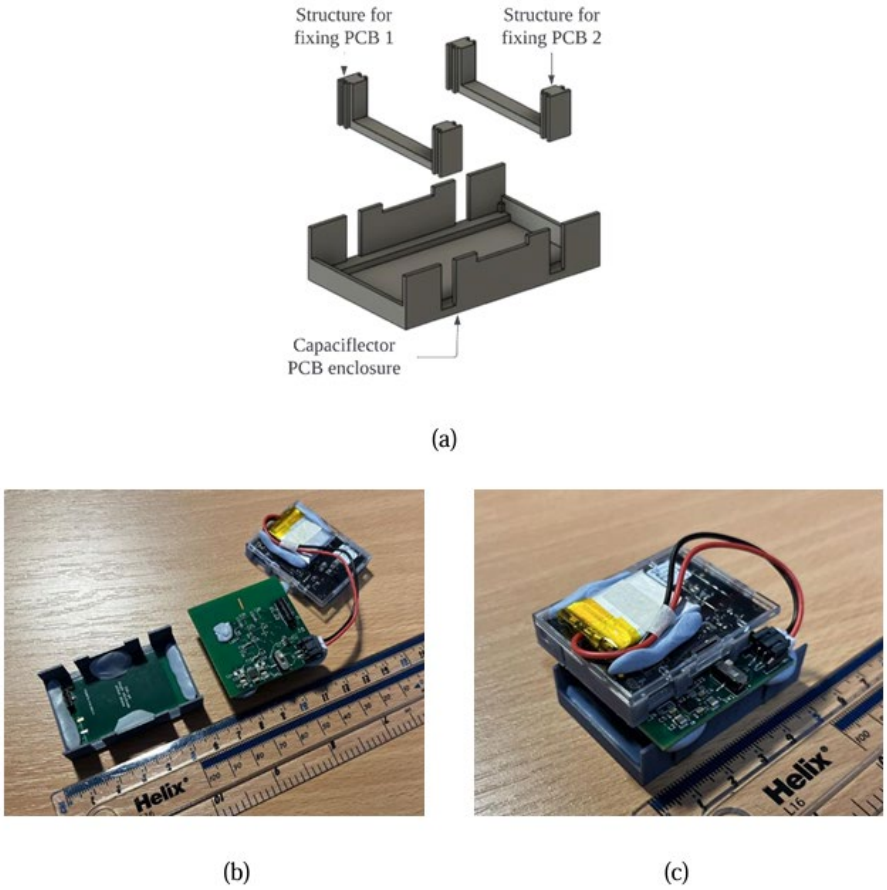

Figure 50 (a) Designed capaciflector housing and components. (b) Capaciflector, FDC2214 capacitance measurement module and CC2650STK. (c) Fully assembled wireless capacitive sensor.

The 3D printed capaciflector shell has 1mm sidewall thickness to ensure its structural rigidity. The dimensions of the bottom of the case are set at 54.4mm long and 34.2mm wide, while its thickness is designed to be only 0.43mm. The thinner bottom thickness is used to shorten the distance between the sensor and the skin surface, which helps reduce the possible negative effects on sensor sensitivity caused by increased distance.

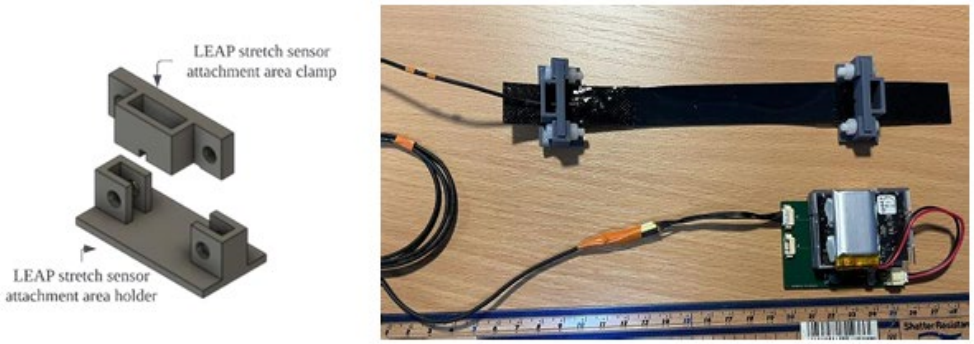

Figure 51 (a) Designed LEAP stretch sensor clamp and its components. (b) The assembled wireless LEAP stretch sensor.

The printed LEAP stretch sensor clamp and its components are designed with a 3mm sidewall thickness, which is intended to ensure the clamp is structurally rigid and securely holds the LEAP sensor attachment area. The bottom dimensions of the clamp were set to be 40mm long, 20mm wide, and 2mm thick.

4.3.2 Mounting method

In this study, the sensor was mounted using URSA double-sided tape[69]. This double-sided tape is a hypoallergenic material and is often used for pasting microphones. Its dimensions are 78mm long, 22mm wide and 0.1mm thick.

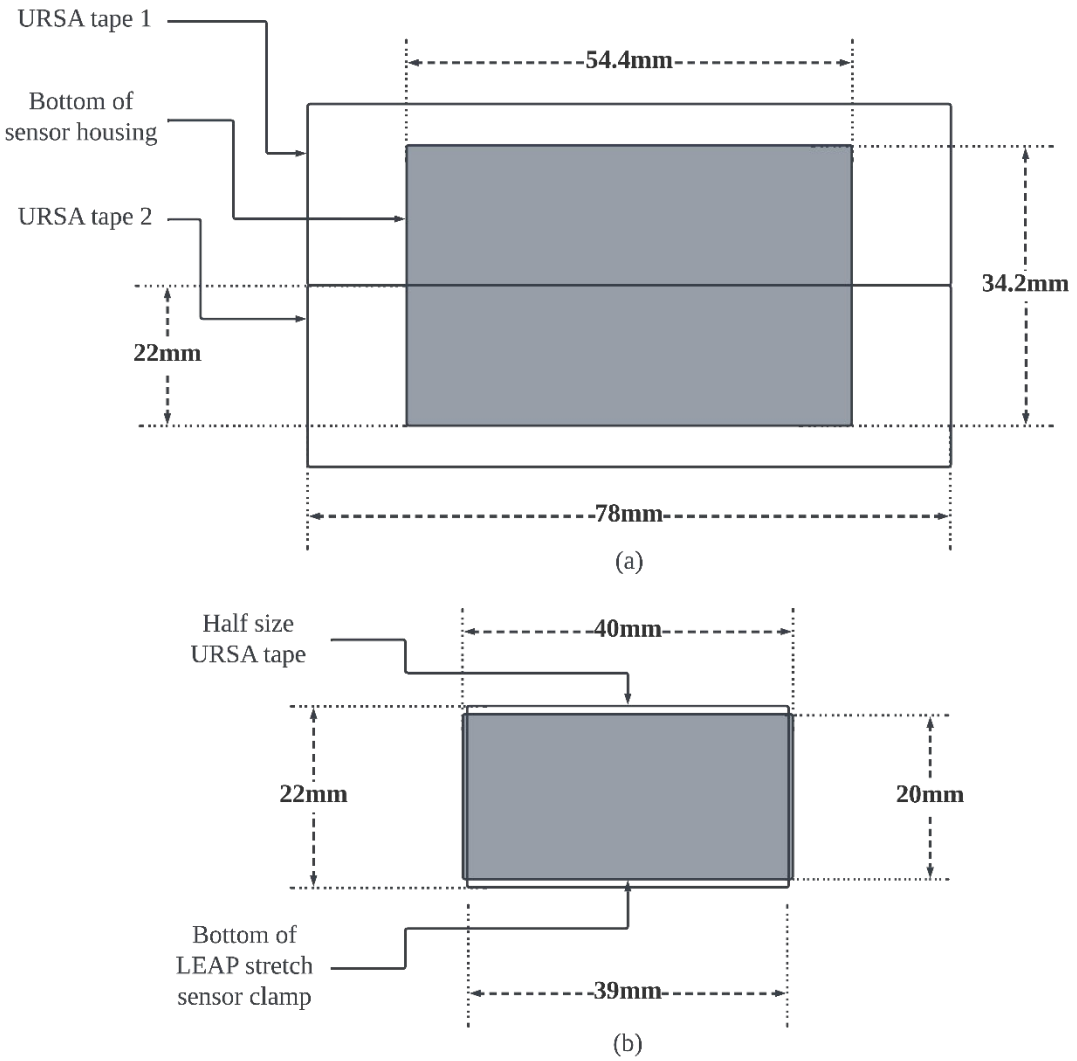

Figure 52 URSA Tape attachment configurations: (a) for use on the bottom of the capaciflector housing (b) for use on the bottom of the LEAP stretch sensor clamp.

For the dimensions of the bottom of the 3D printed capaciflector housing, a configuration of two URSA tapes arranged closely side by side was used. For the bottom of the LEAP stretch sensor clamp, a URSA tape configuration with half the size is used according to its size.

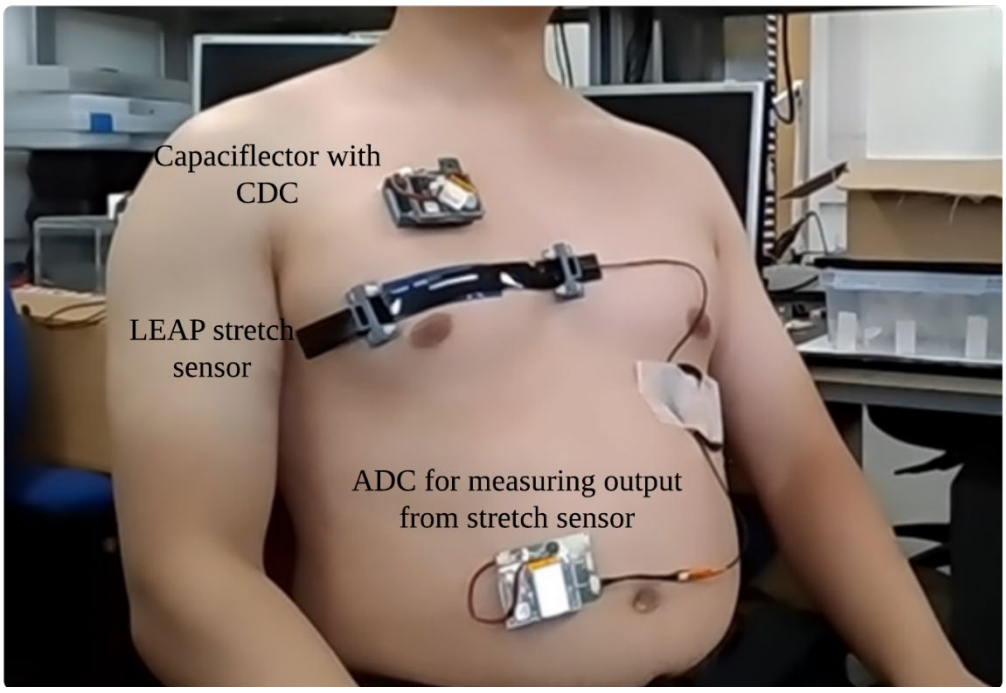

Figure 53 Capaciflector and LEAP stretch sensor were mounted on the right chest of the subject.

The right chest area was selected as the location for the sensor. The capaciflector is installed in the upper middle part of the right chest, and the LEAP stretch sensor is located about 20mm below the capaciflector.

4.3.3 Test environment and test protocol

The experiment was conducted in a specially prepared indoor environment where good ventilation was maintained while the temperature was strictly controlled between 16 and 24 degrees Celsius to ensure environmental stability. In addition, to ensure the accuracy of the experiment, the surrounding environment was cleared so that there were no obstructions within 1 meter around the subjects, thereby reducing interference from external factors.

To control the subject's breathing rhythm, a metronome of 28 beats per minute was used. Using a metronome of 28 beats per minute helps stabilize the breathing rate at around 14 beats per minute, which is consistent with the normal breathing rate of an average person while sitting still. In order to effectively avoid the potential interference of motion artifacts on experimental results, subjects need to sit in a chair during the experiment. They were specifically instructed to place their backs against the back of the chair to maintain body stability, thereby ensuring the accuracy and reliability of the test.

The subject is asked to inhale on one beat, then exhale on the next beat, and repeat this process for about 75 second. In addition, the experiment required subjects to take 5 deep breaths first, followed by 5 shallow breaths. Specific steps are as follows:

1. Take 5 deep breaths;
2. Take 5 normal breaths;
3. Return to step 1 and repeat process.

The difference between deep and shallow breathing depends mainly on the subject's personal feelings, which is an uncontrollable variable. However, since the respiratory data is displayed on the computer screen in real time, the subjects can understand and adjust their breathing intensity based on these data. At the same time, real-time data display also provides researchers with a way to effectively monitor the subject's respiratory status during the experiment. After the test is completed, the subjects can carefully remove the two sensors on their bodies.

It is worth noting that, except for the test protocol of the subjects, the above-mentioned experimental environment remains unchanged in the tests in subsequent chapters. The test protocols for subjects will be adjusted according to different experimental purposes.

4.4 Result

Figure 54 shows the measurement data obtained in the preliminary experiment, the main purpose of which was to verify the effectiveness of the measurement system and to make a preliminary observation of the measured respiratory signal. When set to 14 breaths per minute, the frequency of the respiratory signal is approximately 0.23Hz. By applying a low-pass filter with a cutoff frequency of 0.72Hz, part of the signal noise was successfully filtered out. The red circle in the figure marks the end point of inhalation determined based on the local maximum value of the signal, while the blue circle marks the starting point of inhalation determined based on the local minimum value.

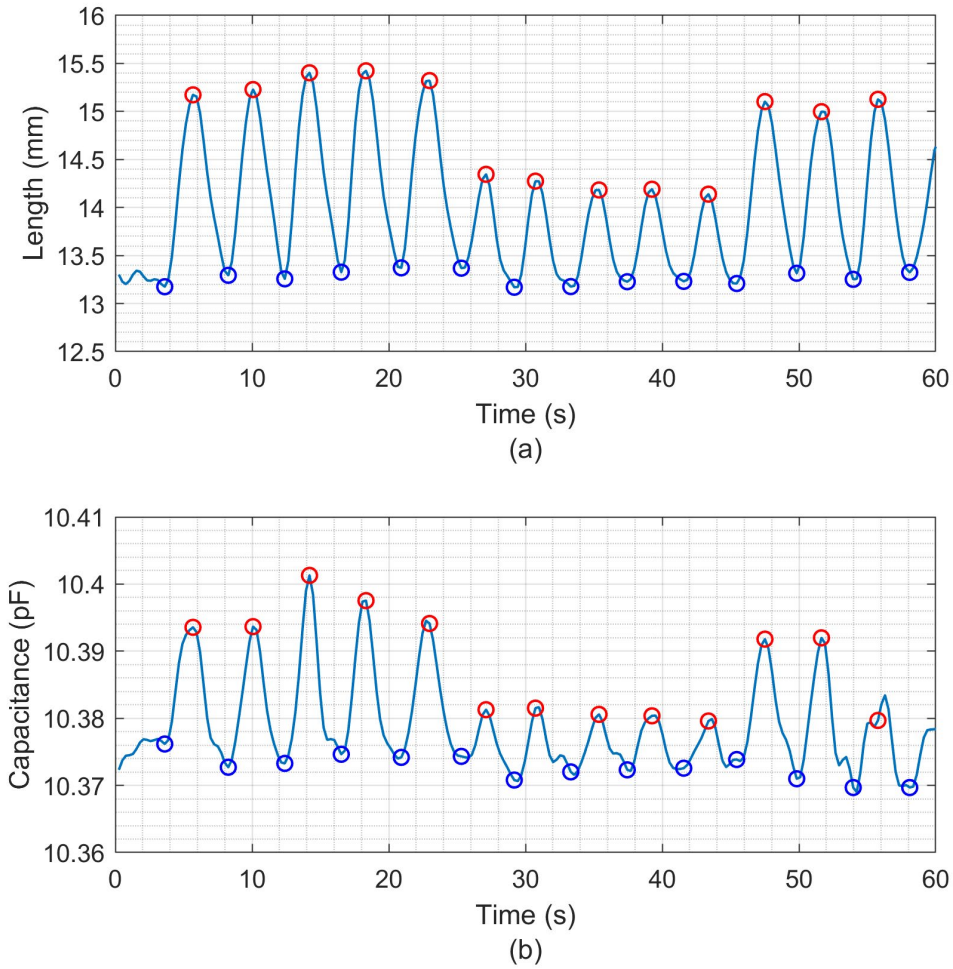

Figure 54 Breathing signal comparison: (a) LEAP stretch sensor (b) Capaciflector

During the 60-second measurement period, 13 spikes were observed, which was roughly consistent with the preset respiratory rate of 14 breaths per minute. In these measurements, the reference stretch sensor showed stretch changes in the range of 1-2mm, while the capaciflector's capacitance changes were roughly between 0.01-0.03pF. Notably, the capaciflector is able to differentiate between different intensities of breathing, although it is displayed on a different scale than the reference stretch sensor. This difference can be attributed, in part, to differences in size and location of measurement between the reference stretch sensor and the capaciflector, resulting in signal differences between deep and shallow breathing.

4.5 Discussion

Experimental results show that the system successfully measured the capacitance change of the capaciflector and the length change of the stretch sensor, and the signals measured by the two sensors showed a certain degree of synchronization. During normal breathing, the capacitance change of the capaciflector is about 0.01pF, and it can distinguish between deep breathing and shallow breathing.

Since the size and measurement location of the stretch sensor are different from those of the capaciflector, the deformation data measured by the stretch sensor cannot be directly used to evaluate the capacitance change caused by unit deformation. Although the capaciflector can differentiate between deep and shallow breathing, data from the reference stretch sensor can be used to detect the occurrence of respiratory events and monitor changes in breathing intensity during the experiment.

Follow-up research can be based on the current measurement platform to further explore whether capaciflector can effectively measure skin deformation and the impact of different sensor designs on its measurement sensitivity.

Chapter 5 Effect of skin stretching on capacitance-based respiration measurement

5.1 Strain dependent dielectric behaviour for complex dielectrics

Deformation of complex dielectrics can lead to changes in their effective dielectric constant and conductivity[70]. Taking carbon black reinforced natural rubber[71] as an example, the movement of the interface between the conductive and dielectric materials within the material affects its effective dielectric constant and conductivity[72].

Human tissue, as a complex dielectric, has its effective dielectric constant significantly affected by its composition and structure[73]. When skin deforms, its internal structure changes, possibly leading to changes in the effective dielectric constant. Simulation studies have shown that electromagnetic energy is mainly concentrated in the superficial layers of body tissue, that is, the skin surface, because the potential intensity excited by the electric field decreases as the distance increases. Therefore, deformations in areas of skin are more easily detected by capacitive sensors than in deeper tissues.

5.2 Experiment setup and test protocol

The test objective of this chapter is to analyse the effect of chest skin deformation on capacitance change through breathing and skin stretching experiments. The contribution of skin deformation to capacitance change can be determined by comparing the capacitance change caused by skin stretching when the subject is not breathing with the capacitance change caused by breathing.

The experiments in this chapter used the experimental platform described in Chapter 4. The stretch sensor was mounted on the lower side of the subject's right chest and was used to provide reference signals during breathing and local skin stretch. The capaciflector working at 1MHz was mounted in the center of the right chest, approximately 20 mm above the stretch sensor.

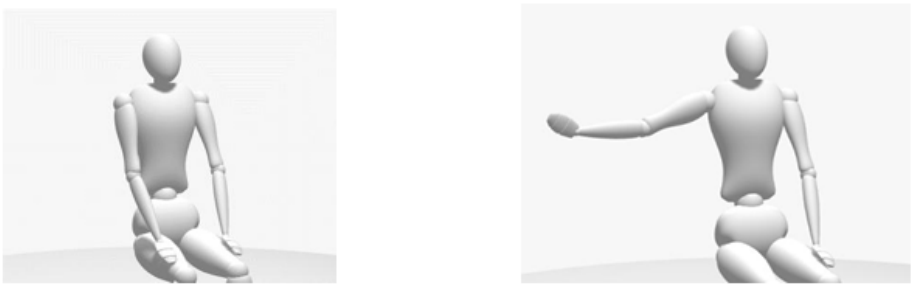

(a) (b)

Figure 55 (a) The initial sitting position of subject; (b) The arm of subject moving to stretch the chest[74].

In order to accurately measure the effect of skin stretching on capaciflector capacitance, the specific actions of the subjects were specified in the experiment. The subjects were required to perform movements according to a metronome rhythm of 28 beats per minute to control the consistency of skin stretching. To avoid any motion artifacts during breathing, subjects were required to sit firmly in a chair before the experiment began. The experimental steps are as follows:

1. inhale;
2. exhale;
3. without inhaling, swing your arms back to stretch the chest skin;
4. return the arm to its original position;
5. return to step 1.

One set of experiments lasts about 75 seconds, and a total of 4 sets of experiments are performed.

5.3 Test subjects

In order to ensure the general applicability of the experimental data, 10 volunteers were recruited to participate in this study. Recruitment criteria required volunteers to have no skin or lung disease. However, given that the experimental equipment is mainly installed in the chest area, this experiment is temporarily limited to male volunteers.

In terms of ethics approvals, this experiment was approved online by the Ethics and Research Governance Team, Faculty of Engineering and Physical Sciences, University of Southampton, UK (ERGO II, project 81239).

Table 16 Body information of experiment participants

Subject number	**Height (cm)**	**Weight (kg)**	**Age**	**Gender**	**BMI**
1	174	80	28	Male	26.4
2	170	63	25	Male	21.7
3	171	58	26	Male	19.8
4	173	64	33	Male	21.3
5	180	88	22	Male	27.1
6	185	105	18	Male	30.6
7	176	70	28	Male	22.5
8	176	103	23	Male	33.2
9	188	90	26	Male	25.4
10	174	70	29	Male	23.1

5.4 Result

Figure 56 shows typical measurements from a subject over one minute. The spikes in the figure correspond to independent breathing and skin stretching events respectively, where the first spike represents an independent breathing signal, the second spike represents an independent skin stretching signal, and subsequent spikes are arranged in this order. Red circles mark local maxima of the signal, indicating the end points of breathing and stretching actions; blue circles mark local minima, marking the start points of these events.

By comparing the data from the stretch sensor and the capaciflector, it can be observed that the capaciflector effectively captures the events of breathing and skin stretching, and that both events have similar effects on the electrical properties of the skin. Specifically, both activities caused changes in capacitance, which ranged from approximately 0.01pF to 0.1pF, and in both cases the capacitance increased. Given that the expansion of the chest during breathing does cause small deformations of the skin, it can be inferred that capaciflector is able to capture respiratory signals by monitoring local deformations of the skin during breathing.

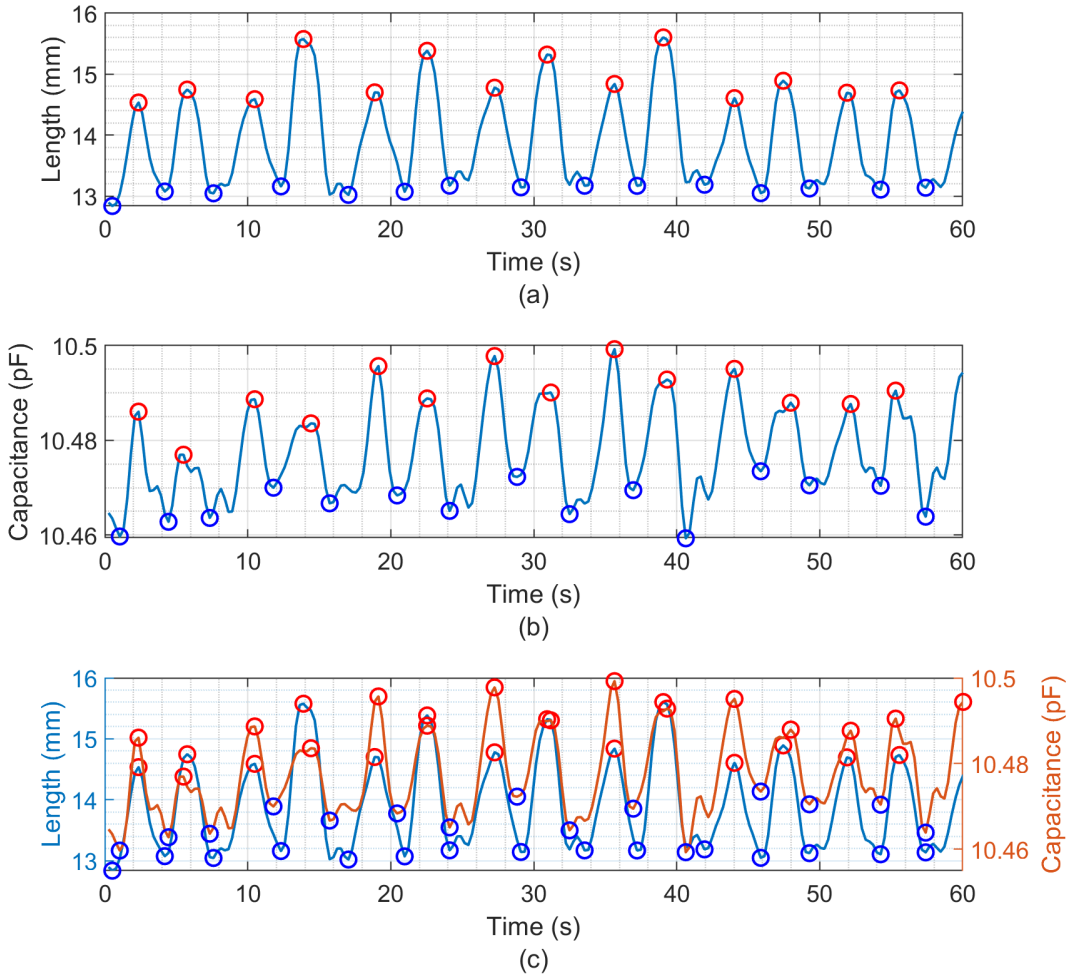

Figure 56 Respiration and skin stretch test results: (a) Reference stretch sensor data; (b) capaciflector data; (c) Comparison of the two measurement results.

In order to verify the consistency between different individuals, this study conducted a detailed analysis of the data measured by each subject using the capaciflector and the reference stretch sensor. The core of the analysis is to observe and compare the time difference between the end moments of breathing and skin stretching activities recorded by the two sensors (i.e., local maximum values). The mean and standard deviation of these time differences were calculated. As a complementary comparison, the actual duration of the inhalation and skin stretching behaviors was also measured by analysing the time difference between local maxima and minima. Based on a metronome of 28 beats per minute, the theoretical duration of the inhale and stretch is expected to be approximately 2 seconds.

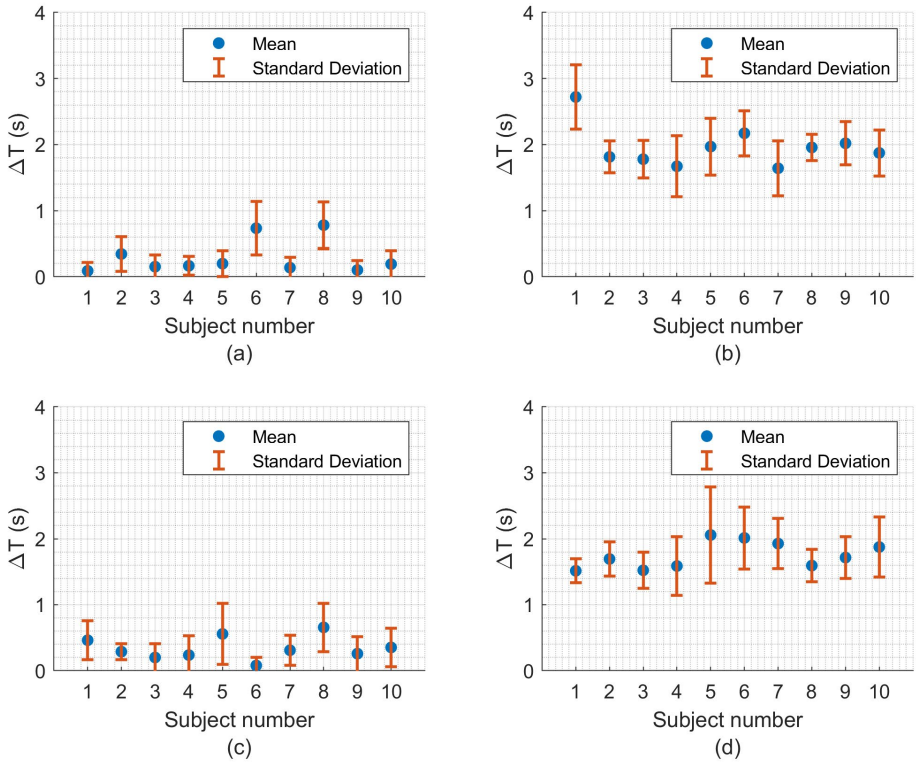

Figure 57 (a) Time difference of local maximum for breath. (b) Time difference between period of inhalation. (c) Time difference of local maximum for stretch. (d) Time difference between period of stretch.

Figure 57 presents summary statistics of measurement data from 10 subjects, where each data point reflects the average of 35 activities for each subject (here each breath and each skin stretch are considered a single event). The analysis results revealed good synchronization between the capaciflector and the reference stretch sensor in capturing inspiratory and skin stretch activities. The average time difference between recorded activity end points remained within 0.5 seconds for both breathing and skin stretching activities. In addition, by comparing the duration of inhalation movements and chest stretching behaviours, it was also found that the 10 subjects showed consistent patterns in these activities. This result further supports the theoretical assumption that capaciflector can effectively capture respiratory signals by monitoring skin stretching activities.

5.5 Discussion

Experimental results showed that when performing inhalation or skin stretching activities alone, the capacitance of the capaciflector used by all 10 subjects showed an increase, and the

magnitude of the capacitance changes produced were concentrated in the range of 0.01 to 0.1pF. Therefore, it can be inferred that capaciflector can effectively capture respiratory signals by monitoring the deformation of the skin during breathing.

Biological tissues, especially skin, as a complex dielectric composed of a variety of materials with different electrical properties, mainly experience interfacial polarization under the action of external AC electric fields. This phenomenon mainly occurs at the junction of materials with different electrical properties, such as charge accumulation between cell membranes and cell fluids[75]. Strain-induced material deformation causes these interface regions to move spatially, causing changes in the material's effective dielectric constant and conductivity[72].

Given that the internal structure of the skin contains conductive cell fluids, charged protein macromolecules, non-conductive cell membranes, and collagen fibres, these complex interfaces may drift under strain. However, it is not yet understood exactly how these interfacial drifts lead to increased capacitance. In order to fully explain this phenomenon, more in-depth simulation studies are necessary. These studies should start from the structural characteristics of the dielectric and establish detailed models, rather than relying solely on dielectric mixing theory based on material composition to build effective dielectric models.

Current measurement systems are not yet able to accurately obtain the numerical relationship between skin stretch and capacitance changes from experimental data, mainly due to two limiting factors: first, the two sensors used are of different sizes; second, their measurement locations in the chest area There are also differences. Although the chest area is relatively flat, skin stretching caused by arm activity does not necessarily affect the area covered by the two sensors evenly in each movement, potentially leading to inconsistencies in the degree of deformation.

In addition, according to the experimental results, due to the limited degree of deformation, the capacitance change range is between 0.01 and 0.1pF. Although the signal is clear, the system may still be affected by electronic noise during long-term measurements. Furthermore, the principle of using skin deformation to obtain respiratory signals shows that the signal is likely to be significantly affected by motion artifacts, and further research is needed to circumvent this effect.

It is also worth noting that the dielectric constant and conductivity of the skin are frequency dependent, so the measurement sensitivity can be adjusted by adjusting the frequency of the sensor excitation electrodes. At the same time, the sensitivity of the capacitive sensor is also related to the range of the fringe electric field generated by it. The measurement sensitivity can also be affected by adjusting the sensor size.

Chapter 6 Effect of working frequency on capaciance-based respiration measurement

6.1 Frequency dependent dielectric properties of human tissue

Human tissue is a complex dielectric, and its dielectric constant and conductivity significantly depend on frequency. The frequency dependence of the dielectric constant is mainly attributed to charge accumulation at the interface of materials with different electrical properties. The degree of charge accumulation is related to the period of the AC electric field: a longer period allows more charges to accumulate in the interface region, thus exhibiting a higher relative dielectric constant under low-frequency electric fields. On the contrary, under high-frequency electric fields, charge accumulation is reduced, resulting in a lower relative permittivity. In terms of electrical conductivity, the cell membrane of human tissue is similar to a capacitor. Its capacitive reactance decreases as the electric field frequency increases, so the impedance of the overall material decreases and the electrical conductivity increases.

Theoretically, strain-related dielectrics tend to exhibit more significant relative permittivity changes under low-frequency electric fields because more charges accumulate in the interface region of materials with different electrical properties. The sensor used in this study has been demonstrated in previous chapters to be able to capture respiratory signals by measuring local deformation of the skin. Therefore, low-frequency electric fields may theoretically have higher sensitivity. However, increasing the frequency increases the penetration depth of the electric field, extending the sensor's measurement range. Further experimental studies are required to fully understand the effect of frequency on measurement sensitivity.

6.2 Experiment setup and test protocol

The test objective of this chapter is to study the effect of operating frequency on the sensitivity of the capaciflector. By measuring breathing at different frequencies, the effect of frequency change on the sensitivity of the sensor is observed, and whether there is an optimal operating frequency is explored.

Based on previous experiments, this study further designed a variety of LC resonant circuits to produce different resonant frequencies, aiming to evaluate the sensitivity of the capaciflector at different operating frequencies. In specific practice, each LC resonant circuit with different

inductor and capacitor configurations corresponds to an independent capacitance measurement unit PCB. During the experiment, measurements at different frequencies were achieved by replacing these PCBs. Theoretically designed inductor and capacitor values, expected resonant frequencies, and set voltages are shown in Table 17.

Table 17 LC Tank Design and Resonance Frequency

Designed L (μH)	**Designed C (pF)**	**Designed Frequency (MHz)**	**Designed Vpk-pk (V)**
4.7	82	8.11	1.5
10	100	5.03	1.5
100	220	1.07	1.5
220	220	0.72	1.5
470	220	0.49	1.5
1000	470	0.23	1.5

There is a certain deviation between the actual capacitive and inductive components used and the theoretical values, so an impedance analyser (Wayne Kerr 6500B) is used to accurately measure them at their operating frequency to obtain the actual values, and then calculate the capacitance value of the capaciflector. The determination of the operating frequency and voltage configuration are achieved by measuring the excitation signal on the active shielding electrode. This measurement is completed using an oscilloscope (Agilent MSO7012B). The reason why active shielding electrodes are selected instead of direct measurement electrodes is because the oscilloscope probe itself has a capacitance of about 15pF. Direct connection to the sensing electrode will introduce additional capacitance, thus affecting the resonant frequency of the LC oscillation circuit and the voltage of the excitation signal. Since the active shield electrode is isolated from the LC oscillation circuit by a high-speed voltage buffer, measurements on the active shield electrode do not significantly affect the resonant frequency and voltage. After obtaining the actual operating frequency of each design, the values of the capacitance and inductance components can be measured accordingly. Specific measurement results are shown in Table 18.

Table 18 The actual inductance (L) and capacitance (C) in the LC oscillation circuit and their resonant frequency

Measured L (μH)	**Measured C (pF)**	**Measured Frequency (MHz)**	**I_drive code for FDC2214**	**Vpk-pk (V)**
5.358	81.81	7.41	0x48	1.53
10.808	106.29	4.54	0x40	1.59
104.51	224.81	1.03	0x50	1.66
230.66	223.36	0.687	0x38	1.56
503.06	222.58	0.465	0x20	1.56
1022.57	474.2	0.226	0x30	1.52

During the experiment, a metronome of 28 beats per minute was continued to be used to control the subject's breathing rhythm. The subjects were instructed to inhale when they heard one beat, exhale when they heard the next beat, and then repeat the process. Each set of tests lasted approximately 75 seconds to ensure adequate data collection. In order to improve the reliability of the data, the experiment was repeated three times at each frequency point, thereby collecting a total of approximately 50 independent respiratory signal samples at each frequency point for subsequent statistical analysis. The subjects in this experiment were the same as those in the previous chapter. In order to reduce the impact of the experimental order on the results, a different experimental order was adopted: odd-numbered subjects performed the experiment from high frequency to low frequency, while even-numbered subjects performed the experiment from low frequency to high frequency.

6.3 Result

Figure 58 below shows typical data from Subject 2 over a 60 second measurement period using the capaciflector operating at 1MHz. The red circles in the figure mark the local maximum points based on analysis of the reference stretch sensor data, representing the end of inhalation, while the blue circles mark the local minimum points, representing the start of inhalation. It is worth noting that capaciflector uses the moments corresponding to the local maxima and minima of the stretch sensor data as markers during analysis. The analysis of this method shows that, although there are some small deviations, the local extreme points recorded by the stretch

sensor are in most cases suitable for identifying the corresponding extreme points in the capaciflector measurement data. These small deviations often have insignificant effects on the overall results.

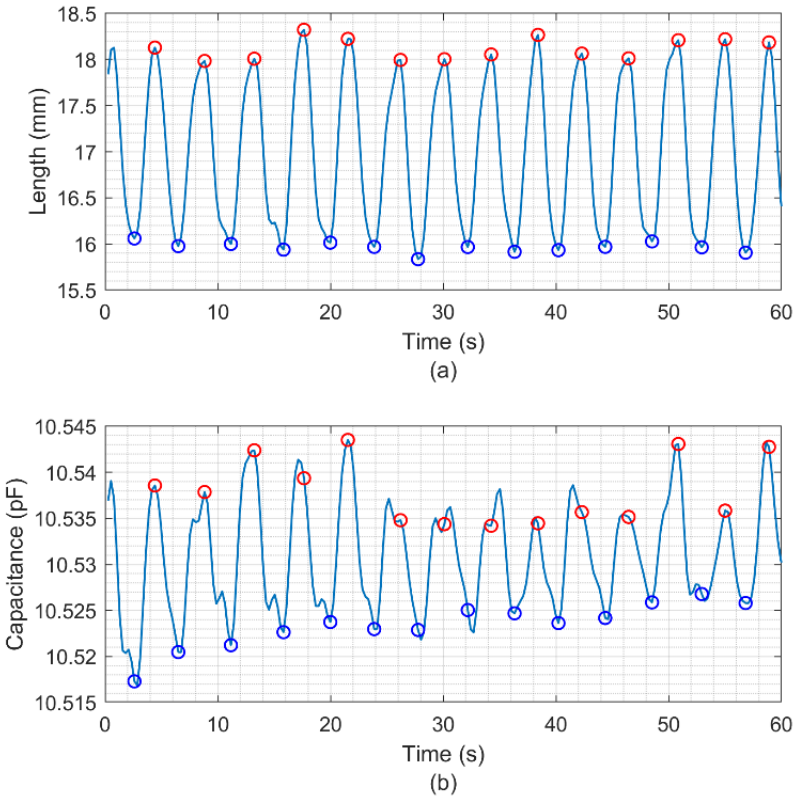

Figure 58 Respiration measurement results: (a) reference stretch sensor (b) capaciflector

By calculating the difference between local maxima and minima, the stretch changes and capacitance changes caused by inhalation can be quantified. This reflects the sensitivity of both sensors to breathing. The sensitivity data at all frequencies were statistically analysed and presented as box plots.

Figure 59 shows the trend of sensitivity changes in the operating frequency range of 200kHz to 7MHz when subject 1 was measured using the capaciflector. Figure 59 (a) presents the raw capacitance data, while Figure 59 (b) shows the normalized sensitivity trend. In this study, normalization is achieved by dividing the sensitivity data at each frequency point by the maximum sensitivity value across the entire frequency range, thus scaling the data to the range of 0 to 1. At the same time, the proportional relationship of the original data is maintained. The black circle in Figure 59 represents the median of each set of data, representing the typical sensitivity value at that frequency point. The trend shown shows that there is no clear linear relationship in sensitivity as a function of frequency. Although the sensitivity at the 200kHz

frequency is slightly higher than other frequencies, the difference is within 2 times. Taking into account the possible effects of breathing intensity, this difference is not enough to prove that the 200kHz frequency has better performance.

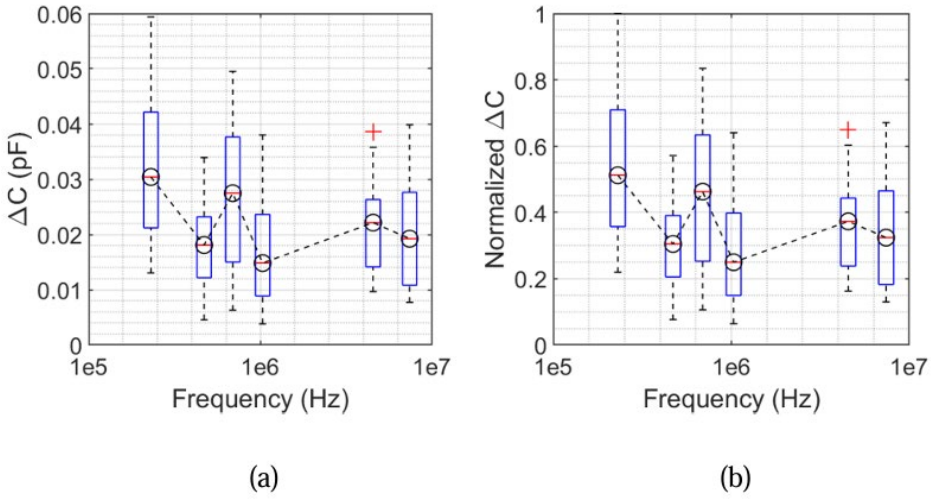

Figure 59 Comparison of capaciflector measurements on Subject 1 at different working frequencies: (a) Original capacitance change; (b) Normalized capacitance change

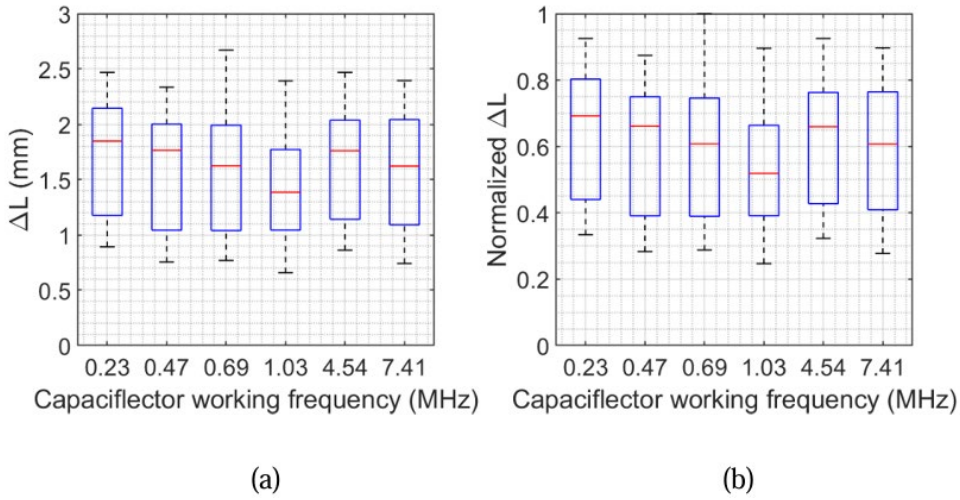

Figure 60 Comparison of reference stretch sensor measurements on Subject 1 at corresponding working frequencies of capaciflector: (a) Original length change; (b) Normalized length change

Figure 60 shows the measurement statistics of the reference stretch sensor at the corresponding operating frequency of the capaciflector. Figure 60 (a) shows that when performing the breath test at a lower frequency, the breath intensity is relatively higher, but the difference is only within a factor of 1.4, although this could potentially affect the measurement results. Figure 60 (b) shows the normalized data, that is, by dividing the data of each frequency point by the maximum value of all frequency measurement data. The numerical range is scaled to 0 to 1 to

facilitate subsequent comparison and statistical analysis. However, measurements from a single subject are not sufficient to generalize the overall picture. The trends of the normalized capacitance change sensitivity as a function of frequency for the 10 subjects are compared in Figure 61. The numerical relationship between capacitance changes and stretch length changes was not clearly defined in the current study, so it was not possible to compensate for the effect of different breathing intensities on capacitance change by scaling the stretch data.

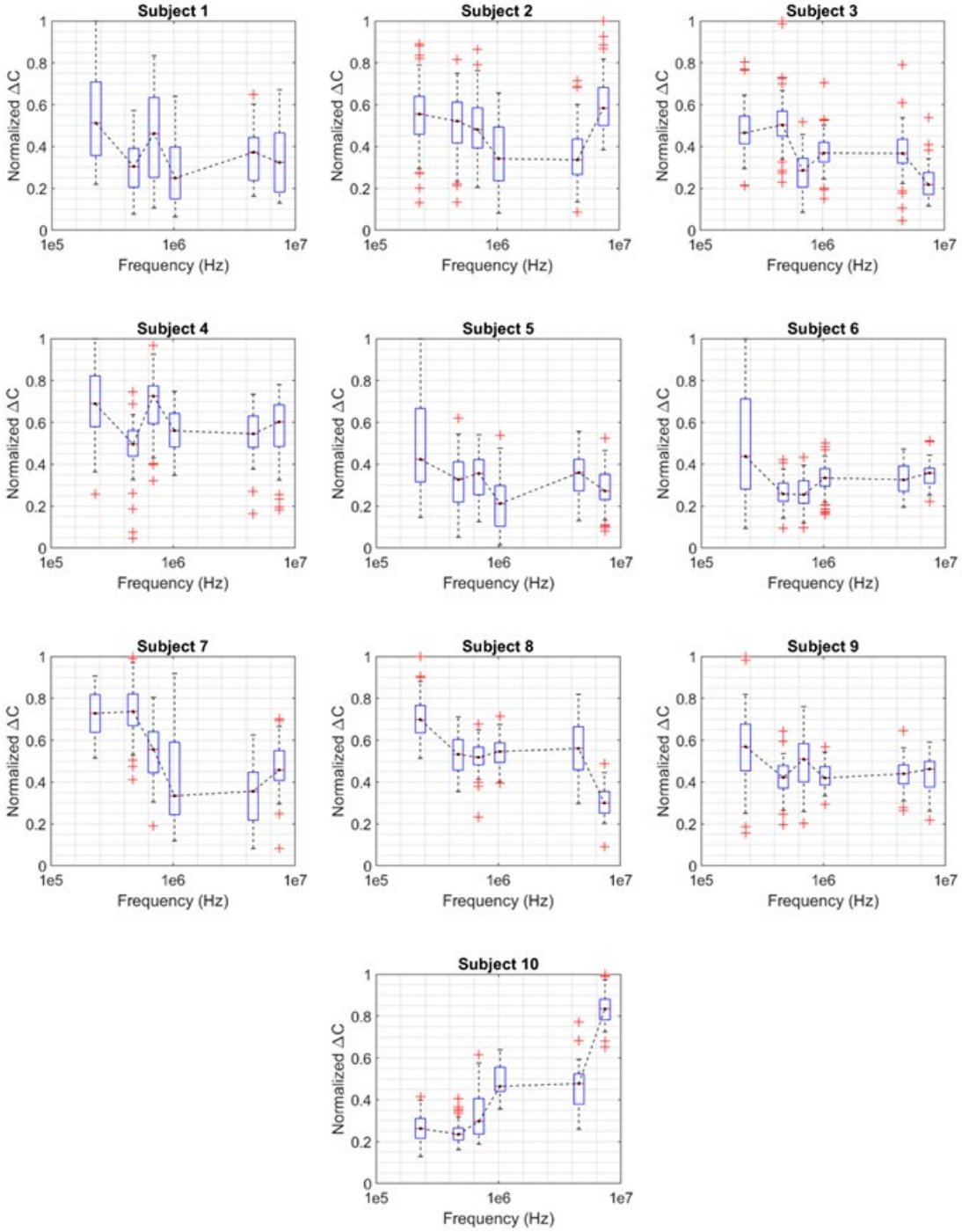

Figure 61 Normalized trends in the effect of frequency changes on respiration-induced capacitance changes: Subject 1 to 10.

According to Figure 61, most subjects have higher sensitivity under low frequency conditions. This phenomenon may be due to the fact that more charges are accumulated on the skin surface at lower frequencies, resulting in more obvious capacitance changes. In particular, subjects 8 and 9 showed the highest sensitivity at about 200 kHz. Subjects 1, 2, 4, and 5 showed higher sensitivity in the range of 200 kHz to 1 MHz. In contrast, subject 10 showed a trend of gradually increasing sensitivity with increasing frequency.

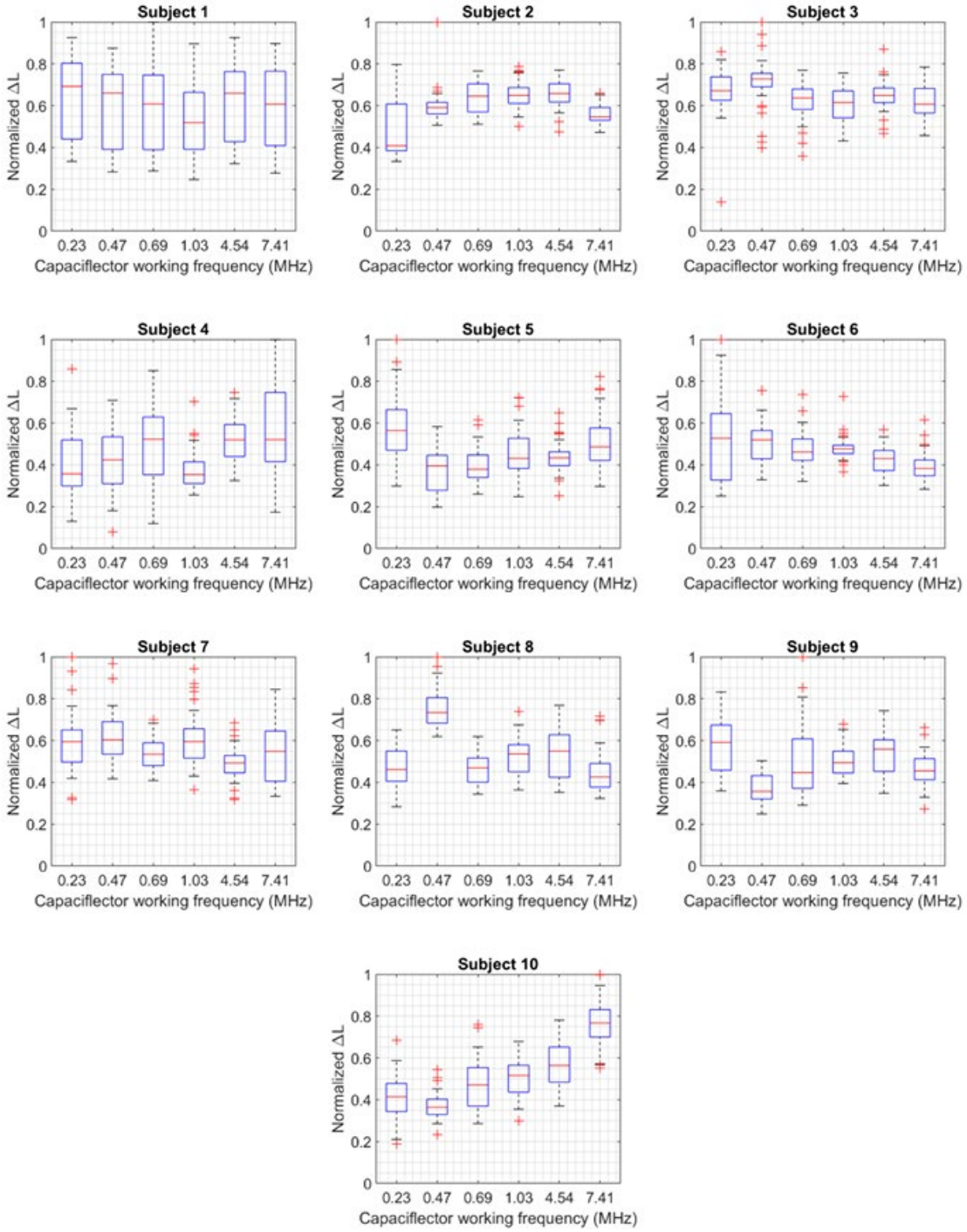

Figure 62 Normalized reference stretch sensor data: Subjects 1 to 10.

To explore whether these sensitivity changes are related to differences in breathing intensity, Figure 62 shows the normalized breathing intensity data measured by the reference stretch sensor at each frequency. Although these data are not directly used to correct the changes in breathing intensity in capacitance measurement, they can help analyse the potential impact of breathing intensity differences on sensitivity. For example, subject 10 had a larger inhalation intensity at high frequencies, which may have led to the phenomenon that its sensitivity increased with increasing frequency. The breathing intensity of other subjects remained relatively consistent at different frequencies. The median breathing intensity of most subjects was between 0.5 and 0.6, indicating that in these experiments, changes in breathing intensity had little effect on sensitivity, so the changes in sensitivity were mainly caused by changes in frequency.

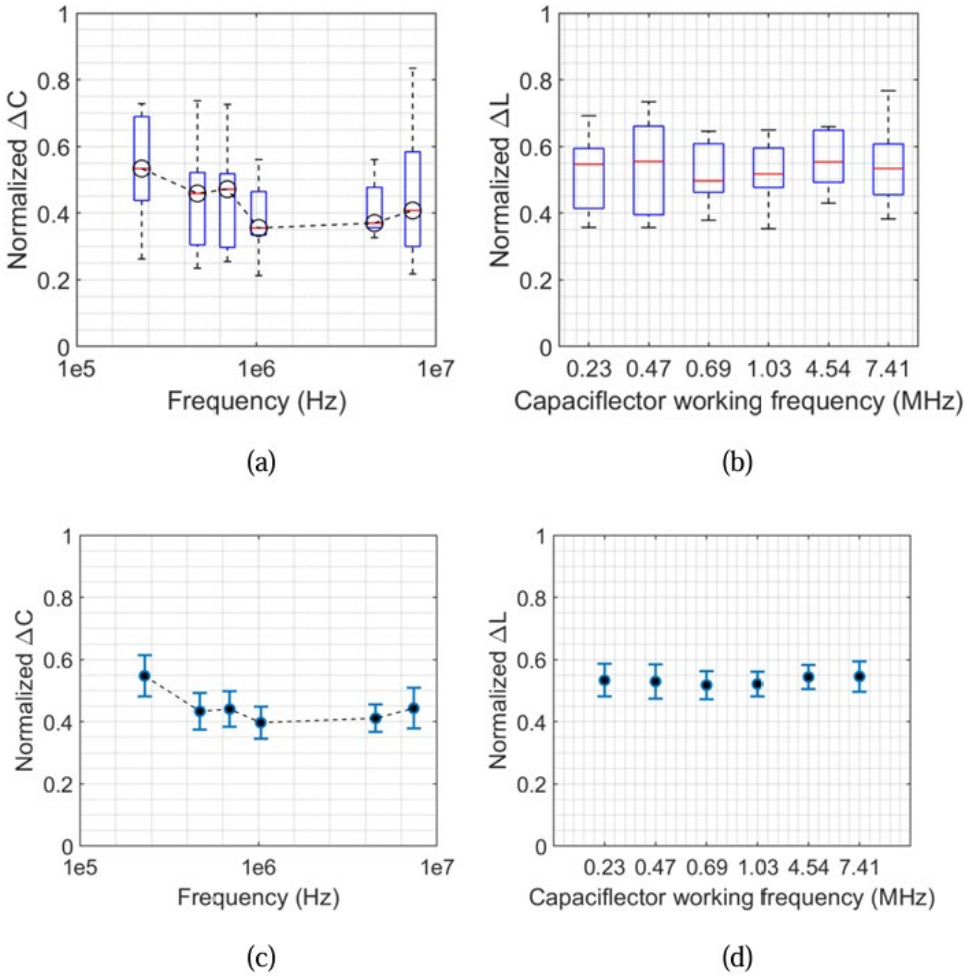

Figure 63 Statistics of the median of normalized data for 10 subjects: (a) boxplot for the normalized capacitance change; (b) boxplot for the normalized local length change; (c) mean and standard errors for the normalized capacitance change; (d) mean and standard errors for the normalized local length change.

By analysing the median of the normalized capacitance change data of 10 subjects, as shown Figure 63 (a) and (b), it can be found that the sensitivity of the capaciflector shows a gradual downward trend in the range of 200kHz to 1MHz, while in the range of 1MHz to 7MHz It shows a slight upward trend. However, the change amplitude of these two trends is not significant, and the change rate is within 1.2 times. At the same time, by observing the normalized data of the reference stretch sensor, the comprehensive statistical results of 10 subjects showed that the breathing intensity of most subjects did not fluctuate significantly during the test process at different capaciflector operating frequencies.

Figure 63 (c) and (d) compare the mean and standard error of the normalized sensitivity of all subjects at each frequency. It can be observed that, similar to the trend shown in the box plot, the sensitivity of the sensor shows a slight upward trend from high frequency to low frequency, with a change of about 1.2 times. The comparison results of the normalized stretch sensor also show that the breathing intensity of the subjects remained basically consistent during different experiments.

6.4 Discussion

The comprehensive test results of 10 subjects showed that in the frequency range from 200kHz to 7MHz, the sensitivity of the capaciflector to breathing first showed a downward trend before 1MHz, and then showed an upward trend between 1MHz and 7MHz. This phenomenon may be related to the frequency dependence of the electrical skin properties. At low frequencies, skin exhibits low electrical conductivity and high dielectric constant, while at high frequencies it exhibits high electrical conductivity and low dielectric constant. The electrical properties of biological tissues such as skin are closely related to their structure[73], including collagen and cell membranes that act as insulators, and intracellular and extracellular fluids that act as weak conductors. The applied alternating electric field polarizes the skin, mainly interfacial polarization. The insulator and conductor interface region experiences charge accumulation. Generally, charge accumulation is greater in low-frequency electric fields because more time can be used for accumulation[70]. Therefore, under similar skin deformation conditions, more interfacial accumulated charges can cause more capacitance changes[72].

Although the operating frequency has an impact on the sensitivity of the capaciflector in respiratory monitoring, this impact is relatively limited in the frequency range of 200kHz to 7MHz. The change amplitude of frequency on sensitivity is limited to within 1.2 times, which means the operating frequency has a slight effect on the sensor sensitivity. Using lower

frequencies has the potential to increase the sensitivity of the sensor. The small effect of frequency on sensitivity may be due to the fact that the electrical properties of skin tissue do not change significantly in the range of 200 kHz to 7 MHz[76].

In practical design, the selection of operating frequency should be mainly based on the specific needs of electronic equipment. It is worth noting that low-frequency operation requires less buffer performance for active shielding, while high-frequency operation requires the use of a high-speed op amp like the BUF602. In addition, high-frequency operation allows the use of smaller capacitors and inductors to build LC resonant circuits, making it possible to achieve higher capacitance resolution. This is because when the fixed capacitance in the LC tank circuit is small, small changes in capacitance will cause large changes in the resonant frequency, thereby improving the resolution of capacitance measurement. Therefore, it is recommended to perform measurements at high frequencies as it provides higher capacitance resolution and is more suitable for detecting weak respiratory signals.

The main limitation of the experiments is reflected in the limitation of the frequency range performed, which is mainly limited by the operating range of the FDC2214 capacitive-to-digital converter used, which can only operate between 10kHz and 10MHz. Resonant frequencies below 200kHz require the use of fixed capacitors greater than 470pF, which will result in the capacitance resolution of the measurement system being insufficient to resolve small capacitance changes of the order of 0.01pF to 0.1pF, making it impossible to clearly detect the respiratory signal, affecting data analysis. The upper limit of frequency is limited by the maximum 10MHz measurement capability of FDC2214, and in order to retain room for frequency variation, a frequency lower than 10MHz needs to be selected. Future studies could conduct experiments over a wider frequency range to more fully understand the effect of frequency on the sensitivity of capacitive respiration sensors.

Chapter 7 Effect of sensor electrode size on capacitance-based respiration measurement

7.1 Design of different capaciflector geometries

A special feature of the design of coplanar parallel plate capacitive sensors is that the size of the electrodes and the distance between them play a decisive role in the measurement. This is mainly because these parameters directly determine the distribution of the electric field. Normally, increasing the distance between electrodes can expand the measurement range of the sensor, but this may lead to a decrease in the electric field strength between the electrodes and negatively affect the sensitivity of the sensor. This means that in specific applications, it is crucial to properly adjust these parameters according to the location and characteristics of the object being measured. Considering the characteristics of human skin, the average thickness of the subcutaneous fat layer is about 11mm, and the total thickness of the epidermis and dermis is about 3mm. The changes in the effective dielectric constant and conductivity caused by the deformation of these layers can comprehensively reflect the skin deformation of the region. Therefore, adjusting the capaciflector's electrode dimensions, especially the length of the electrodes and the spacing between them, is expected to significantly affect its sensitivity to respiratory signal detection.

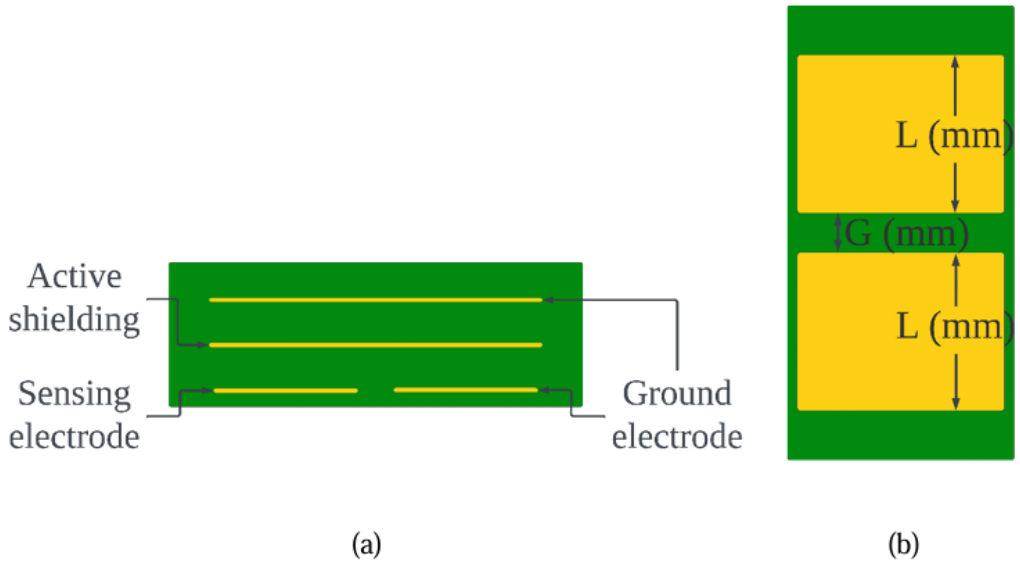

Figure 64 Schematic diagram of the structure of a coplanar parallel plate capacitive sensor with active shielding: (a) side view; (b) bottom view.

Figure 64 shows schematic diagrams of the different capaciflectors designed in this study. The design feature of these sensors is that their electrode length (L) and gap (G) are set to different sizes, while the electrode width remains consistent at 22.8 mm. 9 sensors of different designs were used in this experiment. In order to facilitate description and distinction, they are identified with specific IDs, such as: L12-G2, L12-G4, L12-G6, L16-G2, L16-G4, L16-G6, L20-G2, L20-G4 and L20- G6. The naming of these IDs reflects the structural parameters of each sensor. For example, L16-G4 indicates that the electrode length is 16mm and the electrode gap is 4mm. The experiments were designed to explore the specific impact of changes in electrode size on sensor performance, specifically differences in sensitivity when measuring respiratory signals.

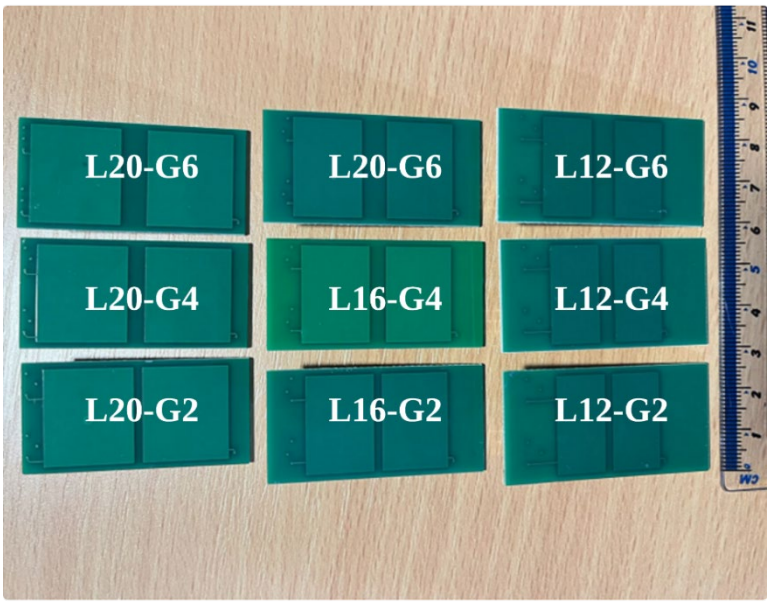

Figure 65 Different sizes of capaciflectors manufactured by JLCPCB

The sensors shown in Figure 65 are as follows: the first column (from top to bottom) is L20-G6, L20-G4, L20-G2; the second column (from top to bottom) is L16-G6, L16-G4, L16- G2; the third column (from top to bottom) is L12-G6, L12-G4, L12-G2.

7.2 Experiment setup and test protocol

The test objective of this chapter is to investigate the effect of sensing electrode size on the sensitivity of the capacitive reflector. By comparing the sensitivity of different electrode sizes, it is determined whether there is an optimised electrode design that can improve the detection of capacitance changes caused by breathing.

To evaluate the specific impact of different sensor designs on capaciflector sensitivity. Using the same capacitance measurement unit, the capaciflector was replaced several times to collect test data for various sensor configurations. The capacitance measurement unit used in the experiment fixed the operating frequency of the capaciflector at 1MHz. This setup is intended to ensure that the impact of other factors on the comparison results is minimized, allowing for a more accurate assessment of the specific impact of changes in electrode size and gap on sensor sensitivity.

The mounting position of the sensor remains the same as in the previous chapter. During the experiment, we continued to use a metronome of 28 beats per minute to standardize the subjects' breathing rhythm. Specifically, subjects were asked to inhale on each beat, exhale on the next beat, and continue this cycle. Each test round lasts approximately 75 seconds to ensure sufficient data can be collected. In order to improve the reliability and accuracy of the data, 3 replicate experiments were conducted for each sensor size configuration, resulting in a total of approximately 50 independent respiratory signal samples collected under each configuration, providing sufficient data for subsequent statistical analysis. data basis. The subjects in the experiment were the same as in the previous chapter. In order to reduce the possible impact of the experimental order, different experimental orders were adopted: odd-numbered subjects were in accordance with L20-G6, L20-G4, L20-G2, L16-G6, L16-G4, L16-G2, L12-G6, L12-G4, and L12-G2, while even-numbered subjects were performed in the reverse order.

7.3 Result

Figure 66 shows the typical measurement results recorded within 60 seconds by subject 1 when conducting experiments using the capaciflector with size ID L16-G4. The red circles in the figure mark the local maximum points based on analysis of the reference stretch sensor data, representing the end of inhalation, while the blue circles mark the local minimum points, representing the start of inhalation. It is worth noting that capaciflector uses the moments corresponding to the local maxima and minima of the stretch sensor data as markers during analysis. The analysis of this method shows that, although there are some small deviations, the local extreme points recorded by the stretch sensor are in most cases suitable for identifying the corresponding extreme points in the capaciflector measurement data. These small deviations often have insignificant effects on the overall results.

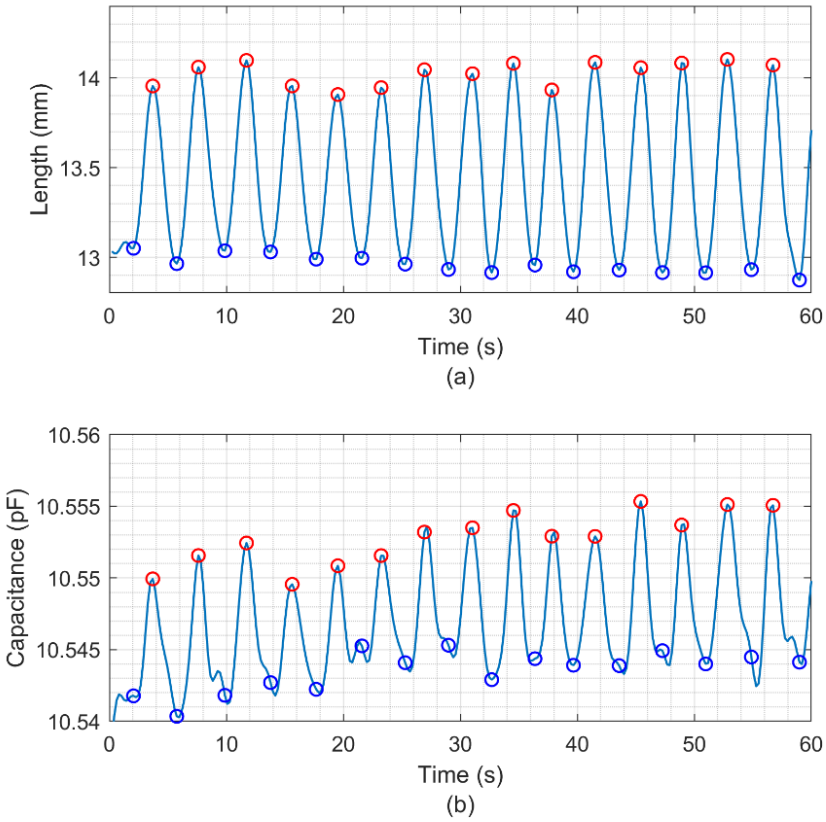

Figure 66 Respiration measurement results: (a) reference stretch sensor (b) capaciflector

By calculating the difference between local maxima and minima, the stretch changes and capacitance changes caused by inhalation can be quantified. This reflects the sensitivity of both sensors to breathing. The sensitivity data at all frequencies were statistically analysed and presented as box plots.

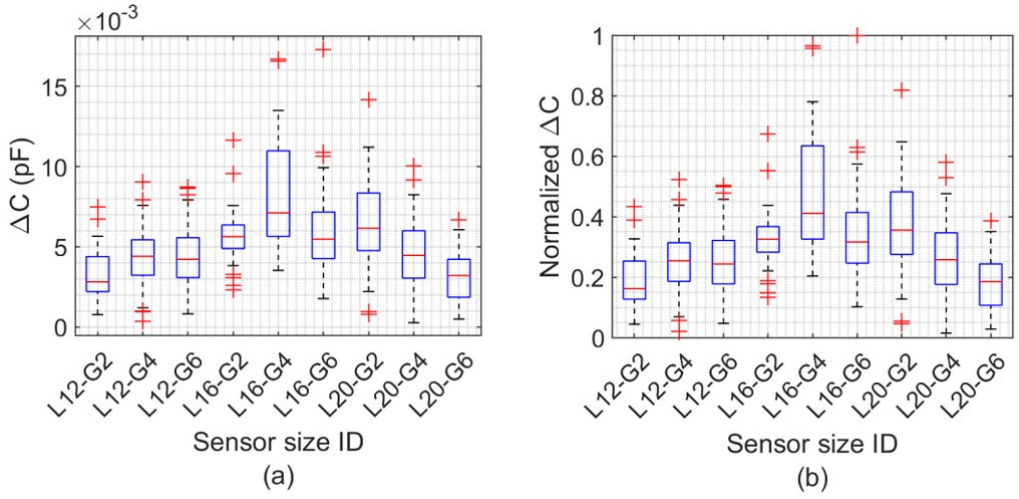

Figure 67 Comparison of capaciflector measurements on Subject 1 at different size of capaciflectors: (a) Original capacitance change; (b) Normalized capacitance change

Figure 67 shows the comparison of sensitivity when measuring using different sizes of capaciflector sensors. Figure 67 (a) presents the raw capacitance data recorded by sensors of various sizes, while Figure 67 (b) shows the normalized sensitivity of these data. Normalization is accomplished by dividing the sensitivity data at each frequency point by the maximum sensitivity value within the entire frequency range. This scales the data to the range of 0 to 1 while retaining the proportional relationship of the original data. Judging from the results, the l16-g4 size sensor performs higher sensitivity.

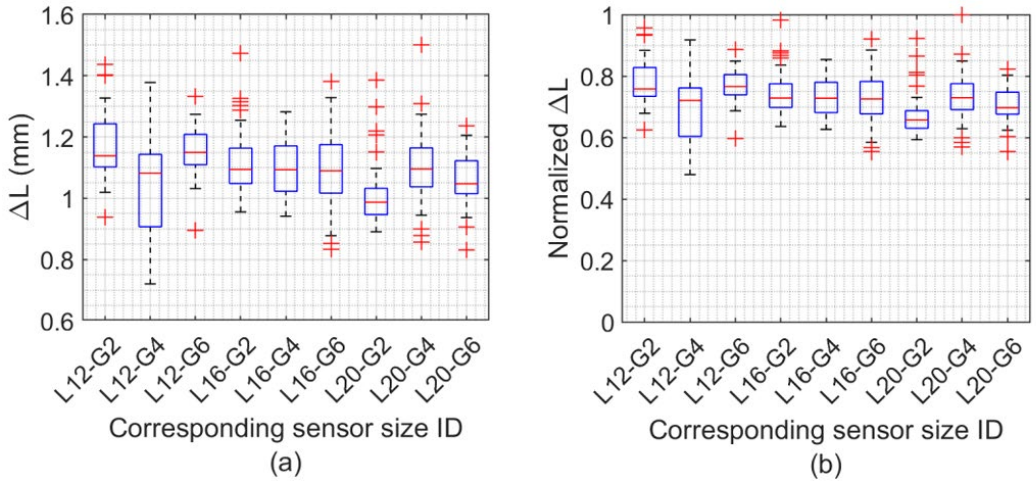

Figure 68 Comparison of reference stretch sensor measurements on Subject 1 at corresponding working frequencies of capaciflector: (a) Original length change; (b) Normalized length change

Figure 68 shows the statistical results of the data recorded by the reference stretch sensor when measuring capaciflector of different sizes. Figure 68 (a) presents the original data, while Figure 68 (b) shows the normalized data. Normalization is achieved by dividing the data at each frequency point by the maximum value among all frequency measurement data, thereby scaling the numerical range to 0 to 1 to facilitate subsequent comparison and statistical analysis. Overall, when conducting the L16-G4 size capaciflector experiment, the breathing intensity of the subjects was not significantly higher than that of other sizes. However, single subject results are not sufficient to prove the generalizability of this. Figure 69 also summarizes the data of 10 subjects, showing the comparison of the sensitivity of different sizes of capaciflector. The numerical relationship between capacitance changes and stretch length changes has not been clearly defined in the current study, so the normalization process of stretch data cannot be used to compensate for the effects of different breathing intensities on capacitance changes.

Figure 69 shows that for subjects 2, 3, 4, 7, 8, 9 and 10, when the capaciflector size is L16-G4, its sensitivity to respiratory signals is more significant compared to other designs. Although the capaciflector size L12-G2 also demonstrated higher sensitivity in tests with subjects 2, 4, and

9, But in tests with other subjects, the capaciflector using the L12-G2 size showed lower sensitivity. In particular, subject 5 had a higher breathing intensity when testing using the L20-G2, L20-G4 and L20-G8 size capaciflectors, which may lead to certain errors in his test data. In the case of Subject 6, although his breathing intensity remained consistent throughout the experiment, his measurements showed a distinctive pattern. In this subject's tests, the sensor's sensitivity seemed to decrease as the distance between the electrodes increased.

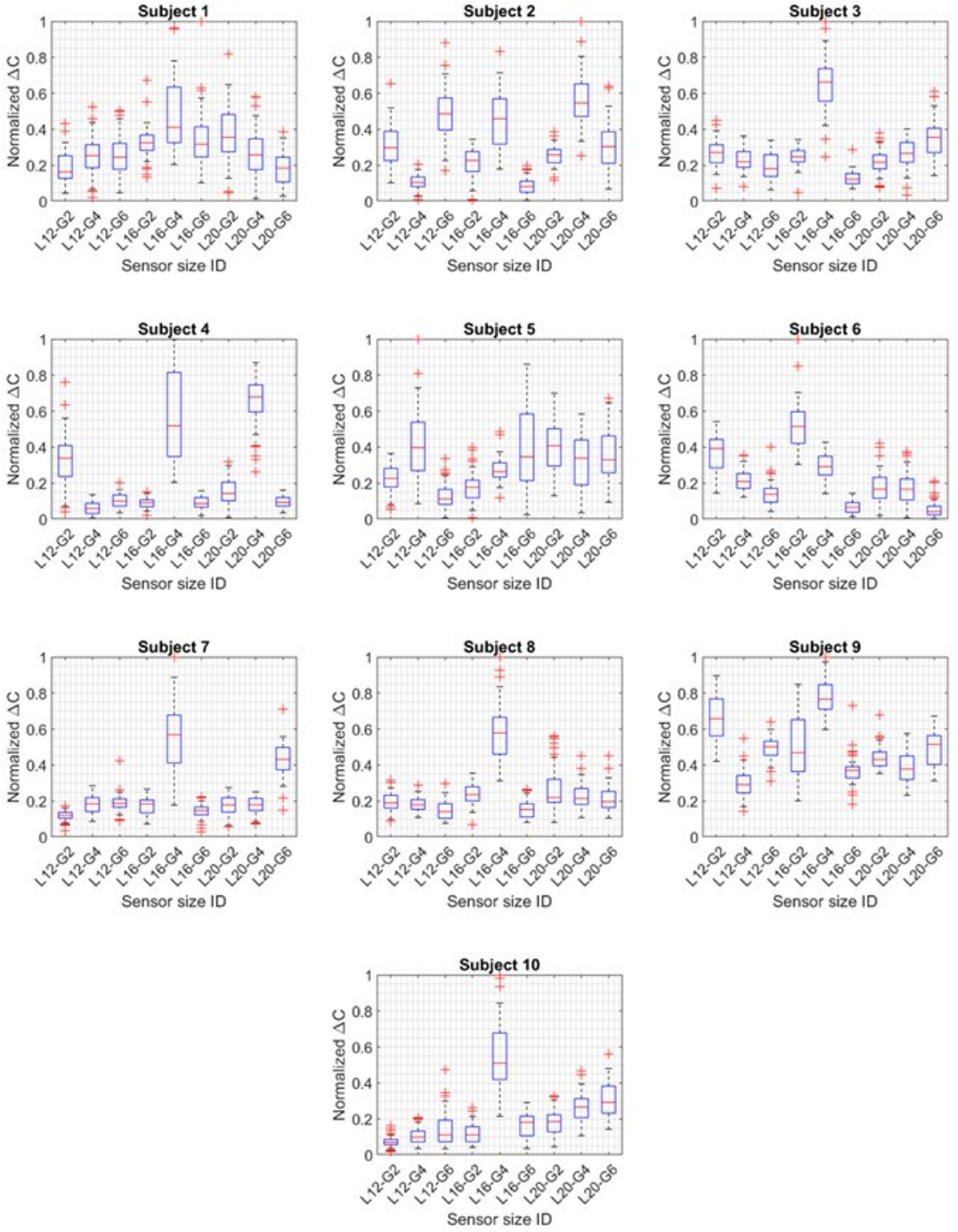

Figure 69 The effect of size for capaciflector on respiration-induced capacitance changes: Subject 1 to 10.

Figure 70 shows the data measured by 9 subjects using the reference stretch sensor. These data are mainly used to evaluate the breathing intensity during the test. Although these data cannot currently be used directly to compensate for differences in sensor capacitance changes due to different breathing intensities, they can help identify and eliminate possible sensor sensitivity errors caused by higher or lower breathing intensities.

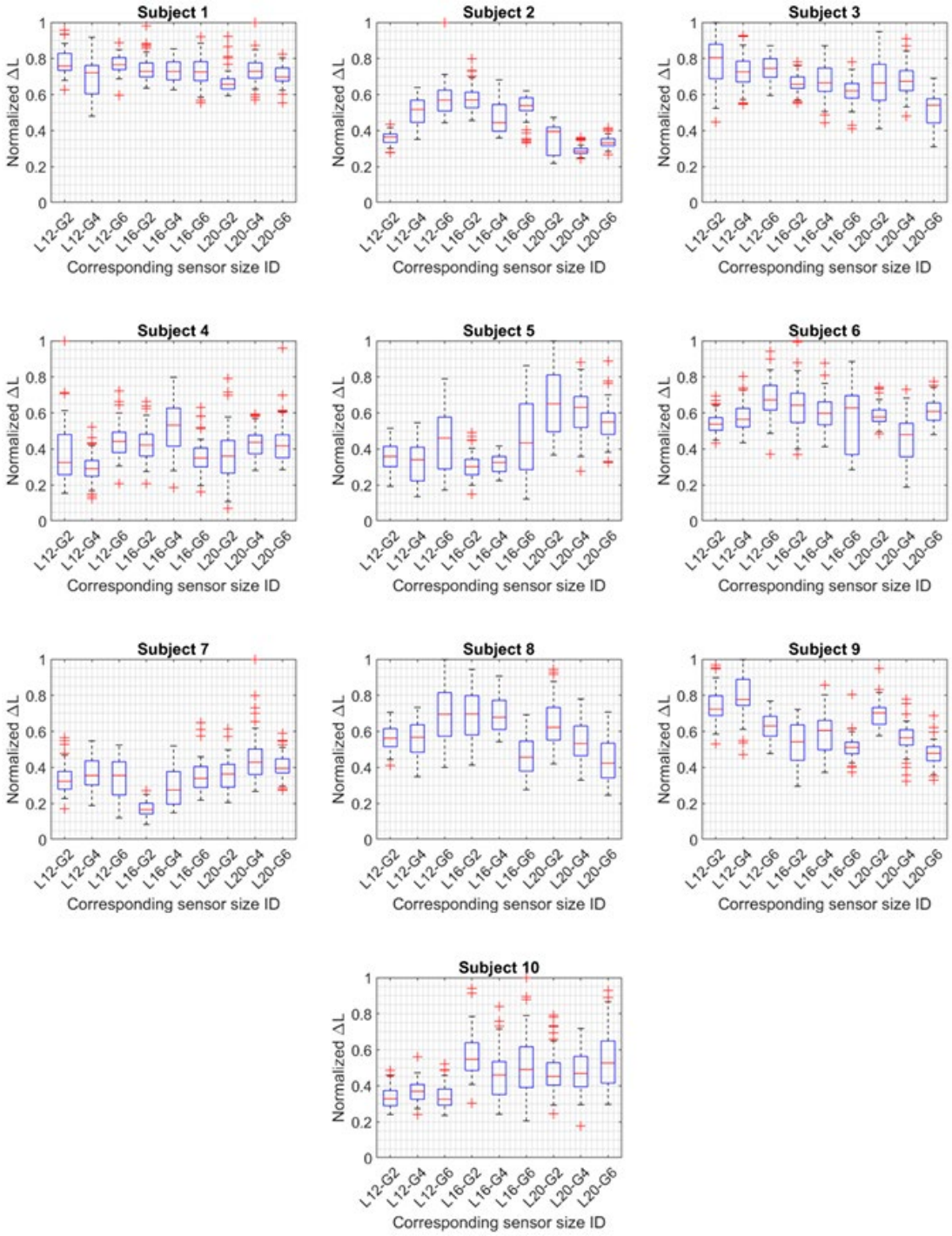

Figure 70 Normalized reference stretch sensor data: Subjects 1 to 10.

Figure 71 (a) and (b) the statistics of the median of the normalized capacitance change data of 10 subjects. It can be seen that the capaciflector with design L16-G4 exhibits relatively higher sensitivity overall, which is approximately twice that of other sizes. Statistics of normalized data from the reference stretch sensor showed that the breathing intensity of the vast majority of subjects remained stable during testing of different capaciflector sizes. The median of its normalized data is mainly concentrated between 0.4 and 0.6, indicating that the respiratory intensity does not fluctuate significantly during the test.

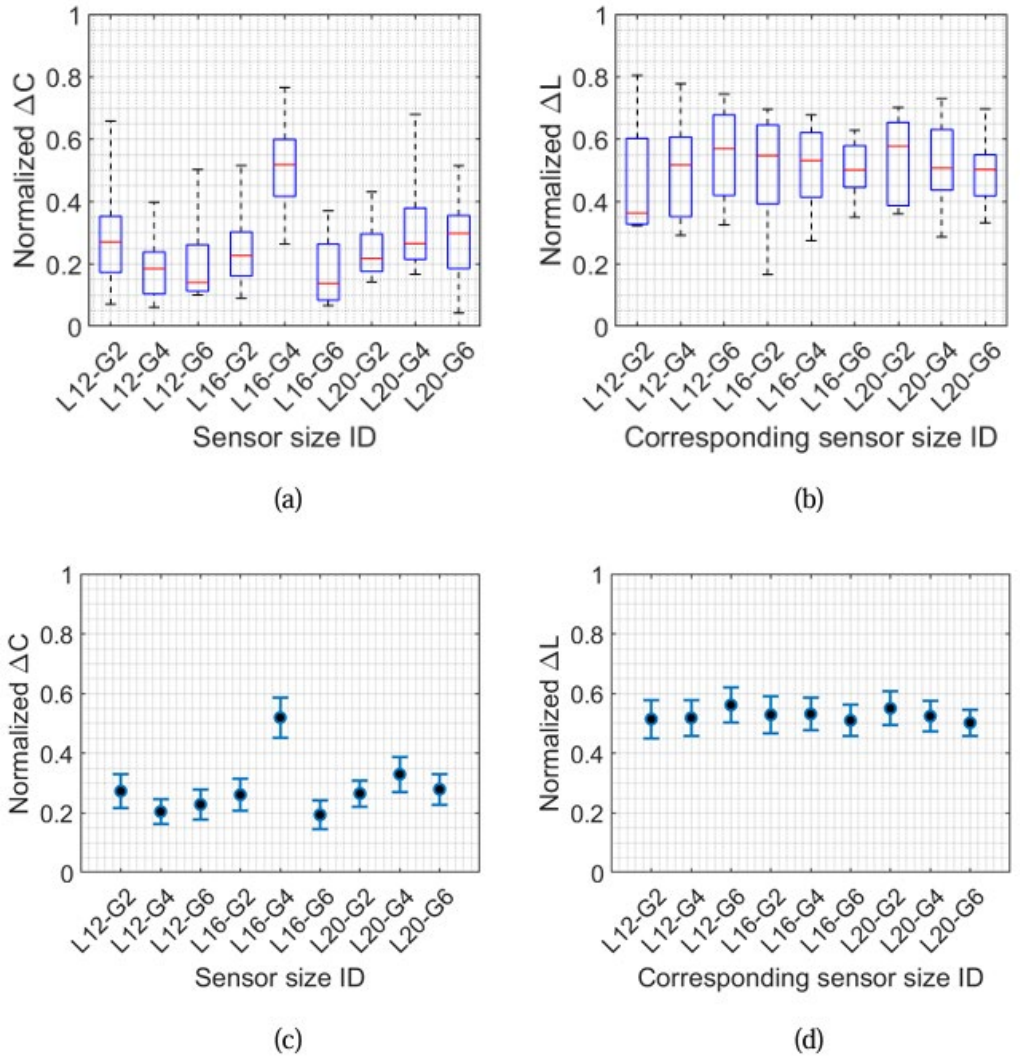

Figure 71 Statistics of the median of normalized data for 10 subjects: (a) boxplot for the normalized capacitance change; (b) boxplot for the normalized local length change; (c) mean and standard errors for the normalized capacitance change; (d) mean and standard errors for the normalized local length change.

Figure 71 (c) and (d) compare the mean and standard error of the normalized sensitivity of all subjects at each design. It can be observed that, similar to the data shown in the box plot, the L16-G4 design shows relative higher sensitivity. The comparison results of the normalized

stretch sensor also show that the breathing intensity of the subjects remained basically consistent during different experiments.

7.4 Discussion

The experimental results show that the electrode length and spacing have a certain effect on the sensitivity of the sensor, but the degree is relatively minor. The L16-G4 design shows relatively high sensitivity, which may be related to its optimised electrode size, which can produce suitable electric field strength and distribution. Changing the length and spacing of the electrodes will affect the characteristics of the electric field, thereby affecting the sensitivity of the sensor. However, based on the limited data available, this effect is not significant. Although the L16-G4 design has some potential in improving sensitivity, the experimental data based on only 10 subjects is not enough to clearly conclude that L16-G4 or L12-G2 is the best design, especially when considering individual differences. To further verify these findings, studies with larger sample sizes are needed. In addition, it is also important to explore factors that may cause these differences, such as skin characteristics and breathing patterns. By expanding the sample size and exploring other electrode configurations, it can help to determine a more generally applicable and effective design.

The higher sensitivity of the L16-G4 design may be related to its ability to produce a balanced electric field strength and distribution. This design may provide a more ideal detection range that can effectively capture deformations in both surface and deep tissues. Increasing the electrode size may expand the sensor's detection depth, but this may also reduce sensitivity to epidermal deformation. Conversely, reducing the electrode size can increase sensitivity to epidermal deformation but limit the overall detection range.

In addition to design factors, the fluctuations in sensitivity of the L12-G2 design may suggest physiological differences between subjects. Individual differences such as skin thickness, moisture content, and breathing patterns may have a significant impact on sensor performance. Although the experimental conditions remain consistent, these physiological differences may still lead to variability in experimental results. Therefore, future studies should control these variables more precisely or analyse the impact of individual differences on the results through larger and more diverse samples. In addition, further exploring the specific effects of these physiological factors on sensor performance is crucial to developing more stable and widely applicable designs.

A significant limitation of the experiments is that only 9 different sensor sizes were used, preventing a full exploration of the relationship between electrode size and spacing and sensor sensitivity. In addition, this experiment has not examined the impact of sensor width on measurement results. Although increasing sensor width can usually expand its measurement area, it has a limited impact on depth detection, so it was not taken into account during the initial design of the experiment. In subsequent studies, sensors with longer electrode lengths and wider spacing can be used to verify whether deformation of deep tissue will have a different impact on sensor capacitance changes than shallow tissue. However, it is important to note that larger sized sensors may require a flexible design to accommodate the non-flat surface features of the human body. Rigid sensors may not lie flat against the skin when designed in large sizes, potentially introducing additional interference. Considering that the L16-G4 size sensor has been able to clearly capture breathing signals in experiments, a flexible breathing sensor similar to the size of a Band-Aid can be designed based on this size. Such a design will be in line with the trend of miniaturization of wearable sensors.

Moreover, a potential research direction is to analyse the relationship between individual breathing duration and capacitance changes. Lung capacity varies from individual to individual, which may affect the capacitance changes detected by the sensor. Future research may reveal the correlation between lung capacity and sensor capacitance changes by performing a detailed analysis of each subject's breathing duration. Such an analysis will not only help to better understand the impact of breathing patterns on sensor sensitivity, but also help optimise the design of sensors to make them more adaptable to individual differences. This direction may lead to discoveries about how physiological parameters affect sensor performance.

Chapter 8 Discussion

Table 19 Experimental findings and suggestions for sensor design optimisation

Chapter no.	**Experimental result**	**Findings**	**Suggestions**
5	Skin stretching experiments show that skin stretching alone can cause a capacitance increase similar to that caused by inhalation, with the capacitance change ranging from 0.01 to 0.1 pF.	Capacitive sensors can effectively capture breathing signals by monitoring skin deformation.	The discovery could lead to the miniaturization of sensors suitable for wearable applications, and future research could verify the applicability of the principle in other configurations.
6	In the range of 200kHz to 7MHz, the effect of frequency on the respiration sensitivity of the sensor is within 1.2 times.	Lower frequencies show potential that slight improve the sensitivity. However, due to its small impact the frequency selection can be adjusted based on the device requirements.	Higher frequencies can improve capacitance resolution, and future research should test over a wider frequency range to optimise sensor design.
7	The length and spacing of electrodes have a certain impact on sensor sensitivity. The L16-G4 design showed high sensitivity, but the existing data is insufficient to confirm that it is the optimal design. The sensitivity fluctuation of L12-G2 may be related to individual differences.	L16-G4 can detect both surface and deep tissue deformations due to its balanced electric field distribution. Individual differences have a significant impact on sensitivity.	Future work will require validation of these findings using larger sample sizes and controlling for variables such as skin properties and breathing patterns to improve sensor robustness.

The capaciflector in this study is a unidirectional projected capacitive sensor designed to be placed close to the skin surface of the chest, with the primary purpose of measuring respiratory activity. The working mechanism of the sensor is based on monitoring changes in the electrical properties of materials, such as changes in conductivity and relative permittivity, within the AC electric field it generates. In conventional designs, these sensors are usually equipped with larger capacitive electrodes (approximately 20cm x 20cm) in order to track the changes in electrical properties of the lungs during breathing and thereby capture respiratory signals[77]. However, in the process of pursuing higher wearing comfort, when the size of the sensor is reduced to about 5cm x 5cm, the coverage area of its detection electric field is also reduced, which may change its basic mechanism of capturing respiratory signals. In particular, considering that the electric field strength generated by the sensor decreases with distance, shallow human tissues, such as skin, may cause more significant changes in capacitance values while the dielectric properties remain unchanged. Experiments to verify this theoretical hypothesis are crucial for the design of projected capacitive respiration sensors, because differences in measurement principles will directly affect the size of the sensor electrodes and the selection of the operating frequency of its detection electric field.

During breathing, changes in the ribcage cause the surrounding skin to undergo squeeze and stretch deformations. Specifically, when inhaling, the expansion of the thorax causes the skin to deform; conversely, during exhalation, the contraction of the thorax and the elastic properties of the skin itself cause the skin to return to its original shape. Skin, as a complex dielectric, has an internal structure that undergoes interfacial polarization under the action of an alternating electric field, which makes the skin's dielectric constant and conductivity closely related to its strain state. Within the skin, charges accumulate under the influence of electric fields at the interfaces between components with different electrical properties. When the skin deforms, the spatial displacement of these microscopic interface areas causes changes in the macroscopic effective dielectric constant and conductivity of the skin.

According to the experimental results on skin stretch measurement in Chapter 5, it can be observed that skin stretch alone can cause a capacitance increase effect similar to that of inhalation, and the amplitude of the capacitance change is also in the range of 0.01 to 0.1pF. Combined with the simulation experiments conducted using capacitive sensors of similar sizes in Chapter 3, it was found that the spatial potential is mainly concentrated in the skin tissue area. These findings collectively support the view that capacitive sensors can effectively capture respiratory signals by monitoring the deformation of the skin. This measurement principle has an important impact on the electrode design of capacitive sensors, indicating that effective measurements can be achieved without designing large-size sensors and deep layer

tissue detection. This discovery facilitates the miniaturization of sensors, making them more suitable for wearable applications.

According to the experimental results of electrodes with different excitation frequencies in Chapter 6, it was found that in the range of 200kHz to 7MHz, the impact of the excitation frequency on the sensor's respiratory sensitivity is within 1.2 times. This finding suggests that operating frequency has a slight impact on the extent of capacitance changes caused by breathing. The lower frequencies have the potential to slightly increase sensor sensitivity. However, due to the relatively small impact, currently the selection of frequency can be relative more determined based on the requirement of the electronic device. For capacitance measurement equipment that relies on an LC resonant circuit, a higher operating frequency allows the use of smaller values of capacitive and inductive components to construct the LC resonant circuit. This can improve the capacitive resolution of the device and enhance its ability to monitor weak respiratory signals. Experimental testing of frequency ranges other than 200kHz to 7MHz has not yet been carried out. This is mainly due to performance limitations of the FDC2214 capacitance measurement unit used. To conduct experiments over a wider frequency range, one would need to rely on other types of chips or specially customized circuit designs. Such extended experiments will help to more fully understand the impact of frequency on sensor performance and further optimise sensor design.

According to Chapter 7, experimental results show that electrode length and spacing have a certain impact on sensor sensitivity. The higher sensitivity of the L16-G4 design may be attributed to its optimised electrode size, which provides appropriate electric field distribution. Although adjusting the electrode length and spacing can affect the electric field characteristics, based on the available data, this effect is not significant. Although the L16-G4 design showed potential for improved sensitivity, data based on only 10 subjects was not sufficient to determine it as the optimal design. Taking into account individual physiological differences, further studies involving larger sample sizes are needed to validate these findings and explore the impact of factors such as skin characteristics and breathing patterns on sensitivity. The improved sensitivity of L16-G4 may be due to its more balanced electric field distribution, which can detect both surface layer and capture deformation of deep tissue. Increasing the size of the electrode may expand the detection depth, but reduce the sensitivity to the surface layer; reducing the size does the opposite. Additionally, sensitivity fluctuations in the L12-G2 design may reflect individual differences such as skin thickness and breathing patterns. Future studies should better control for these variables or use larger sample sizes to account for their effects.

This discovery provides a new perspective on the design of capacitive sensors, especially in dealing with temperature and humidity drift caused by environmental factors. If the sensitivity

to respiration can be significantly affected by fine-tuning the electrode size, while the response to changes in temperature and humidity is small or relatively fixed, then using the signal differences of electrodes of different sizes can effectively reduce the interference of environmental factors on monitoring data. This method can improve the accuracy and reliability of data by comparing and analysing the signals of two electrodes of different sizes, thereby maintaining stable sensor performance in complex environments.

A significant limitation in the experimental design is that the reference stretch sensor is approximately twice as long as the capaciflector used. Furthermore, taking into account avoiding measurement interference, the distance between the stretch sensor and the capaciflector was kept at approximately 2 cm. This configuration makes it impossible to accurately obtain the direct numerical correspondence between the local stretch length and the capacitance change, thus limiting the in-depth exploration of the measurement principle to some extent. To reduce the difference in local deformation measurements between the two sensors, future experiments could consider using smaller custom stretch sensors. This will help to more accurately study the relationship between skin deformation and capacitance changes, further improving the understanding of the effectiveness of respiratory activity monitoring.

Motion artifact is an important issue when monitoring respiratory activity, especially considering that the capaciflector primarily measures skin deformation. Movements of the body, especially the arms, can cause the skin to deform and become a source of interference. When the sensor is attached to the chest, capacitance changes caused by arm movement may be in the same magnitude range as capacitance changes caused by breathing, which may lead to signal confusion and misidentification of body movement signals as breathing signals. To solve this problem, one method is to mount an inertial measurement unit on the arm to track the angle between the arm and the torso, and then determine the specific location of the capacitance change caused by arm movement in the respiratory monitoring data[78]. This will allow the use of signal separation techniques such as independent component analysis to separate interference caused by arm movements from the breathing signal. An easier approach might be to mount the sensors in areas less affected by torso and arm movements.

Another major challenge when using capacitive sensors to measure respiratory signals based on skin deformation is that the capacitance changes caused by skin deformation are relatively small, typically in the range of 0.01pF to 0.1pF. Such small changes place high requirements on the resolution of the capacitor-to-digital converter. To increase sensitivity to respiration, an approach that has not yet been explored in this study is to increase the width of the electrodes. All experiments in this study used 22.5 mm wide sensing electrodes. Although the width itself has little effect on the penetration depth of the electric field, it mainly increases the lateral range

of the measurement, similar to the effect of multiple sets of sensing electrodes placed side by side. This can cover a wider measurement area. Since thoracic expansion caused by breathing can cause skin deformation across the chest region, measuring a wider area helps capture more capacitance changes. Therefore, in theory, increasing the electrode width may be an effective way to improve sensor sensitivity.

However, since the shape of the torso area is not completely flat, this may require the use of flexible sensors. However, since the shape of the torso area is not completely flat, this may require the use of flexible sensors. Using flexible sensors may also introduce new issues, such as the effect of sensor bending on capacitance. Therefore, further experiments and exploration are still needed to solve the problem of motion artifacts.

Chapter 9 Conclusion and future work

9.1 Conclusion

This study experimentally verified the measurement principle of capaciflector in respiratory monitoring and analysed the influence of its design parameters on its measurement sensitivity in wearable respiratory monitoring applications. The research results answered the preset research questions and the specific conclusions are as follows:

9.1.1 Verification of the measurement principle

According to the skin stretching experiment results in Chapter 5, skin stretching alone can cause a capacitance increase similar to inhalation, with a capacitance change amplitude between 0.01 and 0.1 pF. Combined with the simulation experiment in Chapter 3, it was found that the electric field is mainly concentrated in the skin tissue area. This finding verifies that skin deformation is the main factor causing capacitance change, and confirms the measurement principle that breathing signals can be effectively captured by monitoring skin deformation. This principle has an important impact on the electrode design of capacitive sensors, indicating that effective measurement can be achieved without designing large-size sensors, which helps to miniaturize the sensor and make it more suitable for wearable applications.

9.1.2 Effect of operating frequency on sensitivity

The experimental results in Chapter 6 show that in the range of 200kHz to 7MHz, the effect of the operating frequency on the respiration sensitivity of the sensor is within 1.2 times. This shows that lower frequencies have the potential to slightly increase sensor sensitivity. However, due to the effect is not significant, currently the operating frequency can be selected according to the specific needs of the electronic device. For capacitance measurement devices that rely on LC resonant circuits, higher operating frequencies allow the use of smaller capacitors and inductors to build LC resonant circuits, thereby improving the capacitance resolution of the device and enhancing its ability to monitor weak respiration signals. Future experiments can expand the frequency range to more fully understand the impact of frequency on sensor performance and further optimise sensor design.

9.1.3 Effect of electrode size on sensitivity

The experimental results in Chapter 7 show that electrode length and spacing have some effect on sensor sensitivity, and the L16-G4 design shows higher sensitivity, which may be attributed to its optimised electrode size and electric field distribution. However, the effect of adjusting electrode size and spacing on sensitivity may also be affected by individual physiological differences, such as skin thickness, breathing pattern, and hydration. These differences may cause the sensitivity of the sensor to vary among different subjects. The sensitivity fluctuations observed in the L12-G2 design may also reflect individual differences.

To better understand the relationship between electrode size and individual differences, future studies need to further explore the specific effects of these physiological factors on sensitivity through experiments with larger sample sizes. Larger-scale experiments will help optimise electrode design and ensure that the sensor has universal applicability and consistent performance in different individuals. This finding provides new ideas for the design of electrode size and will help improve the accuracy of sensors under different physiological conditions.

9.2 Future work

9.2.1 Use an inertial measurement unit (IMU) to reduce motion artifacts caused by arm movements

An inertial measurement unit (IMU) can measure acceleration and angular velocity and combine this data to calculate a specific angle[78]. In this study, the IMU was placed at the deltoid position, which can effectively track the angle between the upper arm and the trunk. The degree of skin stretching caused by arm movement is related to the angle between the arm and the torso. Therefore, by monitoring this angle, the signal generated by the arm movement can be identified. This can effectively weaken the motion artifacts caused by arm movement on the measurement results of the capacitive respiration sensor and improve the accuracy of the data.

9.2.2 Effect of increasing electrode width on respiratory sensitivity of capaciflector

The width of the electrodes has an important influence on the measuring range of the sensor. In future experiments, it is planned to use four different widths of coplanar parallel plate electrodes, namely 20mm, 40mm, 60mm and 80mm. These electrodes will be manufactured using a two-layer flexible PCB process while retaining the active shielding layer and removing the ground

plane. The next test will follow a similar process in Chapter 7 to explore whether a linear increase in electrode width can correspondingly linearly increase the sensor's sensitivity to respiration. This kind of testing is important for understanding how electrode width affects sensor performance, and can help further optimise the design of the sensor to make it more suitable for monitoring biological signals such as breathing.

9.2.3 Textile-based capaciflector

In order to explore the design of capacitive sensors that are more suitable for wear, in addition to the traditional screen-printing method, it is planned to try to use a new fabrication technology to made a fabric-based capaciflector. This method involves using multiple layers of finished weft-knitted conductive fabric. The specific method is to use thermal bonding technology to bond the conductive fabric to the insulating fabric on both sides to build the structure of the capaciflector[79]. The main advantage of using fabric electrodes is that it can greatly improve the overall wearing comfort, making the sensor more suitable for long-term wear, especially when continuous bio signals need to be monitored. In addition, the flexibility and adaptability of fabric electrodes also allow them to better fit irregular body surfaces, thereby improving measurement accuracy and reliability.

List of References

[1] M. A. Cretikos, R. Bellomo, K. Hillman, J. Chen, S. Finfer, and A. Flabouris, 'Respiratory rate: The neglected vital sign', *Medical Journal of Australia*, vol. 188, no. 11, pp. 657–659, 2008, doi: 10.5694/j.1326-5377.2008.tb01825.x.

[2] P. Contributors, 'Hypoxaemia', Physiopedia, . Accessed: Jul. 10, 2021. [Online]. Available: https://www.physio-pedia.com/index.php?title=Hypoxaemia&oldid=279660

[3] H. Liu, J. Allen, D. Zheng, and F. Chen, 'Recent development of respiratory rate measurement technologies', *Physiol Meas*, vol. 40, no. 7, p. 07TR01, Jul. 2019, doi: 10.1088/1361-6579/ab299e.

[4] I. Perez-Suarez *et al.*, 'Accuracy and Precision of the COSMED K5 Portable Analyser', *Front Physiol*, vol. 9, no. December, pp. 1–12, Dec. 2018, doi: 10.3389/fphys.2018.01764.

[5] P. Sharma, X. Hui, J. Zhou, T. B. Conroy, and E. C. Kan, 'Wearable radio-frequency sensing of respiratory rate, respiratory volume, and heart rate', *NPJ Digit Med*, vol. 3, no. 1, p. 98, Dec. 2020, doi: 10.1038/s41746-020-0307-6.

[6] C. Massaroni, A. Nicolò, D. Lo Presti, M. Sacchetti, S. Silvestri, and E. Schena, 'Contact-Based Methods for Measuring Respiratory Rate', *Sensors*, vol. 19, no. 4, p. 908, Feb. 2019, doi: 10.3390/s19040908.

[7] P. Y. Carry, P. Baconnier, A. Eberhard, P. Cotte, and G. Benchetrit, 'Evaluation of respiratory inductive plethysmography: Accuracy for analysis of respiratory waveforms', *Chest*, vol. 111, no. 4, pp. 910–915, 1997, doi: 10.1378/chest.111.4.910.

[8] J. E. Hall and A. C. Guyton, 'Pulmonary Ventilation', in *Guyton and Hall Textbook of Medical Physiology*, 12th, illust ed., R. Gruliow and L. Stingelin, Eds., Saunders/Elsevier, 2011, ch. 37, pp. 465–472.

[9] P. Aqueveque *et al.*, 'Simple wireless impedance pneumography system for unobtrusive sensing of respiration', *Sensors (Switzerland)*, vol. 20, no. 18, pp. 1–16, 2020, doi: 10.3390/s20185228.

[10] S. Ansari, K. R. Ward, and K. Najarian, 'Motion Artifact Suppression in Impedance Pneumography Signal for Portable Monitoring of Respiration: An Adaptive

Approach', *IEEE J Biomed Health Inform*, vol. 21, no. 2, pp. 387–398, 2017, doi: 10.1109/JBHI.2016.2524646.

[11] Dirk de Jager, 'Enabling Technologies for Distributed Body Sensor Networks', University of Southampton, 2012.

[12] N. M. White, J. Ash, Y. Wei, and H. Akerman, 'A Planar Respiration Sensor Based on a Capaciflector Structure', *IEEE Sens Lett*, vol. 1, no. 4, pp. 1–4, 2017, doi: 10.1109/LSENS.2017.2722481.

[13] N. Hayward *et al.*, 'A capaciflector provides continuous and accurate respiratory rate monitoring for patients at rest and during exercise', *J Clin Monit Comput*, vol. 36, no. 5, pp. 1535–1546, Oct. 2022, doi: 10.1007/s10877-021-00798-7.

[14] N. M. White, J. Ash, Y. Wei, and H. Akerman, 'A Planar Respiration Sensor Based on a Capaciflector Structure', *IEEE Sens Lett*, vol. 1, no. 4, pp. 1–4, Aug. 2017, doi: 10.1109/LSENS.2017.2722481.

[15] D. Wang, 'FDC1004 : Basics of Capacitive Sensing and Applications', 2014.

[16] X. Hu and W. Yang, 'Planar capacitive sensors – designs and applications', *Sensor Review*, vol. 30, no. 1, pp. 24–39, Jan. 2010, doi: 10.1108/02602281011010772.

[17] COMSOL Multiphysics, 'AC/DC Module User's Guide', 2018.

[18] T. Wartzek, S. Weyer, and S. Leonhardt, 'A differential capacitive electrical field sensor array for contactless measurement of respiratory rate', *Physiol Meas*, vol. 32, no. 10, pp. 1575–1590, 2011, doi: 10.1088/0967-3334/32/10/006.

[19] M. Iwamoto, 'Maxwell–Wagner Effect', in *Encyclopedia of Nanotechnology*, 2012, pp. 1276–1284. doi: 10.1007/978-90-481-9751-4_5.

[20] I. R. L. M. and Swa. M. JOHN M. VRANISH, '"CAPACIFLECTOR" COLLISION AVOIDANCE SENSORS FOR ROBOTS', *Computers Elect. Engn*, vol. 17, no. 3, pp. 173–179, 1991.

[21] Keysight Technologies, *Keysight Technologies Impedance Measurement Handbook A guide to measurement technology and techniques*. 2009.

[22] Texas Instruments, 'Relaxation Oscillator Circuit'. Accessed: Dec. 20, 2023. [Online]. Available: https://www.ti.com/lit/an/snoa998/snoa998.pdf

[23] Y. Yu, 'Resonance-Based Capacitive Sensing Using LDC2114', 2017.

[24] M. Cavagnaro, E. Pittella, and S. Pisa, ‘UWB pulse propagation into human tissues’, *Phys Med Biol*, vol. 58, no. 24, pp. 8689–8707, 2013, doi: 10.1088/0031-9155/58/24/8689.

[25] A. V. Korjenevsky, ‘Electric field tomography for contactless imaging of resistivity in biomedical applications’, *Physiol Meas*, vol. 25, no. 1, pp. 391–401, 2004, doi: 10.1088/0967-3334/25/1/042.

[26] S. K. Kundu, S. Kumagai, and M. Sasaki, ‘A wearable capacitive sensor for monitoring human respiratory rate’, *Jpn J Appl Phys*, vol. 52, no. 4 PART 2, pp. 0–7, 2013, doi: 10.7567/JJAP.52.04CL05.

[27] J. Cheng, O. Amft, G. Bahle, and P. Lukowicz, ‘Designing sensitive wearable capacitive sensors for activity recognition’, *IEEE Sens J*, vol. 13, no. 10, pp. 3935–3947, 2013, doi: 10.1109/JSEN.2013.2259693.

[28] M. Terazawa, M. Karita, S. Kumagai, and M. Sasaki, ‘Respiratory motion sensor measuring capacitance constructed across skin in daily activities’, *Micromachines (Basel)*, vol. 9, no. 11, pp. 2–9, 2018, doi: 10.3390/mi9110543.

[29] M. Terasawa, S. Kumagai, and M. Sasaki, ‘Frequency-response-based analysis of respiratory sensor measuring capacitance built across skin’, *Jpn J Appl Phys*, vol. 55, no. 4, pp. 0–6, 2016, doi: 10.7567/JJAP.55.04EM13.

[30] M. Karita, S. Kumagai, and M. Sasaki, ‘Respiration monitoring during 6 min walk using wearable sensor measuring capacitance built across skin’, *Jpn J Appl Phys*, vol. 61, no. SA, p. SA1010, Jan. 2022, doi: 10.35848/1347-4065/ac1e67.

[31] C. Massaroni *et al.*, ‘Respiratory Monitoring during Physical Activities with a Multi-Sensor Smart Garment and Related Algorithms’, *IEEE Sens J*, vol. 20, no. 4, pp. 2173–2180, 2020, doi: 10.1109/JSEN.2019.2949608.

[32] M. Chu *et al.*, ‘Respiration rate and volume measurements using wearable strain sensors’, *NPJ Digit Med*, vol. 2, no. 1, pp. 1–9, 2019, doi: 10.1038/s41746-019-0083-3.

[33] J. D. Pegan *et al.*, ‘Skin-mountable stretch sensor for wearable health monitoring’, *Nanoscale*, vol. 8, no. 39, pp. 17295–17303, 2016, doi: 10.1039/c6nr04467k.

[34] Y. Li *et al.*, ‘A soft polydimethylsiloxane liquid metal interdigitated capacitor sensor and its integration in a flexible hybrid system for on-body respiratory sensing’, *Materials*, vol. 12, no. 9, 2019, doi: 10.3390/ma12091458.

[35] G. Singh, A. Tee, T. Trakoolwilaiwan, A. Taha, and M. Olivo, ‘Method of respiratory rate measurement using a unique wearable platform and an adaptive optical-based approach’, *Intensive Care Med Exp*, vol. 8, no. 1, p. 15, Dec. 2020, doi: 10.1186/s40635-020-00302-6.

[36] F. Taffoni, D. Rivera, A. La Camera, A. Nicolò, J. R. Velasco, and C. Massaroni, ‘A Wearable System for Real-Time Continuous Monitoring of Physical Activity’, *J Healthc Eng*, vol. 2018, pp. 1–16, Mar. 2018, doi: 10.1155/2018/1878354.

[37] W. D. Bennett, K. L. Zeman, and A. M. Jarabek, ‘Nasal contribution to breathing with exercise: Effect of race and gender’, *J Appl Physiol*, vol. 95, no. 2, pp. 497–503, 2003, doi: 10.1152/japplphysiol.00718.2002.

[38] C. Massaroni *et al.*, ‘Validation of a Wearable Device and an Algorithm for Respiratory Monitoring During Exercise’, *IEEE Sens J*, vol. 19, no. 12, pp. 4652–4659, Jun. 2019, doi: 10.1109/JSEN.2019.2899658.

[39] D. Giavarina, ‘Understanding Bland Altman analysis’, *Biochem Med (Zagreb)*, vol. 25, no. 2, pp. 141–151, 2015, doi: 10.11613/BM.2015.015.

[40] T. Dinh *et al.*, ‘Environment-friendly carbon nanotube based flexible electronics for noninvasive and wearable healthcare’, *J Mater Chem C Mater*, vol. 4, no. 42, pp. 10061–10068, 2016, doi: 10.1039/c6tc02708c.

[41] P. Jiang, S. Zhao, and R. Zhu, ‘Smart sensing strip using monolithically integrated flexible flow sensor for noninvasively monitoring respiratory flow’, *Sensors (Switzerland)*, vol. 15, no. 12, pp. 31738–31750, 2015, doi: 10.3390/s151229881.

[42] P. Liu, R. Zhu, and R. Que, ‘A flexible flow sensor system and its characteristics for fluid mechanics measurements’, *Sensors*, vol. 9, no. 12, pp. 9533–9543, 2009, doi: 10.3390/s91209533.

[43] T. Jiang *et al.*, ‘Wearable breath monitoring via a hot-film/calorimetric airflow sensing system’, *Biosens Bioelectron*, vol. 163, no. May, p. 112288, 2020, doi: 10.1016/j.bios.2020.112288.

[44] T. Dinh *et al.*, 'Solvent-free fabrication of biodegradable hot-film flow sensor for noninvasive respiratory monitoring', *J Phys D Appl Phys*, vol. 50, no. 21, 2017, doi: 10.1088/1361-6463/aa6cd6.

[45] C. Occhiuzzi, C. Caccami, S. Amendola, and G. Marrocco, 'Breath-monitoring by means of Epidermal Temperature RFID Sensors', *2018 3rd International Conference on Smart and Sustainable Technologies, SpliTech 2018*, no. 1, 2018.

[46] F. Güder *et al.*, 'Paper-Based Electrical Respiration Sensor', *Angewandte Chemie - International Edition*, vol. 55, no. 19, pp. 5727–5732, 2016, doi: 10.1002/anie.201511805.

[47] R. Xie *et al.*, 'Wearable Leather-Based Electronics for Respiration Monitoring', *ACS Appl Bio Mater*, vol. 2, no. 4, pp. 1427–1431, 2019, doi: 10.1021/acsabm.9b00082.

[48] S. Borini *et al.*, 'Ultrafast Graphene Oxide Humidity Sensors', *ACS Nano*, vol. 7, no. 12, pp. 11166–11173, Dec. 2013, doi: 10.1021/nn404889b.

[49] M. C. Caccami, M. Y. S. Mulla, C. Di Natale, and G. Marrocco, 'Wireless monitoring of breath by means of a graphene oxide-based radiofrequency identification wearable sensor', *2017 11th European Conference on Antennas and Propagation, EUCAP 2017*, pp. 3394–3396, 2017, doi: 10.23919/EuCAP.2017.7928355.

[50] M. C. Caccami, M. Y. S. Mulla, C. Occhiuzzi, C. Di Natale, and G. Marrocco, 'Design and Experimentation of a Batteryless On-Skin RFID Graphene-Oxide Sensor for the Monitoring and Discrimination of Breath Anomalies', *IEEE Sens J*, vol. 18, no. 21, pp. 8893–8901, 2018, doi: 10.1109/JSEN.2018.2867208.

[51] G. Sierra, V. Telfort, B. Popov, L. G. Durand, R. Agarwal, and V. Lanzo, 'Monitoring respiratory rate based on tracheal sounds. First experiences', *Annual International Conference of the IEEE Engineering in Medicine and Biology - Proceedings*, vol. 26 I, pp. 317–320, 2004, doi: 10.1109/iembs.2004.1403156.

[52] Acurable, 'AcuPebble'. Accessed: Oct. 19, 2020. [Online]. Available: https://acurable.com/

[53] P. Corbishley and E. Rodríguez-Villegas, 'Breathing detection: Towards a miniaturized, wearable, battery-operated monitoring system', *IEEE Trans Biomed Eng*, vol. 55, no. 1, pp. 196–204, 2008, doi: 10.1109/TBME.2007.910679.

[54] G. Rodriguez-Villegas, Esther; Aguilar Pelaez, Eduardo; Chen, 'Feature characterization for breathing monitor', US10226225B2, 2011

[55] N. M. White and J. D. Turner, 'Thick-film sensors: past, present and future', *Meas Sci Technol*, vol. 8, no. 1, pp. 1–20, 1997.

[56] COMSOL Multiphysics, 'The Finite Element Methods (FEM)', Multiphysics Cyclopedia. Accessed: Aug. 20, 2021. [Online]. Available: https://www.comsol.com/multiphysics/finite-element-method?parent=physics-pdes-numerical-042-62

[57] C. Multiphysics, 'Computing the Effect of Fringing Fields on Capacitance'. Accessed: Aug. 20, 2021. [Online]. Available: https://uk.comsol.com/model/download/524141/models.acdc.capacitor_fringing_fields.pdf

[58] C. Gabriel, S. Gabriel, and E. Corthout, 'The dielectric properties of biological tissues: I. Literature survey', *Phys Med Biol*, vol. 41, no. 11, pp. 2231–2249, 1996, doi: 10.1088/0031-9155/41/11/001.

[59] C. Li, G. Guan, R. Reif, Z. Huang, and R. K. Wang, 'Determining elastic properties of skin by measuring surface waves from an impulse mechanical stimulus using phase-sensitive optical coherence tomography', *J R Soc Interface*, vol. 9, no. 70, pp. 831–841, 2012, doi: 10.1098/rsif.2011.0583.

[60] P. Nopp, E. Rapp, H. Pfutzner, H. Nakesch, and C. Rusham, 'Dielectric properties of lung tissue as a function of air content', *Phys Med Biol*, vol. 38, no. 6, pp. 699–716, 1993, doi: 10.1088/0031-9155/38/6/005.

[61] LEAP Technology, 'STRETCH SENSORS'. Accessed: Nov. 30, 2023. [Online]. Available: https://leaptechnology.com/

[62] A. A. Nassr, W. H. Ahmed, and W. W. El-Dakhakhni, 'Coplanar capacitance sensors for detecting water intrusion in composite structures', *Meas Sci Technol*, vol. 19, no. 7, p. 075702, Jul. 2008, doi: 10.1088/0957-0233/19/7/075702.

[63] Texas Instruments, 'FDC2x1x EMI-Resistant 28-Bit,12-Bit Capacitance-to-Digital Converter for Proximity and Level Sensing Applications'. Accessed: Dec. 01, 2023. [Online]. Available: https://www.ti.com/lit/ds/symlink/fdc2214.pdf

[64] F. Reverter, X. Li, and G. C. M. Meijer, ‘Stability and accuracy of active shielding for grounded capacitive sensors’, *Meas Sci Technol*, vol. 17, no. 11, pp. 2884–2890, Nov. 2006, doi: 10.1088/0957-0233/17/11/004.

[65] Texas Instruments, ‘High-Speed, Closed-Loop Buffer’. Accessed: Dec. 01, 2023. [Online]. Available: https://www.ti.com/lit/ds/symlink/buf602.pdf

[66] Adafruit, ‘Lithium Ion Polymer Battery - 3.7v’. Accessed: Dec. 02, 2023. [Online]. Available: https://www.adafruit.com/

[67] MathWorks, ‘MATLAB - Bluetooth Low Energy Communication’. Accessed: Dec. 07, 2023. [Online]. Available: https://uk.mathworks.com/help/matlab/bluetooth-low-energy-communication.html

[68] Bostik, ‘Blu Tack’, 1970, Accessed: Dec. 08, 2023. [Online]. Available: https://diy.bostik.com/en-UK/products/stationery-craft/blu-tack

[69] URSA Straps, ‘URSA Tape’. Accessed: Dec. 08, 2023. [Online]. Available: https://ursastraps.com/product/ursa-tape/

[70] G. Juarez-Martinez *et al.*, ‘Maxwell–Wagner Effect’, in *Encyclopedia of Nanotechnology*, Dordrecht: Springer Netherlands, 2012, pp. 1276–1285. doi: 10.1007/978-90-481-9751-4_5.

[71] M. Huang, L. B. Tunnicliffe, J. Zhuang, W. Ren, H. Yan, and J. J. C. Busfield, ‘Strain-Dependent Dielectric Behavior of Carbon Black Reinforced Natural Rubber’, *Macromolecules*, vol. 49, no. 6, pp. 2339–2347, Mar. 2016, doi: 10.1021/acs.macromol.5b02332.

[72] Y. Huang and L. S. Schadler, ‘Understanding the strain-dependent dielectric behavior of carbon black reinforced natural rubber – An interfacial or bulk phenomenon?’, *Compos Sci Technol*, vol. 142, pp. 91–97, Apr. 2017, doi: 10.1016/j.compscitech.2017.02.003.

[73] S. Huclova, D. Erni, and J. Fröhlich, ‘Modelling and validation of dielectric properties of human skin in the MHz region focusing on skin layer morphology and material composition’, *J Phys D Appl Phys*, vol. 45, no. 2, 2012, doi: 10.1088/0022-3727/45/2/025301.

[74] SetPose, ‘SetPose’. Accessed: Dec. 09, 2023. [Online]. Available: https://setpose.com/

[75] J. C. Lin, *Electromagnetic Fields in Biological Systems*. Boca Raton: CRC Press, 2016. doi: 10.1201/b11257.

[76] S. Gabriel, R. W. Lau, and C. Gabriel, 'The dielectric properties of biological tissues: II. Measurements in the frequency range 10 Hz to 20 GHz', 1996.

[77] D. Teichmann, J. Foussier, Jing Jia, S. Leonhardt, and M. Walter, 'Noncontact Monitoring of Cardiorespiratory Activity by Electromagnetic Coupling', *IEEE Trans Biomed Eng*, vol. 60, no. 8, pp. 2142–2152, Aug. 2013, doi: 10.1109/TBME.2013.2248732.

[78] E. Piuzzi *et al.*, 'Impedance plethysmography system with inertial measurement units for motion artefact reduction: Application to continuous breath activity monitoring', in *2015 IEEE International Symposium on Medical Measurements and Applications (MeMeA) Proceedings*, IEEE, May 2015, pp. 386–390. doi: 10.1109/MeMeA.2015.7145233.

[79] T.-Y. Wu, L. Tan, Y. Zhang, T. Seyed, and X.-D. Yang, 'Capacitivo: Contact-Based Object Recognition on Interactive Fabrics using Capacitive Sensing', in *Proceedings of the 33rd Annual ACM Symposium on User Interface Software and Technology*, New York, NY, USA: ACM, Oct. 2020, pp. 649–661. doi: 10.1145/3379337.3415829.